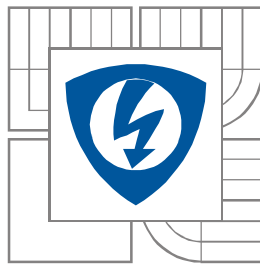


**BRNO UNIVERSITY OF TECHNOLOGY**

**Faculty of Electrical Engineering and Communication**

**Department of Radio Electronics**



**TRIANGULAR-SLOT MONOPOLE ANTENNA  
FOR ON-BODY COMMUNICATIONS**

**Diploma Thesis**

**Study Specialization: Electronics and Communications**

**Author: Alejandro Martín Cantero**

**Supervisor: Prof. Dr. Ing. Zbyněk Raida**



## ACKNOWLEDGEMENTS

---

I would like to thank all the people who have helped and supported me throughout the development of the project, without them it would not have been possible. First I would like to give special thanks to Prof. Dr. Ing. Zbyněk Raida for the opportunity he gave me working with him and for his help and advice throughout the project.

I would also like to thank Ing. Kamil Pítra, Ing. Vladimír Hebelka and Mr. J. Lacik for all their help during the process of design and measurement. Also, I would like to thank the laboratories where the research was performed.



The research described in my thesis was performed in laboratories of the SIX Research Center, the registration number CZ.1.05/2.1.00/03.0072, the operational program Research and Development for Innovation.

I thank my colleague Francisco Ruíz González for having developed his project in parallel to mine, for all his patience, all his help and for being a good friend.

Finally, I would like to thank all those who accompanied me on the way until this point; my parents who always believed in me and made me the way more easy, my brother for all his help when I needed it, my college friends because without them I would not have gotten this far, and finally, my girlfriend Maria Dolores and all those who had the patience to support me during the development of this project, without any of them this would not be possible.

## ABSTRACT

---

The objective of this project is to optimize and redesign a Triangular monopole slot antenna designed to work in On-Body communications. Originally, the antenna was working in the 5.8 GHz ISM band and in the first steps of the design we had to modify the antenna to establish its resonant frequency in the 2.4 GHz band. Finally, we changed the antenna substrate to CuClad 217LX, since this substrate is more flexible and therefore more optimum for communications on the human body. During the development of this project, we show the theoretical simulations of the designs and experimental tests of the antenna.

# CONTENTS

<b>ACKNOWLEDGEMENTS .....</b>	<b>1</b>
<b>ABSTRACT .....</b>	<b>2</b>
<b>LIST OF FIGURES .....</b>	<b>5</b>
<b>LIST OF TABLES .....</b>	<b>10</b>
<b>1. INTRODUCTION.....</b>	<b>11</b>
<b>2. PLANAR ANTENNAS FED BY CPW: AN OVERVIEW .....</b>	<b>13</b>
2.1 MICROSTRIP PATCH ANTENNAS.....	13
2.1.1 Overview .....	13
2.1.2 Properties of a Basic Microstrip Patch .....	14
2.1.2.1 Dimensions .....	15
2.1.2.2 Antenna Impedance and Impedance Matching .....	15
2.1.2.3 Radiation Pattern and Directivity .....	17
2.1.2.4 Antenna Gain and Efficiency .....	18
2.1.2.5 Polarization.....	18
2.1.2.6 Bandwidth .....	18
2.1.3 Advantages and drawbacks.....	19
2.1.4 Slot Antenna concept .....	20
2.2 MICROSTRIP LINE FEEDING .....	21
2.2.1 Coplanar waveguide feeding.....	22
2.3 ELECTROMAGNETIC SIMULATION SOFTWARE.....	24
2.3.1 CST Microwave Studio.....	24
<b>3. TRIANGULAR MONOPOLE ANTENNA .....</b>	<b>26</b>
3.1 OVERVIEW.....	26
3.2 ORIGINAL ANTENNAS.....	27
3.2.1 Antennas from the Paper .....	27
3.2.2 Simulated antennas.....	27
3.2.2.1 Frequency Response S11.....	28
3.2.2.2 H-Field .....	29
3.2.2.3 E-Field .....	30
3.2.2.4 Current Distribution .....	32
3.2.2.5 Farfield.....	33
3.2.3 Conclusions.....	35
3.3 MODIFICATIONS FROM THE ORIGINAL.....	35
3.3.1 Frequency Response S11.....	36

3.3.2	H-Field .....	37
3.3.3	E-Field.....	38
3.3.4	Current Distribution .....	39
3.3.5	Farfield.....	40
3.3.6	Conclusions.....	42
3.4	NEW SUBSTRATE .....	42
3.4.1	Substrate CuClad 217LX .....	43
3.4.2	Simulations.....	43
3.4.2.1	Frequency Response S11.....	44
3.4.2.2	H-Field .....	44
3.4.2.3	E-Field .....	46
3.4.2.4	Current Distribution .....	47
3.4.2.5	Farfield.....	48
3.4.3	Conclusions.....	50
<b>4.</b>	<b>MEASUREMENTS.....</b>	<b>52</b>
4.1	FABRICATION AND MEASUREMENT METHODS.....	52
4.2	MEASUREMENTS RESULTS.....	55
4.3	COMPARISON BETWEEN MEASUREMENTS AND SIMULATIONS .....	56
<b>5.</b>	<b>CONCLUSIONS AND FUTURE WORK .....</b>	<b>60</b>
	<b>REFERENCES .....</b>	<b>61</b>
	<b>APPENDIX A .....</b>	<b>i</b>
1.	POLARIZATION CST EXPLANATION .....	i
2.	TRANSMISSION COEFFICIENT SIMULATION .....	iv
3.	PARAMETER S22 OF FIGURE 15 CONFIGURATION.....	vii
4.	MEASUREMENTS AT 4 LAMBDA DISTANCE (40 CM) .....	ix

## LIST OF FIGURES

---

### Chapter 1

Fig. 1.1. A wearable computer assembly produced at the University of Birmingham

Fig. 1.2. Example of antennas for on-body communications

### Chapter 2

Fig. 2.1. Structure of a microstrip patch antenna

Fig. 2.2. Geometry of a basic patch microstrip antenna

Fig. 2.3. E-field distribution under the patch

Fig. 2.4. Current distribution on the patch surface

Fig. 2.5. Impedance, E-field and H-field distribution along the patch's length

Fig. 2.6. Typical radiation pattern of a simple patch

Fig. 2.7. Geometry slot antenna

Fig. 2.8. Rectangular Slot antenna with dimensions  $a$  and  $b$

Fig. 2.9. Slot antenna and complementary dipole

Fig. 2.10. Schematic of a Microstrip line feeding

Fig. 2.11. Schematic of a CPW

Fig. 2.12. CPW Electric-E and Magnetic-H field distribution

Fig. 2.13. CST Microwave Studio user interface

### Chapter 3

Fig. 3.1. Geometry of a CPW-fed equilateral triangular-ring slot antenna with tuning-stub (left) and with back-patch (right)

Fig. 3.2. CPW-fed double triangular slot antenna

Fig. 3.3. Personal design based on the original antenna

Fig. 3.4. Original antenna Frequency response of the reflection coefficient of the antenna

Fig. 3.5. Original antenna H-Field vector distribution

Fig. 3.6. Original antenna H-Field, X component

Fig. 3.7. Original antenna H-Field, Y component

Fig. 3.8. Original antenna H-Field, Z component

Fig. 3.9. Original antenna H-Field, Abs component

Fig. 3.10. Original antenna H-Field, Normal component

Fig. 3.11. Original antenna H-Field, Tangential component

Fig. 3.12. Original antenna E-Field vector distribution

Fig. 3.13. Original antenna E-Field, X component

Fig. 3.14. Original antenna E-Field, Y component

Fig. 3.15. Original antenna E-Field, Z component

Fig. 3.16. Original antenna E-Field, Abs component

Fig. 3.17. Original antenna E-Field, Normal component

Fig. 3.18. Original antenna E-Field, Tangential component

Fig. 3.19. Original antenna Current Distribution, vector distribution

Fig. 3.20. Original antenna Current Distribution, X component

Fig. 3.21. Original antenna Current Distribution, Y component

Fig. 3.22. Original antenna Current Distribution, Z component

Fig. 3.23. Original antenna Current Distribution, Abs component

Fig. 3.24. Original antenna Current Distribution, Normal component

Fig. 3.25. Original antenna Current Distribution, Tangential component

Fig. 3.26. Original antenna Abs radiation pattern

Fig. 3.27. Original antenna Phi component 3D radiation pattern

Fig. 3.28. Original antenna Theta component 3D radiation pattern

Fig. 3.29. Original antenna Directivity pattern: Phi component ( $\Phi=0$ ) (Left) and Theta component ( $\Phi=90$ ) (Right)

Fig. 3.30. New designed antenna whose resonant frequency is at 2.4 GHz

Fig. 3.31. Antenna at 2.4 GHz Frequency response of the reflection coefficient of the antenna

Fig. 3.32. Antenna at 2.4 GHz H-Field vector distribution

Fig. 3.33. Antenna at 2.4 GHz H-Field, X component

Fig. 3.34. Antenna at 2.4 GHz H-Field, Y component

Fig. 3.35. Antenna at 2.4 GHz H-Field, Z component

Fig. 3.36. Antenna at 2.4 GHz H-Field, Abs component

Fig. 3.37. Antenna at 2.4 GHz H-Field, Normal component

Fig. 3.38. Antenna at 2.4 GHz H-Field, Tangential component



Fig. 3.39. Antenna at 2.4 GHz E-Field vector distribution

Fig. 3.40. Antenna at 2.4 GHz E-Field, X component

Fig. 3.41. Antenna at 2.4 GHz E-Field, Y component

Fig. 3.42. Antenna at 2.4 GHz E-Field, Z component

Fig. 3.43. Antenna at 2.4 GHz E-Field, Abs component

Fig. 3.44. Antenna at 2.4 GHz E-Field, Normal component

Fig. 3.45. Antenna at 2.4 GHz E-Field, Tangential component

Fig. 3.46. Antenna at 2.4 GHz Current Distribution, vector distribution

Fig. 3.47. Antenna at 2.4 GHz Current Distribution, X component

Fig. 3.48. Antenna at 2.4 GHz Current Distribution, Y component

Fig. 3.49. Antenna at 2.4 GHz Current Distribution, Z component

Fig. 3.50. Antenna at 2.4 GHz Current Distribution, Abs component

Fig. 3.51. Antenna at 2.4 GHz Current Distribution, Normal component

Fig. 3.52. Antenna at 2.4 GHz Current Distribution, Tangential component

Fig. 3.53. Antenna at 2.4 GHz Abs radiation pattern

Fig. 3.54. Antenna at 2.4 GHz Phi component 3D radiation pattern

Fig. 3.55. Antenna at 2.4 GHz Theta component 3D radiation pattern

Fig. 3.56. Antenna at 2.4 GHz Directivity pattern: Phi component ( $\Phi=0$ ) (Left) and Theta component ( $\Phi=90$ ) (Right)

Fig. 3.57. Final antenna design, with CuClad 217LX substrate

Fig. 3.58. Final design Frequency response of the reflection coefficient of the antenna

Fig. 3.59. Final design H-Field vector distribution

Fig. 3.60. Final design H-Field, X component

Fig. 3.61. Final design H-Field, Y component

Fig. 3.62. Final design H-Field, Z component

Fig. 3.63. Final design H-Field, Abs component

Fig. 3.64. Final design H-Field, Normal component

Fig. 3.65. Final design H-Field, Tangential component

Fig. 3.66. Final design E-Field vector distribution

Fig. 3.67. Final design E-Field, X component

Fig. 3.68. Final design E-Field, Y component

Fig. 3.69. Final design E-Field, Z component

Fig. 3.70. Final design E-Field, Abs component

Fig. 3.71. Final design E-Field, Normal component

Fig. 3.72. Final design E-Field, tangential component

Fig. 3.73. Final design Current Distribution, vector distribution

Fig. 3.74. Final design Current Distribution, X component

Fig. 3.75. Final design Current Distribution, Y component

Fig. 3.76. Final design Current Distribution, Z component

Fig. 3.78. Final design Current Distribution, Normal component

Fig. 3.77. Final design Current Distribution, Abs component

Fig. 3.79. Final design Current Distribution, Tangential component

Fig. 3.80. Final design Abs radiation pattern

Fig. 3.81. Final design Phi component 3D radiation pattern

Fig. 3.82. Final design Theta component 3D radiation pattern

Fig. 3.83. Final design Directivity pattern: Phi component ( $\Phi=0$ ) (Left) and Theta component ( $\Phi=90$ ) (Right)

Fig. 3.84. Comparison S11 parameter between antenna with Arlon substrate and antenna with CuClad 217LX substrate

## **Chapter 4**

*Fig. 4.1. Triangular-Slot antenna finally built*

*Fig. 4.2. Network Analyzer used in the measurements*

*Fig. 4.3. Phantom used for S11 measurement*

*Fig. 4.4. Phantom measure (Right) and real body measure (Left)*

*Fig. 4.5. Phantom used in the transmission coefficient measurement*

*Fig. 4.6. Transmission coefficient measurement in free space*

*Fig. 4.7. Transmission coefficient measurement with the phantom*

*Fig. 4.8. Reflection coefficient measurements*

*Fig. 4.9. Transmission coefficient measurements*

*Fig. 4.10. Comparison between measurements and simulation in Free Space*

*Fig. 4.11. Comparison between measurements and simulation on human tissue*

*Fig. 4.12. Configuration of an experiment for measuring transmission between two antennas*

*Fig. 4.13. Transmit antenna: fractal-line slot dipole*

*Fig. 4.14. Comparison of frequency response of reflection coefficient at the input of antennas (red, orange) and transmission coefficient (green).*

## **Appendix A**

*Figure 1. Abs-component*

*Figure 2. Theta component*

*Figure 3. Phi component*

*Figure 4. Axes change*

*Figure 5. Abs-component with axes changed*

*Figure 6. Theta component with axes changed*

*Figure 7. Phi component with axes changed*

*Figure 8. Orientation of antennas*

*Figure 9. Transmission configuration*

*Figure 10. S11 and S21 parameters*

*Figure 11. Farfield with antennas structure*

*Figure 12. Transmission configuration*

*Figure 13. S11 and S21 parameters*

*Figure 14. Farfield with antennas structure*

*Figure 15. Transmission configuration*

*Figure 16. S11 and S21 parameters*

*Figure17. Farfield with antennas structure*

*Figure 18 Transmission configuration*

*Figure 19 S parameter of Figure 24 configuration*

*Figure 20 Farfield from Port 1 (Triangular monopole antenna)*

*Figure 21 Farfield from Port 2 (Like-Fractal dipole antenna)*

*Figure 22 Transmision configuration*

*Figure 23 S parameter of Figure 28 configuration*

*Figure 24 Gain from Port 1 (Triangular monopole antenna)*

*Figure 25 Directivity from Port 1 (Triangular monopole antenna)*

*Figure 26 Gain from Port 2 (Like-Fractal dipole antenna)*

*Figure 27 Directivity from Port 2 (Like-Fractal dipole antenna)*

## LIST OF TABLES

---

### Chapter 2

*Table 2.1. Comparison between microstrip and CPW design techniques*

### Chapter 3

*Table 3.1. Original antenna value of the antenna parameters*

*Table 3.2. Original antenna Resonant Frequency results obtained by CST*

*Table 3.3. Antenna at 2.4 GHz value of the antenna parameters*

*Table 3.4. Antenna at 2.4 GHz Resonant Frequency results obtained by CST*

*Table 3.5. Final design value of the antenna parameters*

*Table 3.6. Final design Resonant Frequency results obtained by CST*

### Chapter 4

*Table 4.1. Values of reflection coefficient measurements*

*Table 4.2. Parameters of fractal-line slot dipole antenna on CuClad217LX substrate.*

## 1. INTRODUCTION

---

Ever-growing miniaturization of electronic devices, combined with the recent developments in wearable computer technology, have been leading to the creation of a wide range of devices that can be carried by their user in the pocket or attached to their body. [1]

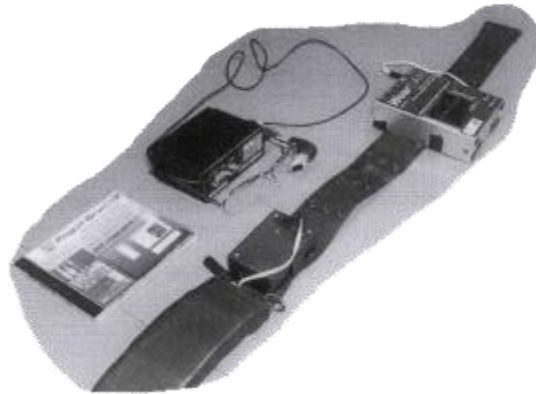


*Fig. 1.1. A wearable computer assembly produced at the University of Birmingham [2]*

Currently, paramedics, warehouse operators, and other specialist occupations use wearable computers. It has also been suggested that wearable computers might also become a fashion accessory, as well as supporting entertainment and information services to the general population. The currently available Bluetooth-connected mobile-phone headsets are an example of an on-body communications system. There is an argument that the Bluetooth standard was not created for such an application, and may thus not be optimal. It is clear that a full understanding of the very different demands of this application is needed to allow the development of fully optimized systems. [2]

Also, the health care market has become a four trillion dollar industry worldwide. With this enormous growth comes the need for new information technologies to achieve two critical goals: cutting costs while improving the quality of care. A long list of factors, including an intensely competitive health care market, strong pressure to prevent medical errors, and the need to comply with regulations, are combining to trigger rapid growth in technology spending. Interest in mobile monitoring technologies and electronic medical records is exploding as hospitals and clinics of all sizes strive to provide physicians and caregivers with advanced access to clinical information. Diagnosis, surveillance, and treatment are increasingly dependent on monitoring information. [3]

In this project we will focus on the development and design of antennas for on-body communications. There are two primary requirements for antennas for on-body links. First, the antenna needs to be insensitive to the proximity to the body; and second, the antenna needs

to have a radiation pattern shape that minimizes the link loss. The matching of the antennas is naturally affected by their proximity to the body, due to the influence of the body on the antenna reactive fields.

The path gain is highly dependent both on antenna type and link geometry. The antenna positions also determine the propagation mode. For example, for the belt-to-chest path, it is evident that propagation will be predominantly due to a surface or creeping wave. Similarly, the belt-to-wrist path will be in some cases a free-space path, when the hand is in front of the body; and in others, it will be a shadowed free-space path with diffraction around the body, when the arm is behind the body. In the case of a grazing wave around the surface, it is clear that an antenna with a radiation pattern peak along the body surface and with vertical polarization is needed. For a free-space link, an antenna with maximum radiation away from the body is needed. In all cases, radiation into the body should be minimized, since the relatively small skin depth of a few centimeters at these frequencies suggests that little energy is propagated through the body. Due to the large number of possible link geometries and body postures, it is rather difficult to specify ideal antenna characteristics.

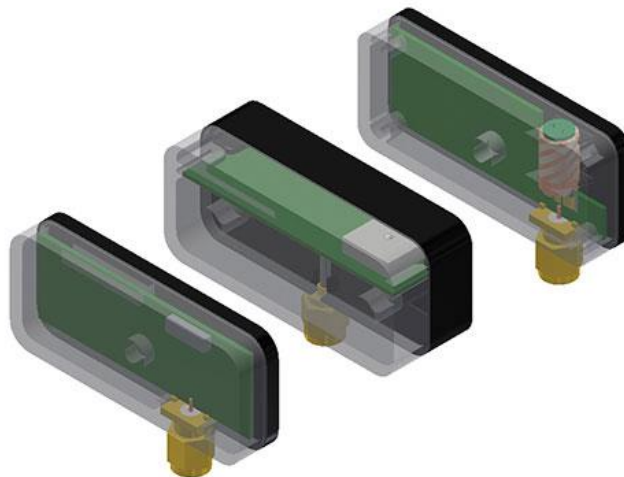


*Fig. 1.2. Example of antennas for on-body communications [4]*

The patch gives strong radiation away from the surface, suitable for the free-space links.

Since the electrical conductivity of a human body is significantly high, electric field intensity of the creeping wave has to be perpendicular to the surface of a human body. The required polarization can be achieved by electrical monopoles, which are perpendicular to the skin, or by slots (magnetic conductors) which are placed in parallel to the skin. From practical reasons, we concentrate on slot antennas. [5]

## 2. PLANAR ANTENNAS FED BY CPW: AN OVERVIEW

### 2.1 MICROSTRIP PATCH ANTENNAS

#### 2.1.1 Overview

As shown in Fig. 2.1, the structure of a microstrip antenna is quite simple. There are three layers, the first one, on top, is the patch with  $L \times W$  dimensions and the microstrip transmission line. The second one is the substrate (some dielectric circuit board) of thickness  $h$  with permittivity or dielectric constant. And the last one is the ground plane, whose thickness is not critically important. Typically the substrate's height is much smaller than the wavelength of operation, but not much smaller than 0.05 of a wavelength. [6]

It is important to remember that both layers, ground plane and patch plane, are made of high conductivity metal (typically copper).

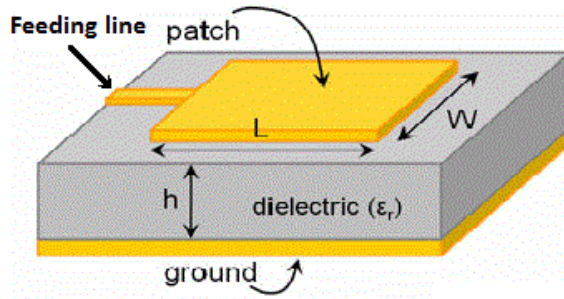


Fig. 2.1. Structure of a microstrip patch antenna [7]

The next step is related with the configuration of the antenna. We can change the parameters of it by modifying the dimensions of  $L$ ,  $W$ ,  $h$  and  $\epsilon_r$ . As we can see in the formula below, the central frequency will be approximately given by [11]:

$$f_c \approx \frac{c}{2L\sqrt{\epsilon_r}} = \frac{1}{2L\sqrt{\epsilon_0\epsilon_r\mu_0}} \quad (1)$$

Here,  $c$  is velocity of light,  $\epsilon_r$  is the dielectric constant of the substrate,  $L$  is the length of the patch,  $\epsilon_0$  and  $\mu_0$  is the permittivity of vacuum and permeability of vacuum, respectively.

Hence, there is an inverse relation between the central frequency and  $L$ . And we notice that the  $L$  dimension of the antenna should be one half of a wavelength within the dielectric medium.

When we modify the width  $W$  of the patch, we control the input impedance and at the same time, the radiation patterns. Talking about the impedance, we can say that the wider the patch becomes the lower the input impedance is. Larger widths also can increase the bandwidth.

Another interesting point is the modification of the permittivity of our substrate because if we decrease it, then we would increase the bandwidth. Moreover, we can control the fringing fields by changing the permittivity. So, when we reduce the value of the permittivity, we obtain wider fringing fields and therefore we get better radiation.

Finally, it is important to stand up the importance of the height of the substrate ( $h$ ) which controls the bandwidth. We can compare this sentence with the general rule which says that “an antenna occupying more space in a spherical volume will have a wider bandwidth”. Hence, if we increase the height of the substrate, we will increase the bandwidth of it. [6]

### 2.1.2 Properties of a Basic Microstrip Patch

The basic form of a patch antenna is a flat plate over a ground plane. This is by far the most popular type of microstrip antenna. The Fig. 2.2 shows the geometry of the rectangular microstrip antenna, not including the ground plane and dielectric which would be underneath. The dimension  $L$  is universally taken to mean the long dimension, which causes resonance at its half-wavelength frequency. The radiating edges are at the ends of the  $L$ -dimension of the rectangle, which sets up the single polarization. Radiation that occurs at the ends of the  $W$ -dimension is far less and is referred to as the cross-polarization. [8]

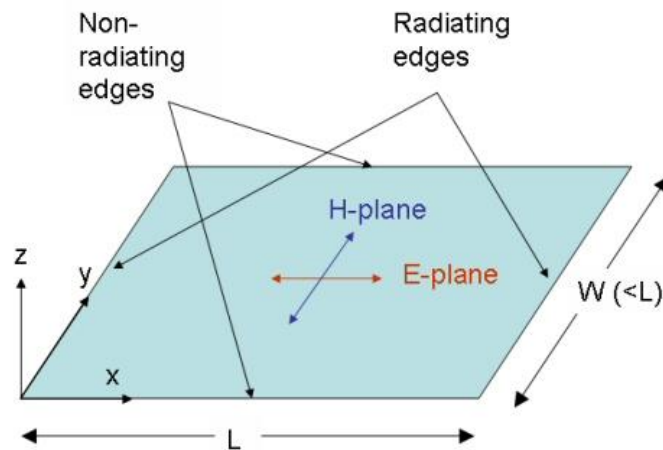


Fig. 2.3. Geometry of a basic patch microstrip antenna [8]

The electric field is zero at the center of the patch, maximum (positive) at one side, and minimum (negative) on the opposite side. It should be mentioned that the minimum and maximum continuously change side according to the instantaneous phase of the applied signal. The Fig. 2.4 is a side view which attempts to show a snapshot of the E-field under the patch. Note that the fields under the  $L$ -edges are of opposite polarity, due to the half-wave nature of the patch. [8][9]



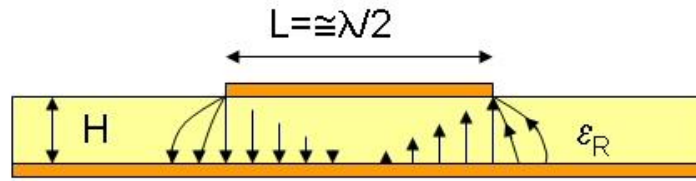


Fig. 2.5. E-field distribution under the patch [8]

### 2.1.2.1 Dimensions

There are an infinite number of resonant modes; the resonant frequency of each is governed by the size and shape of the patch and the relative permittivity of the substrate. The resonant length determines the resonant frequency and is about  $\lambda/2$  for a rectangular patch excited in its fundamental mode. A better approximation for the resonant length is: [10]

- $L$  = resonant length
  - $\lambda_d$  = wavelength in PC board
  - $\lambda_0$  = wavelength in free space
  - $\epsilon_r$  = dielectric constant of the substrate
- $$L \approx 0.49 \cdot \lambda_d = 0.49 \cdot \frac{\lambda_0}{\sqrt{\epsilon_r}} \quad (2) [9]$$

There are other parameters that can influence the resonant frequency like the ground plane size, the conductor thickness and the patch width (impedance).

### 2.1.2.2 Antenna Impedance and Impedance Matching

Antenna Impedance is presented as the ratio of voltage to current at the antenna's terminals. The fundamentals of antenna theory require that the antenna be "impedance matched" to the transmission line or the antenna will not radiate. The concept of voltage standing wave ratio (VSWR) is introduced as a measure of how well matched an antenna is. [6]

For coaxial-fed antennas, the input impedance is dependent on the feed position. It is usually large when the feed is near the edge of the patch and decreases as the feed moves inside the patch. Its magnitude can vary from tens to hundreds of ohms. [10]

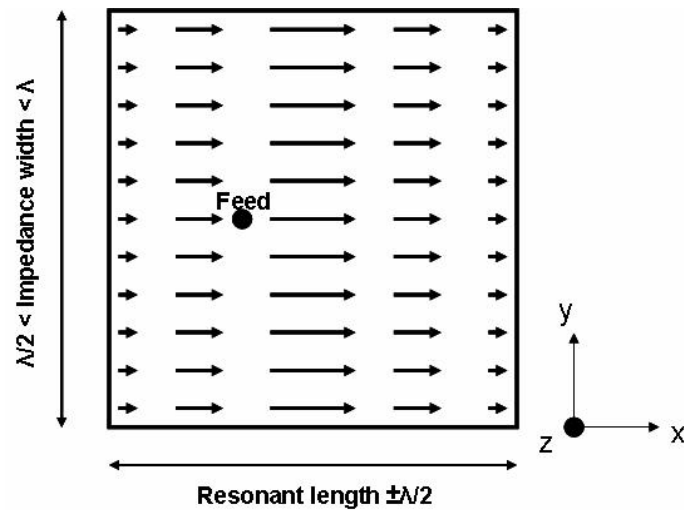


Fig. 2.6. Current distribution on the patch surface [9]

Looking at the current and voltage variation along the patch, the current is maximal at the center and minimal near the left and right edges, while the electrical field is zero in the center and maximal near the left and right edges. [9]

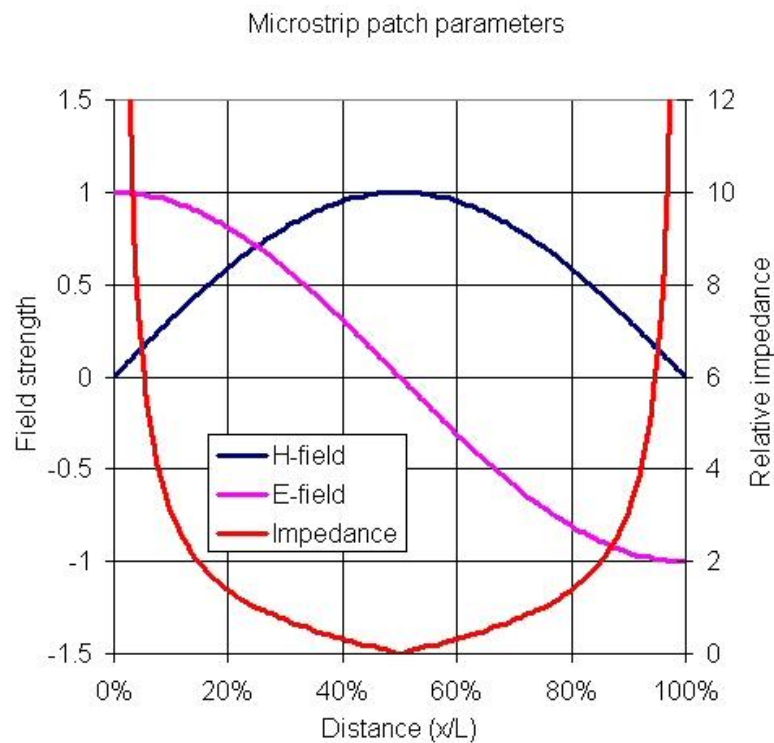


Fig. 2.7. Impedance, E-field and H-field distribution along the patch's length [8]

Perhaps another intuitive way to look at the input impedance to a microstrip patch is to think about how far you are from an open circuit. If you feed it at the center, you are looking at a short circuit in both directions, because you are a quarter-wave from a short circuit. If you feed it at the edge you see an open circuit, because you are a half-wave from another open. [8]

### 2.1.2.3 Radiation Pattern and Directivity

A radiation pattern defines the variation of the power radiated by an antenna as a function of the direction away from the antenna. This power variation as a function of the arrival angle is observed in the antenna's far field. [6]

The patch's radiation pattern shows that the antenna radiates more power in a certain direction than another direction. The antenna is said to have certain directivity. This is commonly expressed in dB. An estimation of the expected directivity of a patch can be derived with ease. The fringing fields at the radiating edges can be viewed as two radiating slots placed above a ground plane. Assuming all radiation occurs in one half of the hemisphere, this results in 3 dB directivity. [9]

This case is often described as a perfect front-to-back ratio, which means all radiation towards the front and no radiation towards the back. This front-to-back ratio is highly dependent on ground plane size and shape in practical cases. Another 3 dB can be added since there are 2 slots. The slots are typically taken to have a length equal to the impedance width of the patch and a width equal to the substrate height. [9]

The rectangular patch excited in its fundamental mode has a maximum directivity in the direction perpendicular to the patch (broadside). The directivity decreases when moving away from broadside towards lower elevations. [9]

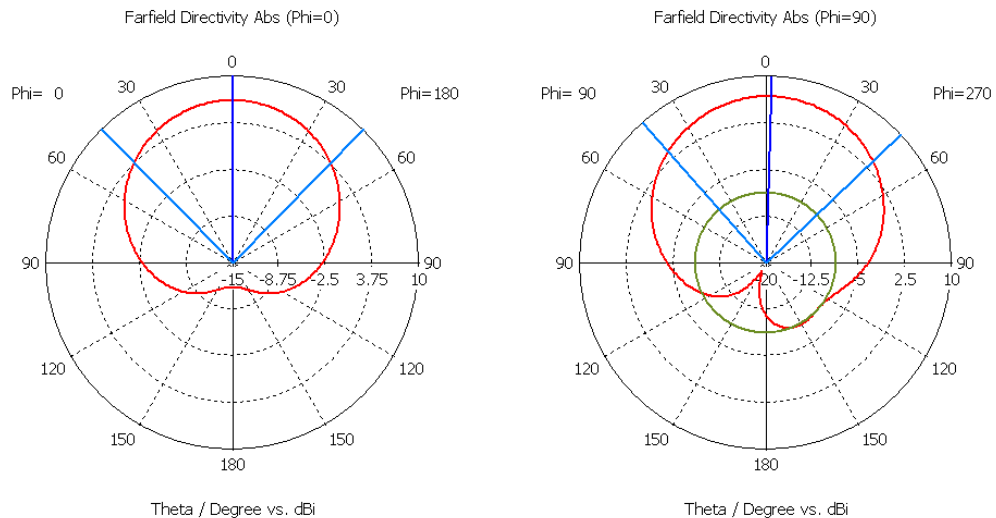


Fig. 2.8. Typical radiation pattern of a simple patch [9]

So far, the directivity has been defined with respect to an isotropic source and hence has the unit dBi. An isotropic source radiates an equal amount of power in every direction. [9]

#### 2.1.2.4 Antenna Gain and Efficiency

An antenna's efficiency is a measure of how much power is radiated by the antenna relative to the antenna input power. Antenna gain is defined as antenna directivity times a factor representing the radiation efficiency. The input power is transformed into radiated power and surface wave power while a small portion is dissipated due to conductor and dielectric losses of the materials used. Surface waves are guided waves captured within the substrate and partially radiated and reflected back at the substrate edges. [6][9]

Antenna gain can also be specified using the total efficiency instead of the radiation efficiency only. This total efficiency is a combination of the radiation efficiency and efficiency linked to the impedance matching of the antenna. [9]

#### 2.1.2.5 Polarization

The plane wherein the electric field varies is also known as the polarization plane. The basic patch covered until now is linearly polarized since the electric field only varies in one direction. This polarization can be either vertical or horizontal depending on the orientation of the patch. A transmit antenna needs a receiving antenna with the same polarization for optimum operation. [9]

There is another kind of polarization such as circular polarization. In a circular polarized antenna, the electric field varies in two orthogonal planes with the same magnitude and a 90° phase difference.

#### 2.1.2.6 Bandwidth

Bandwidth is another fundamental antenna parameter. Bandwidth describes the range of frequencies over which the antenna can properly radiate or receive energy. Often, the desired bandwidth is one of the determining parameters used to decide upon an antenna. For instance, many antenna types have very narrow bandwidths and cannot be used for wideband operation. [6]

Only impedance bandwidth is specified most of the time. However, it is important to realize that several definitions of bandwidth exist like impedance bandwidth, directivity bandwidth, polarization bandwidth, and efficiency bandwidth. Directivity and efficiency are often combined as gain bandwidth. [9]

### 2.1.3 Advantages and drawbacks

Microstrip patch antennas were first proposed in the 1970s, since that moment a constantly evolution in this area has occurred. This kind of antennas has several advantages over conventional microwave antenna with one similarity of frequency range from 100 MHz to 100 GHz. So, we are going to sum up the most important advantages [11] [12]:

- Light weight, low cost, low volume, low profile and robust nature

Printed circuits are thin and thus require less volume than their waveguide or coaxial counterparts. Printed circuits antennas consist mainly of non-metallic materials like foam materials as substrates, such antennas have an extremely low weight compared to conventional antennas.

- Polarization

An advantage inherent to patch antennas is the ability to have polarization diversity. Patch antennas can easily be designed to have vertical, horizontal, right hand circular (RHCP) or left hand circular (LHCP) polarizations, using multiple feed points, or a single feed point with asymmetric patch structures. [13]

- Dual frequency antennas

Dual-frequency operation is possible by using either dual-stacked patches or a patch with a loaded diode or a stub.

- Excitation technique

Patches allow a lot of different excitation techniques to be used, compatible with any technology of the active circuitry and beam forming networks.

- Suitable for integration with MICs (Microwave Integrated Circuits) and optoelectronic integrated circuits (OIECs)

MICs are much easier to handle and less expensive than the alternative waveguides.

Unfortunately, the expression, “there is no such thing as a free lunch”, also applies to microstrip patch technology [14]. Despite the previously mentioned features, microstrip patch antennas suffer from several inherent drawbacks [11][12]:

- Narrow bandwidth.
- Poor radiation efficiency resulting from surface wave excitation and conductor and dielectric losses.
- Lower gain.
- Extraneous radiation from feeds and junctions.
- Low power handling capacity.
- Polarization purity is difficult to achieve.

### 2.1.4 Slot Antenna concept

The slot antenna was invented in 1938 by Alan Blumlein, while working for EMI. He invented it in order to produce a practical type of antenna for VHF television broadcasting that would have horizontal polarization, an omni-directional horizontal radiation pattern and a narrow vertical radiation pattern. [15]

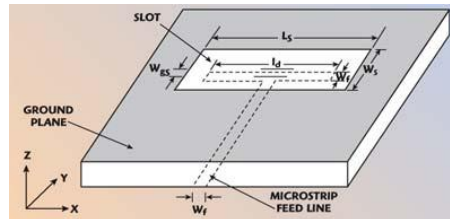


Fig. 2.7. Geometry slot antenna [16]

A slot antenna consists of a metal surface, usually a flat plate, with a hole or slot cut out. When the plate is driven as an antenna by a driving frequency, the slot radiates electromagnetic waves in similar way to a dipole antenna. The shape and size of the slot, as well as the driving frequency, determine the radiation distribution pattern. Often the radio waves are provided by a waveguide, and the antenna consists of slots in the waveguide. Slot antennas are often used at UHF and microwave frequencies instead of line antennas when greater control of the radiation pattern is required. Slot antennas are widely used in radar antennas, for the sector antennas used for cell phone base stations, and are often found in standard desktop microwave sources used for research purposes. [15]

A slot antenna's main advantages are its size, design simplicity, robustness, and convenient adaptation to mass production using PC board technology. Slot antennas are used typically at frequencies between 300 MHz and 24 GHz. The polarization of the slot antenna is linear. The slot size, shape and what is behind it (the cavity), offer design variables that can be used to tune performance. [6][15]

Consider an infinite conducting sheet, with a rectangular slot cut, whose dimensions are  $a \times b$ , as shown in Fig. 2.8. If we can excite some reasonable fields in the slot (often called the aperture), we have a slot antenna.

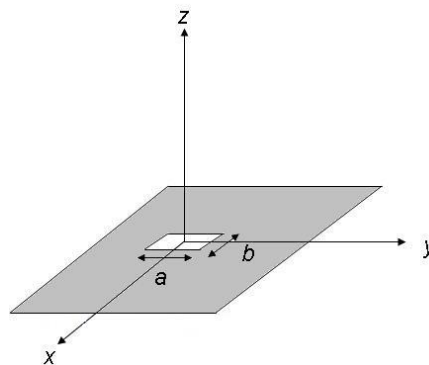


Fig. 2.8. Rectangular Slot antenna with dimensions  $a$  and  $b$  [6]

The slot length is a half wavelength at the desired frequency and the width is a small fraction of a wavelength. The antenna is frequently compared to a conventional half-wave

dipole consisting of two flat metal strips. The physical dimensions of the metal strips are such that they would just fit into the slot cut out of the large metal sheet. This type of antenna is called the *complementary dipole*. [17]

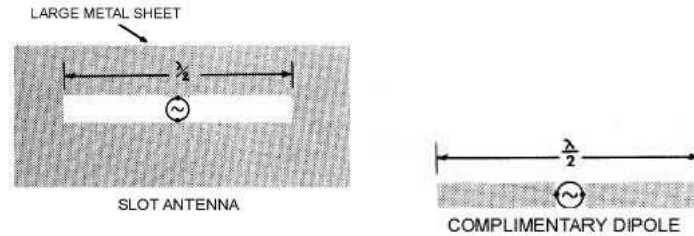


Fig. 2.9. Slot antenna and complementary dipole [17]

Note that a voltage source is applied across the short end of the slot antenna. This induces an E-field distribution within the slot, and currents that travel around the slot perimeter, both contributed to radiation. The complementary antenna is similar to a dipole antenna. The voltage source is applied at the centre of the dipole, so that the voltage source is rotated. The electric and magnetic fields are interchanged. In the case of the dipole antenna shown in Fig. 2.9, the electric lines are horizontal while the magnetic lines form loops in the vertical plane. With the slot antenna, the magnetic lines are horizontal and the electric lines are vertical. The electric lines are built up across the narrow dimensions of the slot. As a result, the polarization of the radiation produced by a horizontal slot is vertical. If a vertical slot is used, the polarization is horizontal. [6][17]

Hence, if we know the fields from one antenna we know the fields of the other antenna, since it is easy to visualize the fields from a dipole antenna, the fields and impedance from a slot antenna can become intuitive because the polarization of the two antennas are reversed. [6]

A second difference between the slot antenna and its complementary dipole is that the direction of the lines of electric and magnetic force abruptly reverse from one side of the metal sheet to the other. In the case of the dipole, the electric lines have the same general direction while the magnetic lines form continuous closed loops. [17]

When energy is applied to the slot antenna, currents flow in the metal sheet. These currents are not confined to the edges of the slot but rather spread out over the sheet. Radiation then takes place from both sides of the sheet. In the case of the complementary dipole, however, the currents are more confined; so a much greater magnitude of current is required to produce a given power output using the dipole antenna. [17]

## 2.2 MICROSTRIP LINE FEEDING

Microstrip line feed is one of the easier methods to fabricate as it is a just conducting strip connecting to the patch and therefore can be consider as extension of patch. It is simple to model and easy to match by controlling the inset position. However the disadvantage of this method is that as substrate thickness increases, surface wave and spurious feed radiation increases which limit the bandwidth. [18]

As we can see in Fig. 2.10, this feeding method consists on a strip of thin metallic film on the surface of the substrate. Besides, on the other side of the substrate there is a metallic layer which is the ground plane.

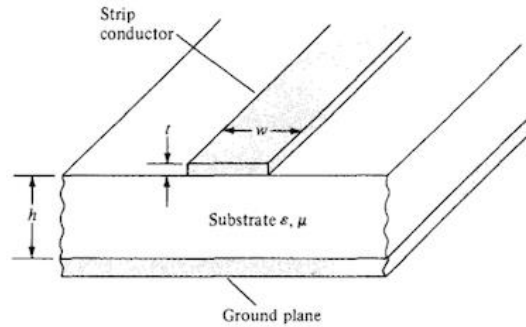


Fig. 2.10. Schematic of a Microstrip line feeding [19]

### 2.2.1 Coplanar waveguide feeding

Coplanar waveguide is a type of electrical transmission line which can be fabricated using printed circuit board technology, and is used to convey microwave-frequency signals. Conventional coplanar waveguide (CPW) consists of a strip of thin metallic film deposited on the surface of a dielectric slab with two ground electrodes running adjacent and parallel to the strip on the same surface, as shown in Fig. 2.11. All three conductors are on the same side of the substrate, and hence are *coplanar*. The return conductors are separated from the central track by a small gap, which has an unvarying width along the length of the line. Away from the central conductor, the return conductors usually extend to an indefinite but large distance, so that each is notionally a semi-infinite plane. [20][21]

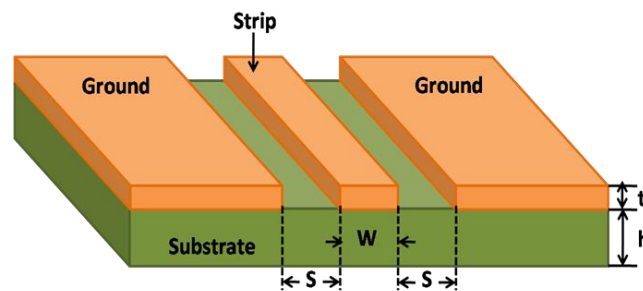


Fig. 2.11. Schematic of a CPW [22]

The electromagnetic wave carried by a coplanar waveguide exists partly in the dielectric substrate, and partly in the air above it. In general, the dielectric constant of the substrate will be different (and greater) than that of the air, so that the wave is travelling in an inhomogeneous medium. In consequence CPW will not support a true TEM wave; at non-zero frequencies, both the E and H fields will have longitudinal components (a hybrid mode). [21]

There is no low-frequency cut-off because of the quasi-TEM mode of propagation. However, the RF electric field between the centre conducting strip and the ground electrodes tangential to the air-dielectric boundary produces a discontinuity in displacement current



density at the interface, giving rise to an axial, as well as transverse, component of RF magnetic field. [20]

As we have said, CPW has a zero cut-off frequency (suitable for wideband), but its low order propagation mode is indicated with Quasi-TEM because it is not a real TEM mode. At higher frequencies, the field becomes less-TEM, and more TE in nature. The CPW magnetic field is elliptically polarized, as shown in Fig. 2.12. [23]

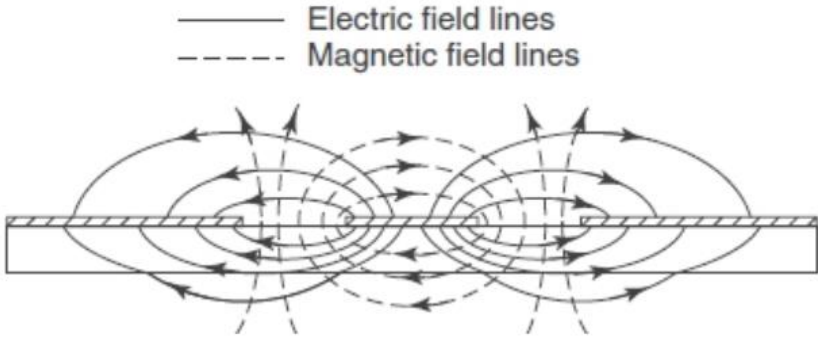


Fig. 2.12. CPW Electric-E and Magnetic-H field distribution [23]

In the last years, an increase in the design of CPW (**CoPlanar Waveguide**) circuits on GaAs could be noticed. The main reason for this is the fact that the CPW design technique allows to reduce the circuit size by about 30% and in addition, the expensive backside processing and the difficult via etching in the microstrip case becomes obsolete. In contrast, CPW design results in the disadvantages of slightly higher losses and poor power handling capabilities. Table 2.1 shows a brief comparison of microstrip and CPW design techniques. [24]

Moreover, compared to the microstrip line, CPW possesses advantages of being more convenient for shunt and series connections on the same side of the substrate avoiding via holes. Therefore, CPW-fed antenna is preferred in our design.



		 Microstrip	 CPW
Design Aspects	Dispersion	High	Low
	Losses	Low	High
	Coupling	High	Low
	Design flexibility	Low	High
Cost Aspects	Circuit processing	Large	Small
	Backside processing	Yes	No
	Via holes	Yes	No

Table 2.1. Comparison between microstrip and CPW design techniques [24]

## 2.3 ELECTROMAGNETIC SIMULATION SOFTWARE

Computational electromagnetics, computational electrodynamics or electromagnetic modelling is the process of modelling the interaction of electromagnetic fields with physical objects and the environment.

It typically involves using computationally efficient approximations to Maxwell's equations and is used to calculate antenna performance, electromagnetic compatibility, radar cross section and electromagnetic wave propagation when not in free space.

During the development of this project, it will be used the CST Microwave Studio.

### 2.3.1 CST Microwave Studio [25]

CST Microwave Studio is a fully featured software package for electromagnetic analysis and design in the high frequency range. It simplifies the process of creating the structure by providing a powerful graphical solid modelling front end which is based on the ACIS modelling kernel. After the model has been constructed, a fully automatic meshing procedure is applied before a simulation engine is started.

Since no one method works equally well for all applications, the software contains several different simulation techniques (time domain solvers, frequency domain solvers, integral equation solver, multilayer solver, asymptotic solver, and eigenmode solver) to best suit various applications.

The largest simulation flexibility is offered by the **time domain solvers**, which can obtain the entire broadband frequency behaviour of the simulated device from a single calculation run. These solvers are remarkably efficient for most high frequency applications such as connectors, transmission lines, filters, and antennas, amongst others.

Two time domain solvers are available, both using a hexahedral grid, either based on the Finite Integration Technique (FIT) or on the Transmission-Line Matrix (TLM) method.

The time domain solvers are less efficient for structures that are electrically much smaller than the shortest wavelength of interest. In such cases it may be advantageous to solve the problem by using the **frequency domain solvers**. *During the development of this project, it has been used the time domain solvers.*

CST MICROWAVE STUDIO therefore contains an **integral equation based solver** which is particularly suited to solving problems related to electrically large structures, volumetric discretization methods generally suffer from dispersion effects and thus require a very fine mesh.

Nonetheless, the Multilevel Fast Multipole Method (MLFMM) solver may become inefficient for electrically extremely large structures. In this case, the **asymptotic solver** is the most suitable one by using the so-called ray-tracing technique.

For structures which are mainly planar, such as microstrip filters or printed circuit boards, this particular property can be exploited in order to gain efficiency. The **multilayer solver**, based on the Method of Moments, does not require discretization of the transversally infinite dielectric and metal stack up.

Efficient filter design often requires the direct calculation of the operating modes in the filter rather than an S-parameter simulation. For these applications, CST MICROWAVE STUDIO also features an **eigenmode solver**.

The last, but certainly not least, outstanding feature is the full parameterization of the structure modeller, which enables the use of variables in the definition of all geometric and material properties of your component. In combination with the built-in optimizer and parameter sweep tools, CST MICROWAVE STUDIO is capable of both the analysis and design of electromagnetic devices.

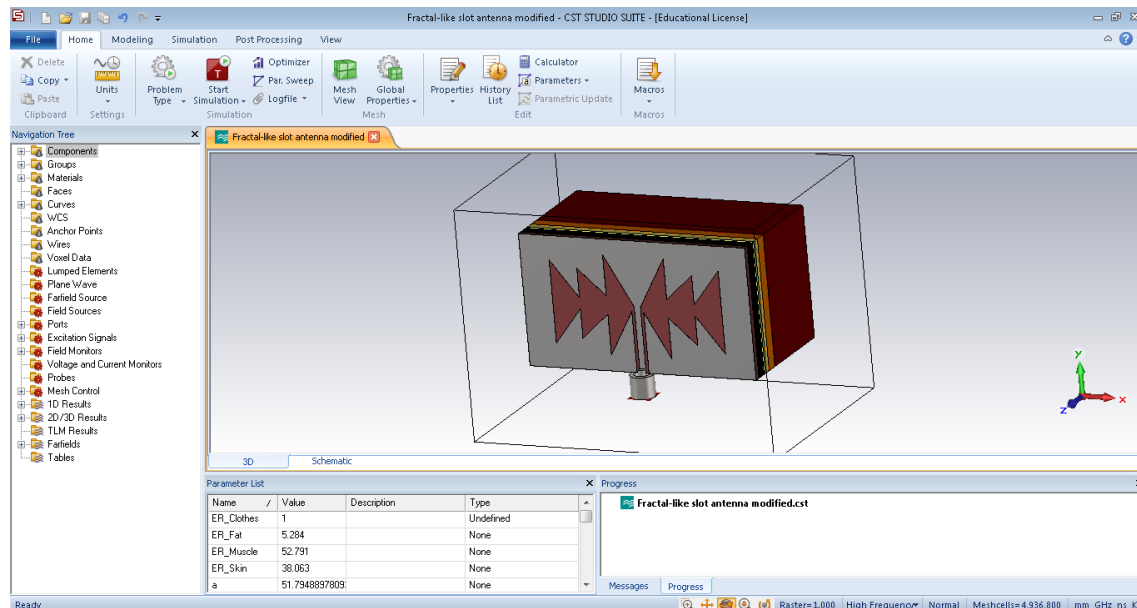


Fig. 2.13. CST Microwave Studio user interface

For the development of this thesis it has been used the CST MICROWAVE STUDIO, taking particular advantage of the wide range of possibilities that it offers to us, from the design of the antenna to the simulation of it.

It has been used the time domain solver during the development of this work, in order to compute the current distribution, radiation patterns and S11 parameters.

### 3. TRIANGULAR MONOPOLE ANTENNA

In this project we were asked to make our own design of a Triangular Monopole slot antenna from previous design reflected in the paper "Slot Antennas for On-Body Communication". This chapter explains the different phases and changes made to the original antenna before reaching our final design. First of all the objective was to lower the resonance frequency down to 2.4 GHz, to finally make some few modifications to change the substrate and keeping the antenna resonance frequency at 2.4 GHz. The main aim is to communicate our antenna with a Fractal-Like Bow-tie dipole antenna at the frequency of 2.4 GHz.

#### 3.1 OVERVIEW

Ring slot antennas have been analyzed and designed for wireless communication systems. It is found that the perimeter of the slot ring is equivalent to about one and a half guided wavelengths of the first operating frequency of the conventional coplanar waveguide fed (CPW) ring slot antennas, and about one guided wavelength for microstrip feedline at proper tuning-stub length. [26][27]

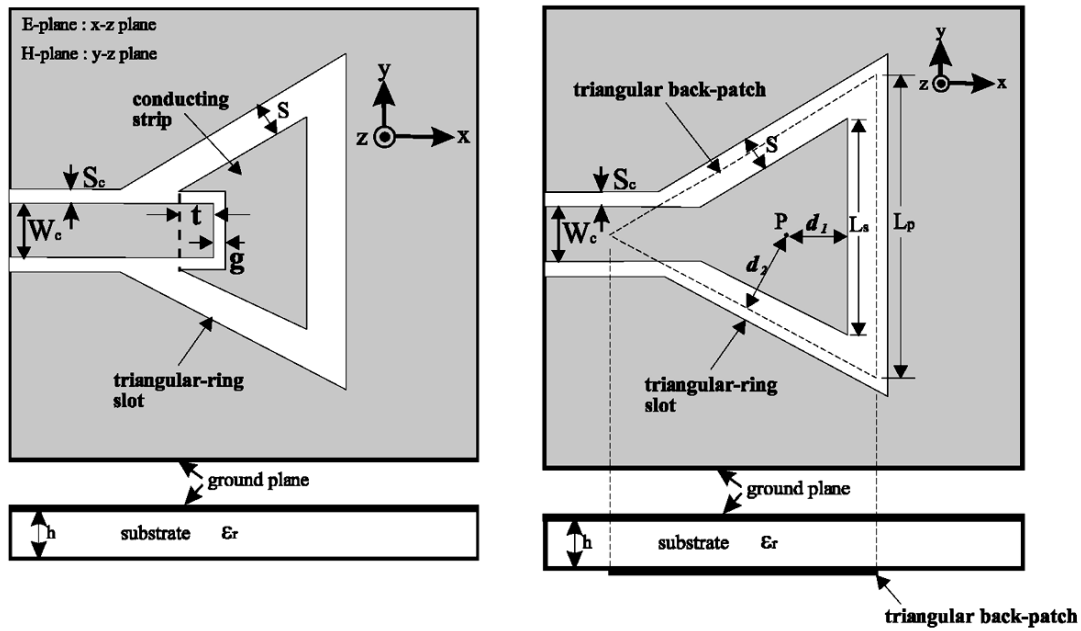


Fig. 3.1. Geometry of a CPW-fed equilateral triangular-ring slot antenna with tuning-stub (left) and with back-patch (right) [27]

Owing to the area of the triangular-ring slot antenna is smaller than rectangular or circular ring slot antenna, triangular-ring slot antenna design is more suitable for wireless communication system. Moreover, introducing a tuning-stub to a conventional CPW-fed triangular-ring slot antenna, the first operating frequency will be lowered. The tuning-stub gap and the ring slot will form a closed path for electric-field distribution and this arrangement will excite the first operating frequency at about one guided wavelength.

## 3.2 ORIGINAL ANTENNAS

### 3.2.1 Antennas from the Paper

In this point we are going to talk about the CPW-fed double triangular slot antenna on which our antenna design is based. The CPW-fed double triangular slot antenna consists of two equilateral triangles. The first triangle is directly connected to the feeding line. The second triangle is connected to the tuning stub on the top. Both triangles are spliced together by the top side. [26]

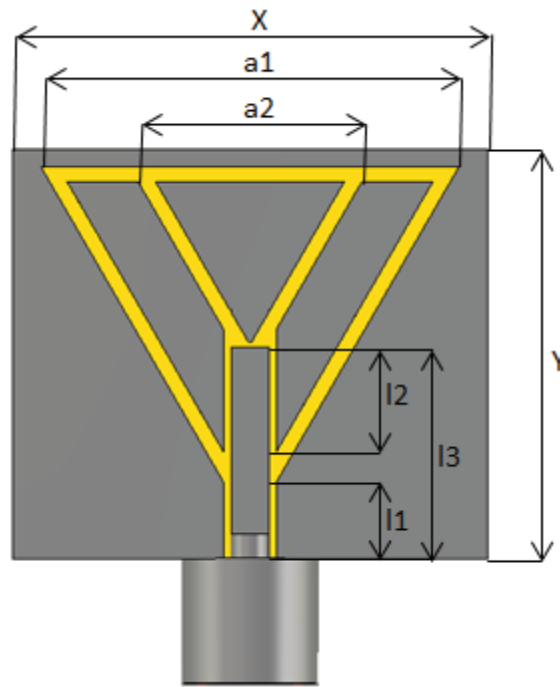


Fig. 3.2. CPW-fed double triangular slot antenna [26]

For an on-body communication, the antenna can be operated in the ISM frequency band from 5.725 GHz to 5.875 GHz (ITU-R 5.138, 5.150 and 5.280). [26]

### 3.2.2 Simulated antennas

To understand the operation of the triangular slot antenna whose design is shown in [26], we made the design and the corresponding simulation of it using CST Microwave Studio program. The first design was done following all the parameters and dimensions of the original antenna.

Therefore, respecting the dimensions of the antenna shown in Fig 3.2, the dimensions used in this design are as shown in Table 3.1. All length parameters are given in millimeters.

Parameter	Value
Substrate	Arlon
$\epsilon_r$	3.38
Metallic Thickness	0.1
Substrate Thickness	1.54
X	19
Y	16.45
a1	16.71
a2	8.94
l1	3.10
l2	4.19
l3	8.5
Width of the signal strip	1.5
Gap between signal strip and the ground plane	0.3

Table 3.1. Original antenna value of the antenna parameters

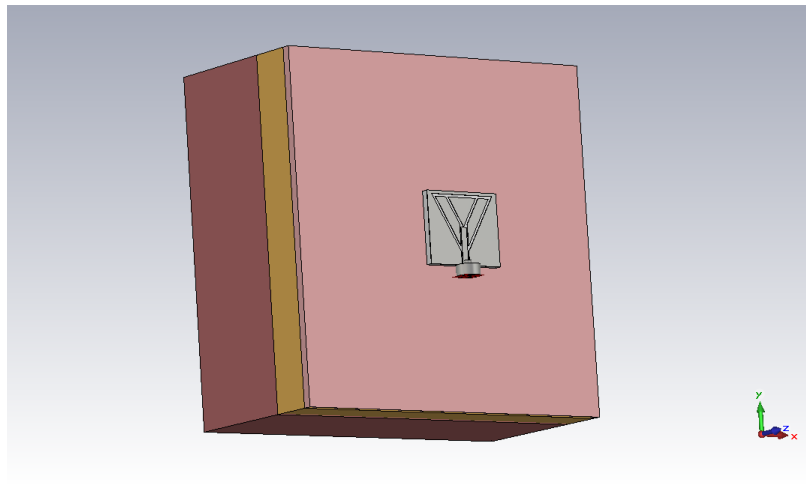


Fig. 3.3. Personal design based on the original antenna

### 3.2.2.1 Frequency Response S11

The frequency response of the reflection coefficient can help us to know in which frequencies can work our antenna. A good value of the parameter S11 for the work area is a value less than -10 dB. The resonant frequency will be at the minimum value of S11 parameter, which indicates the optimal working frequency of our antenna.

The Reflection Coefficient of our antenna was simulated by CST Microwave Studio and it is shown in Fig. 3.4:

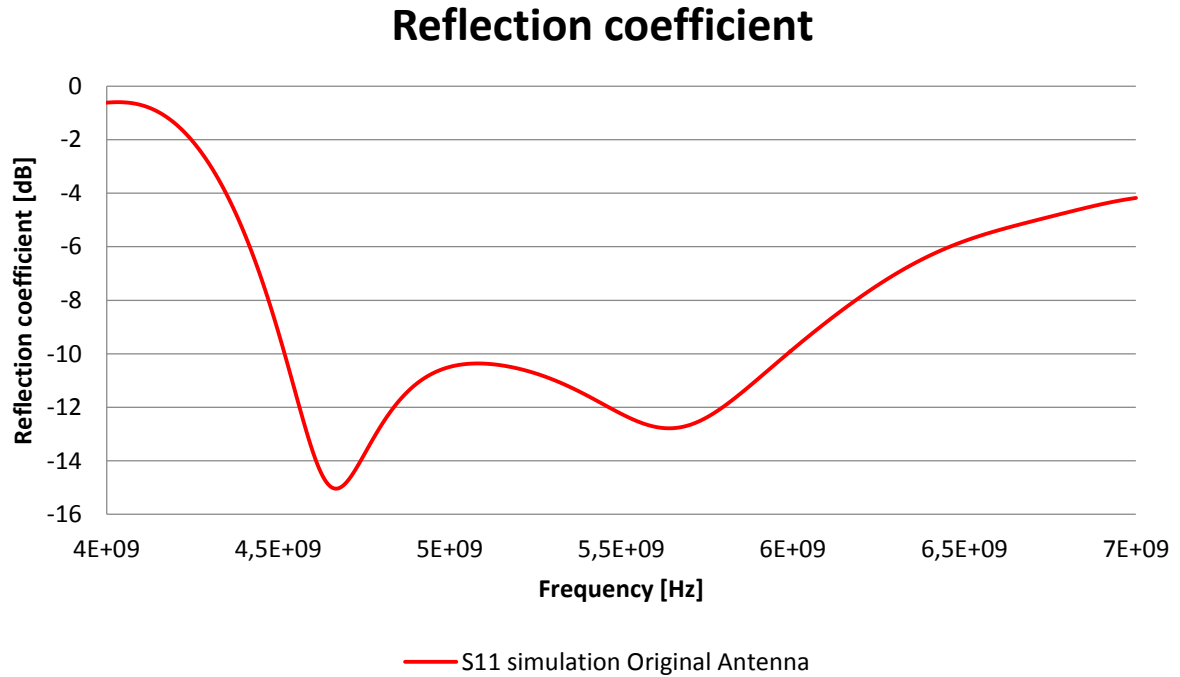


Fig. 3.4. Frequency response of the reflection coefficient of the antenna

The Table 3.2 shows the resonant frequency, which is the minimum value of the reflection coefficient:

Frequency	Reflection Coefficient	Bandwidth	Frequency Range
4.669 GHz	-15.038799 dB	31.4%	4.5183GHz-5.984207GHz
5.638 GHz	-12.783675 dB	26%	4.5183GHz-5.984207GHz

Table 3.2. Original antenna Resonant Frequency results obtained by CST

#### 3.2.2.2 H-Field

In this point we show the distribution of the magnetic field (H-field) at the surface of our antenna. The results were obtained by simulating with CST Microwave Studio. In Fig. 3.5 to 3.11 are shown the results in two different ways: vector form (Fig. 3.5) and scalar form with its different components.

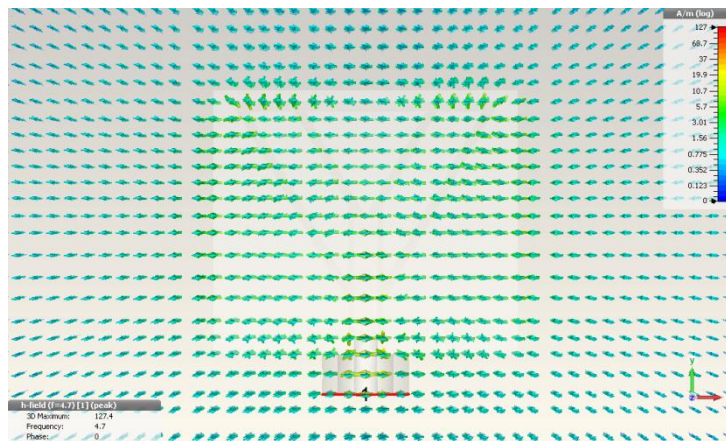


Fig. 3.5. Original antenna H-Field vector distribution

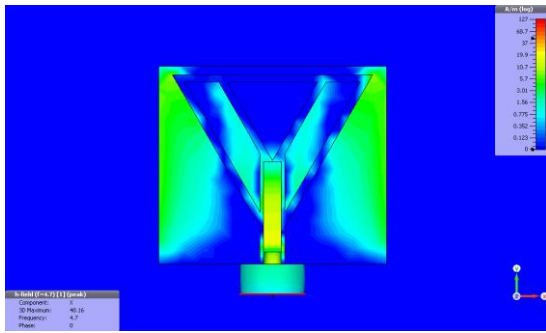


Fig. 3.6. Original antenna H-Field, X component

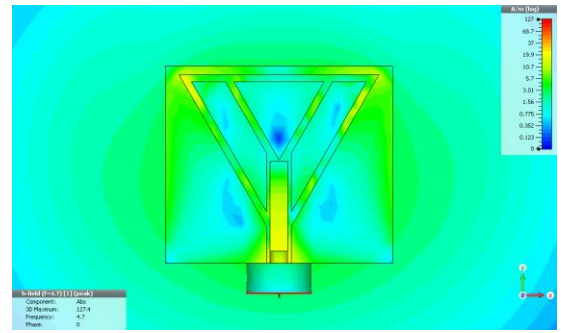


Fig. 3.9. Original antenna H-Field, Abs component

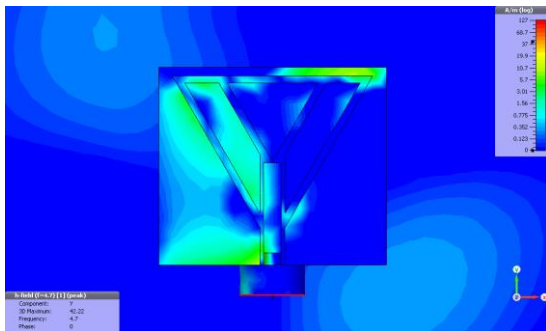


Fig. 3.7. Original antenna H-Field, Y component

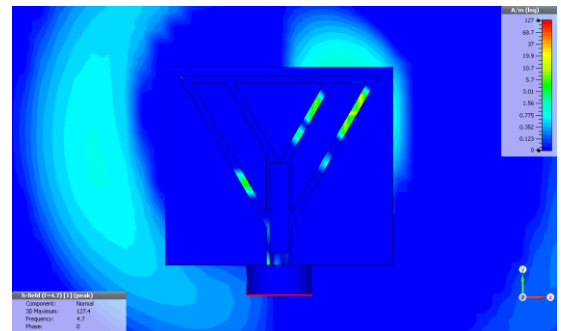


Fig. 3.10. Original antenna H-Field, Normal component

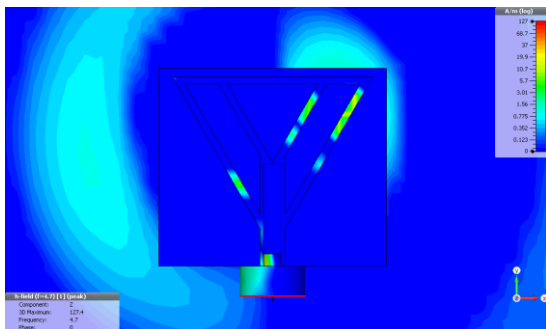


Fig. 3.8. Original antenna H-Field, Z component

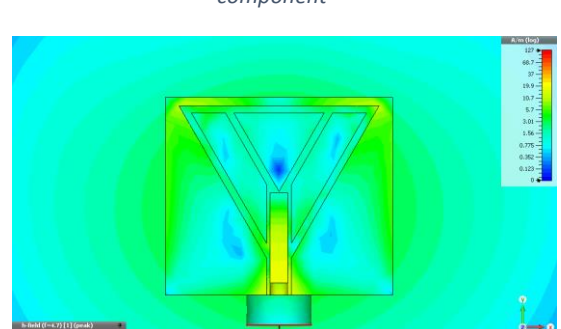


Fig. 3.11. H-Field, Original antenna Tangential component

### 3.2.2.3 E-Field

The electric field (E-field) simulation is shown in this point. The results were also obtained by simulating with CST Microwave Studio. In Fig. 3.12 to 3.18 are shown the results of the mentioned simulation such as vector form (Fig. 3.12) and scalar form with its different components.



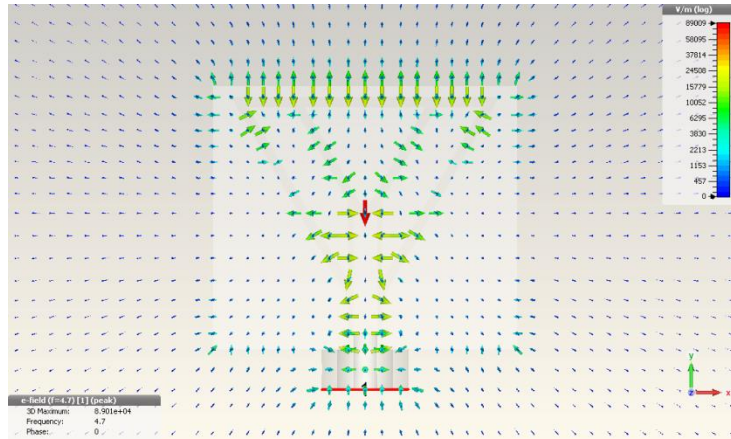


Fig. 3.12. Original antenna E-Field vector distribution

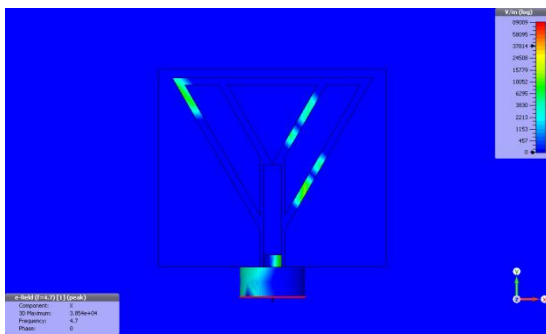


Fig. 3.13. Original antenna E-Field, X component

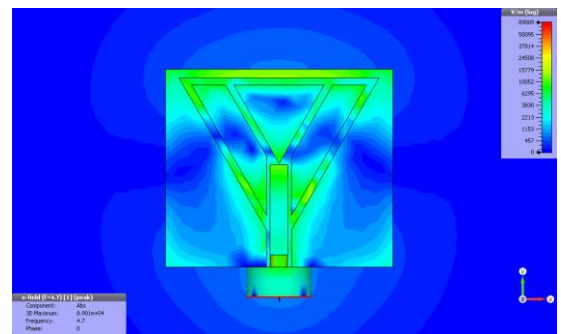


Fig. 3.16. Original antenna E-Field, Abs component

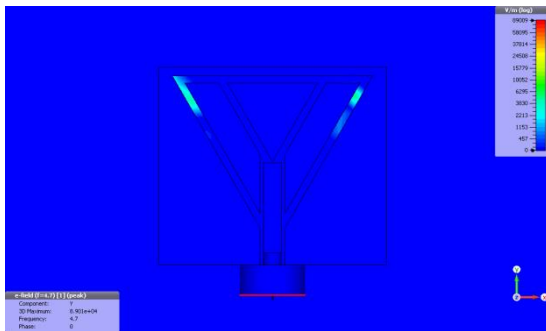


Fig. 3.14. Original antenna E-Field, Y component

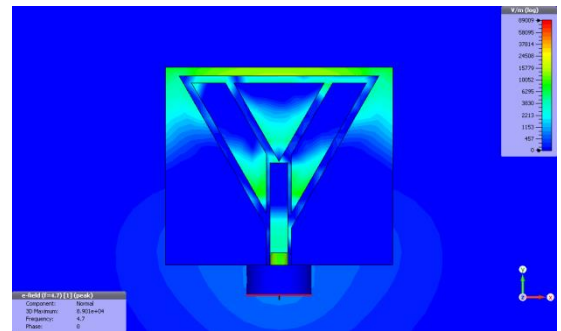


Fig. 3.17. Original antenna E-Field, Normal component

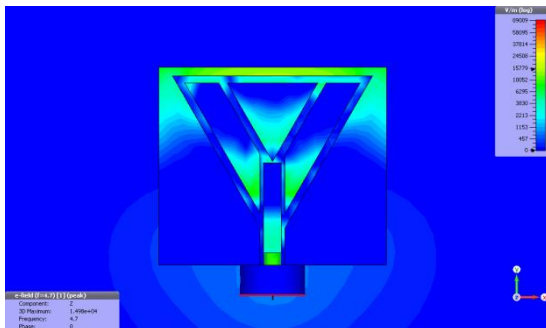


Fig. 3.15. Original antenna E-Field, Z component

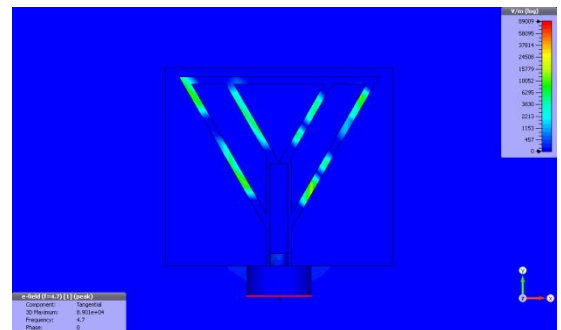


Fig. 3.18. Original antenna E-Field, tangential component

### 3.2.2.4 Current Distribution

We show in this point the surface current distribution. The results of that simulation are shown in Fig. 3.19 to 3.25 in both ways: vector form (Fig. 3.19) and scalar form with its different components. All these results were also obtained by simulating with CST Microwave Studio.

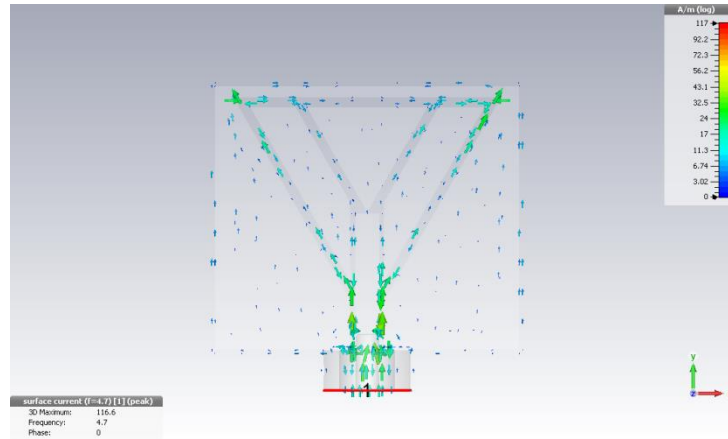


Fig. 3.19. Original antenna Current Distribution, vector distribution

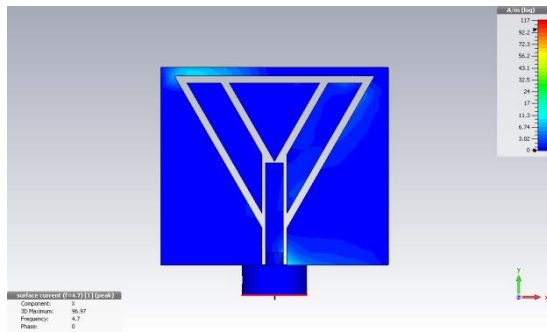


Fig. 3.20. Original antenna Current Distribution, X component

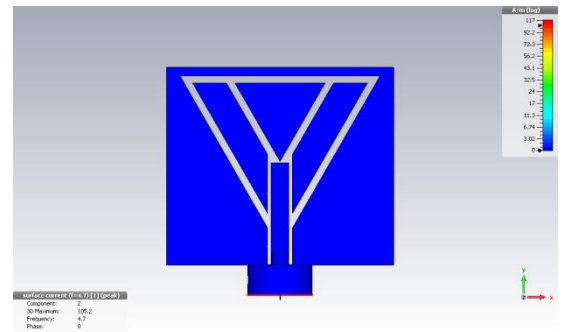


Fig. 3.22. Original antenna Current Distribution, Z component

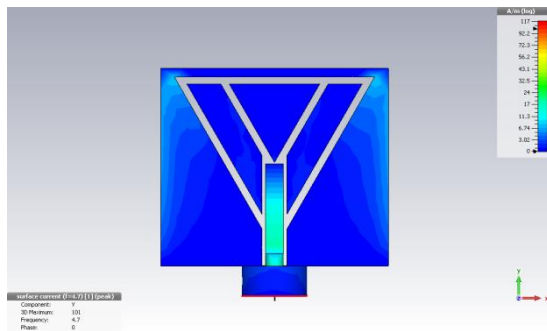


Fig. 3.21. Original antenna Current Distribution, Y component

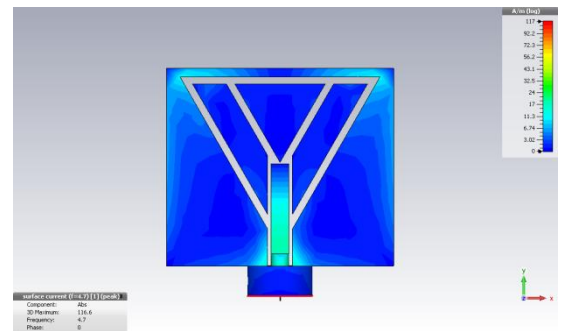


Fig. 3.23. Original antenna Current Distribution, Abs component

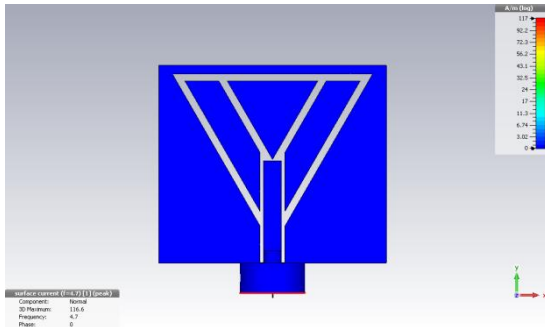


Fig. 3.24. Original antenna Current Distribution, Normal component

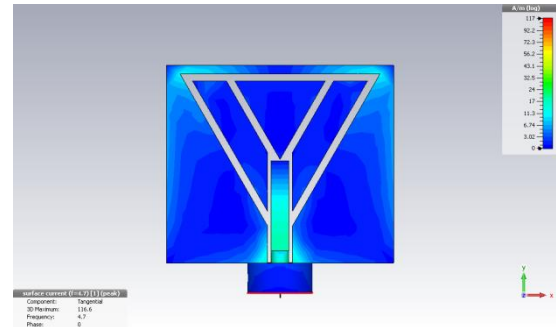


Fig. 3.25. Original antenna Current Distribution, Tangential component

### 3.2.2.5 Farfield

At this point, we will study the radiation patterns of the antenna. First of all, we show the 3D radiation patterns of the Phi component (Fig. 3.27) and the Theta component (Fig. 3.28). In Fig. 3.26 we can see the absolute radiation pattern.

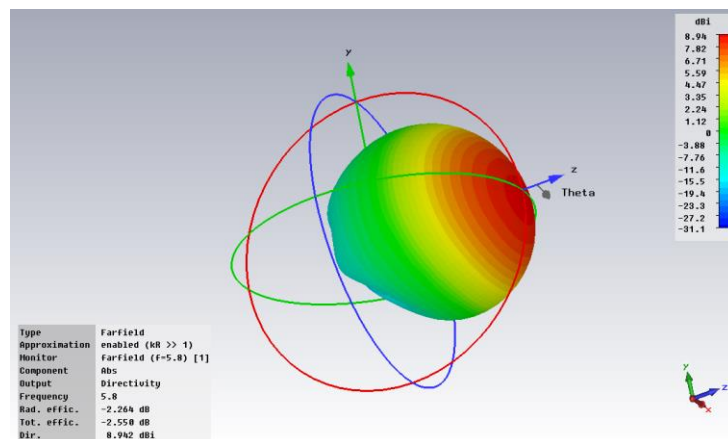
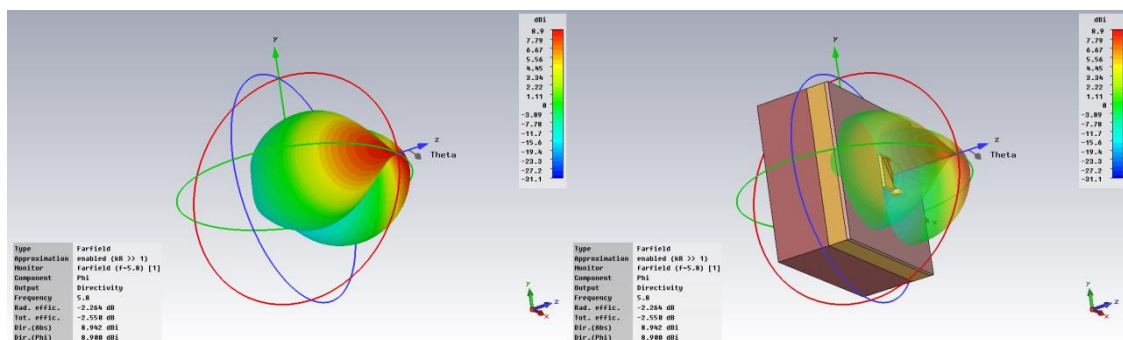


Fig. 3.26. Original antenna Abs radiation pattern



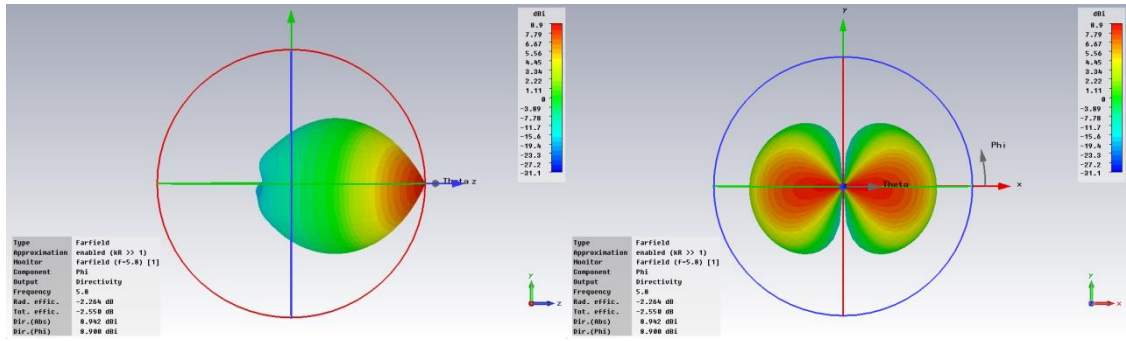


Fig. 3.27. Original antenna Phi component 3D radiation pattern

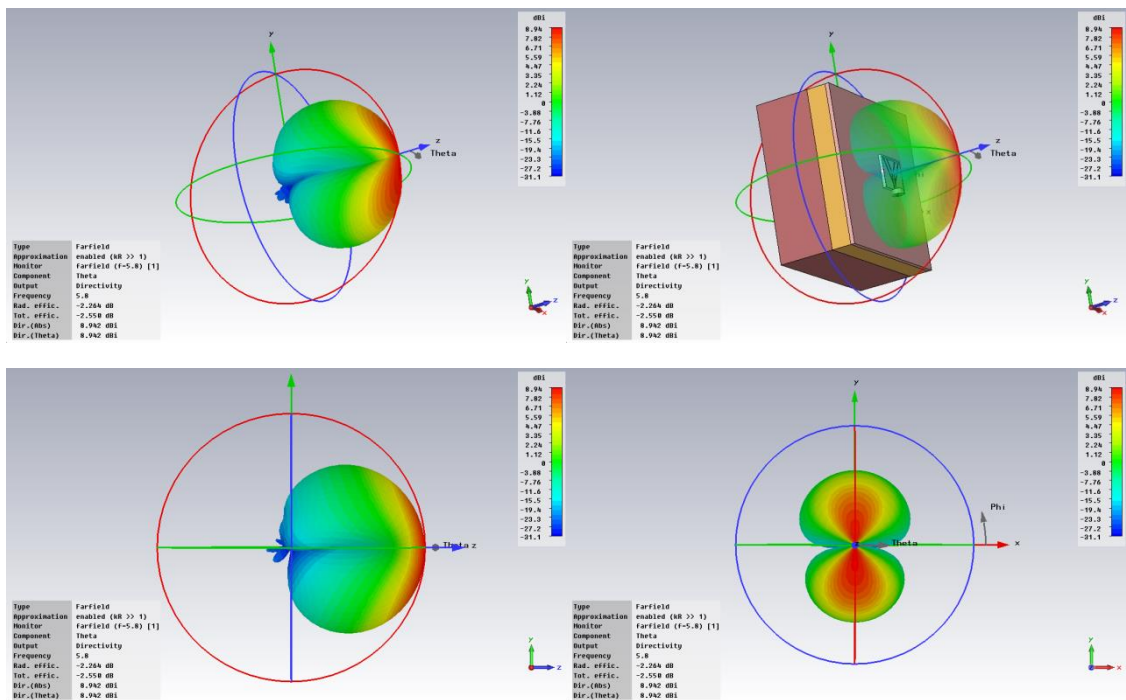


Fig. 3.28. Original antenna Theta component 3D radiation pattern

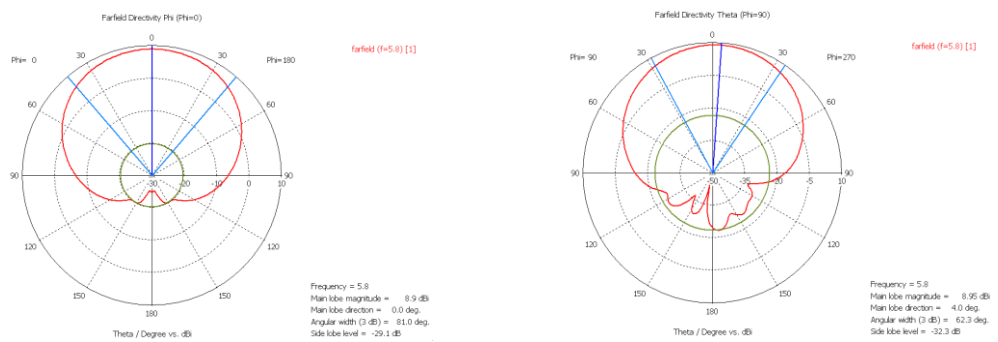


Fig. 3.29. Original antenna Directivity pattern: Phi component (Phi=0) (Left) and Theta component (Phi=90) (Right)

At the end of this point, we show the directivity pattern (Fig. 3.29). As we can see, the antenna radiates most of its output power to the front, that is, at 0 degrees. In the opposite direction, the antenna hardly radiates power due to human tissue.

### 3.2.3 Conclusions

The results are quite similar to those shown in [26], which is what we expected. The differences between the two results are due to the fact that the substrate used is not exactly the same in both designs. In our design the optimum resonance frequency is 4.669 GHz, although there was a minimum at the resonance frequency of the original antenna. Also the directivity pattern is similar to the directivity pattern of the original antenna, as expected.

## 3.3 MODIFICATIONS FROM THE ORIGINAL

In this chapter we will describe the changes made on the original antenna for lowering its resonance frequency down to 2.4 GHz. Changes will be made on the dimensions of the antenna, always keeping the same substrate as the original antenna. We made the design and the corresponding simulation of it using CST Microwave Studio.

Therefore, since the parameters of the antenna are as shown in Fig 3.2, the dimensions of this new design are shown in Table 3.3. It is important to notice the changes made in several parameters from the previous design. All length parameters are given in millimeters.

Parameter	Value
Substrate	Arlon
$\epsilon_r$	3.38
Metallic Thickness	0.1
Substrate Thickness	1.54
X	35.15
Y	31.255
a1	33.42
a2	17.88
l1	3.10
l2	4.19
l3	8.5
Width of the signal strip	1.5
Gap between signal strip and the ground plane	0.3

Table 3.3. Antenna at 2.4 GHz value of the antenna parameters

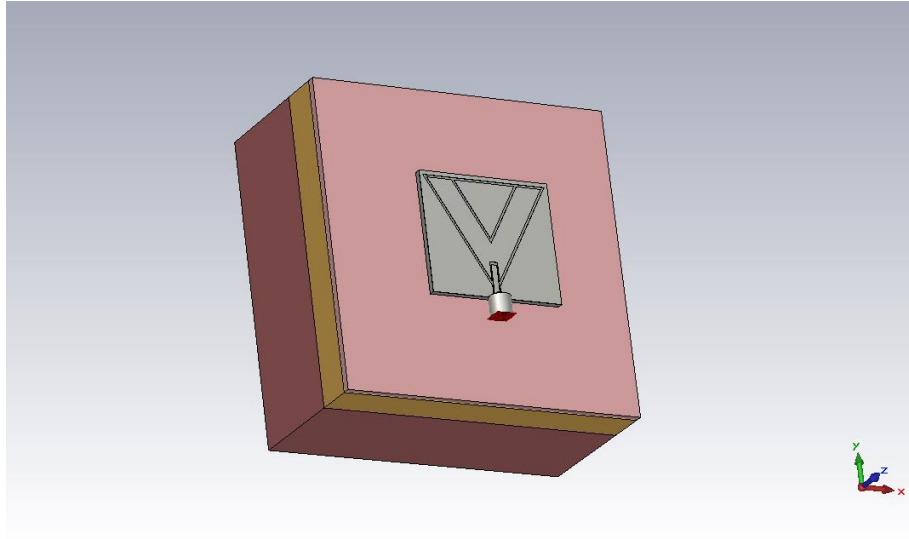


Fig. 3.30. New designed antenna whose resonant frequency is at 2.4 GHz

### 3.3.1 Frequency Response S11

The Reflection Coefficient of our antenna was simulated by CST Microwave Studio and it is shown in Fig. 3.31:

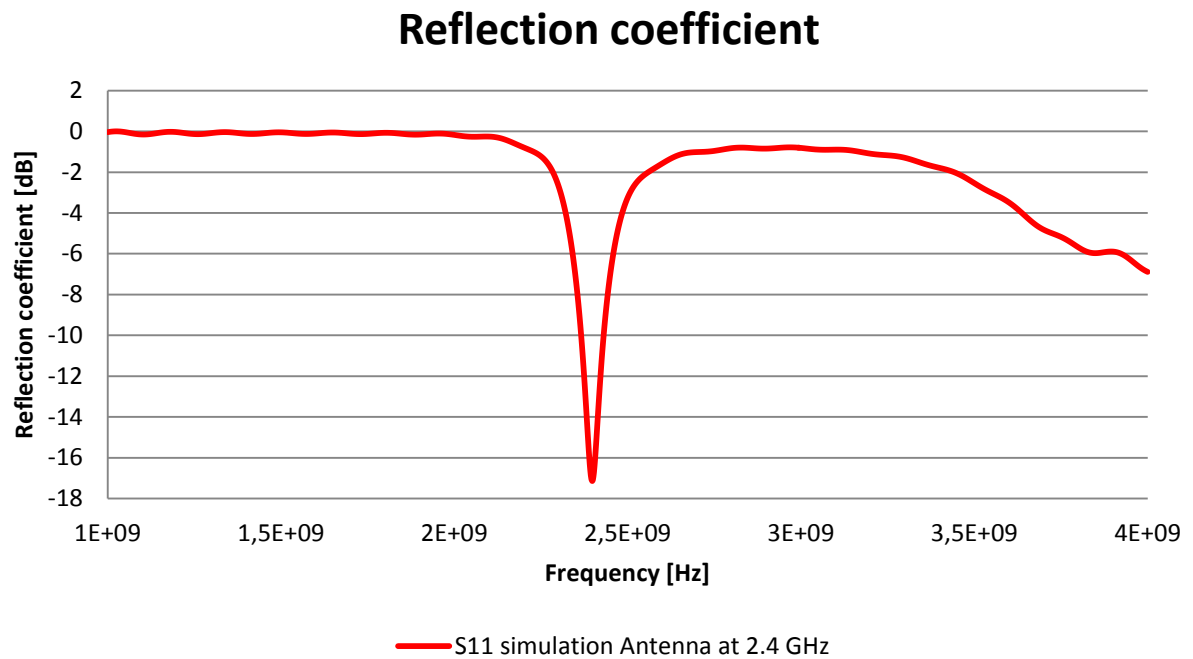


Fig. 3.31. Antenna at 2.4 GHz Frequency response of the reflection coefficient of the antenna

The Table 3.4 shows the resonant frequency, which is the minimum value of the reflection coefficient:

Frequency	Reflection Coefficient	Bandwidth	Frequency Range
2.398 GHz	-17.141249 dB	2.73%	2.3656GHz-2.4310GHz

Table 3.4. Antenna at 2.4 GHz Resonant Frequency results obtained by CST



### 3.3.2 H-Field

In this point we show the distribution of the magnetic field (H-field) at the surface of our antenna. The results were obtained by simulating with CST Microwave Studio. In Fig. 3.32 to 3.38 are shown the results in two different ways: vector form (Fig. 3.32) and scalar form with its different components.

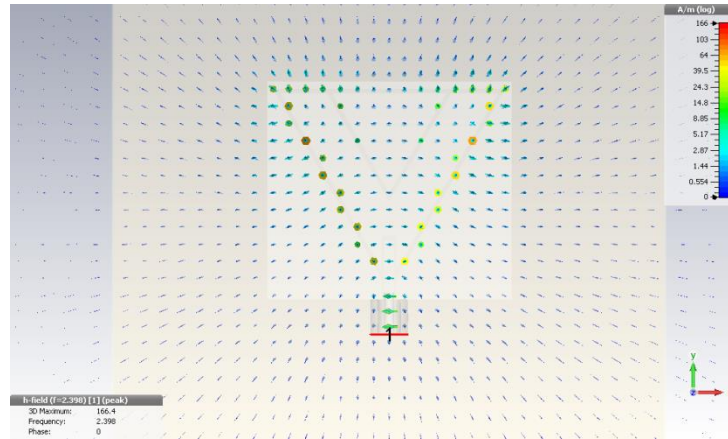


Fig. 3.32. Antenna at 2.4 GHz H-Field vector distribution

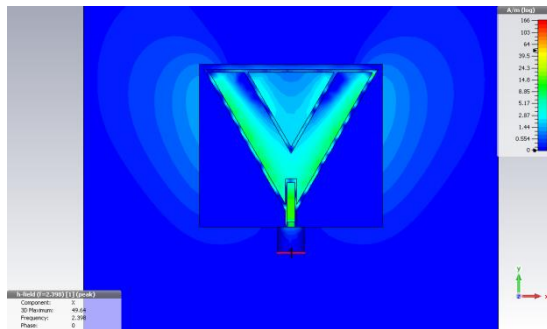


Fig. 3.33. Antenna at 2.4 GHz H-Field, X component

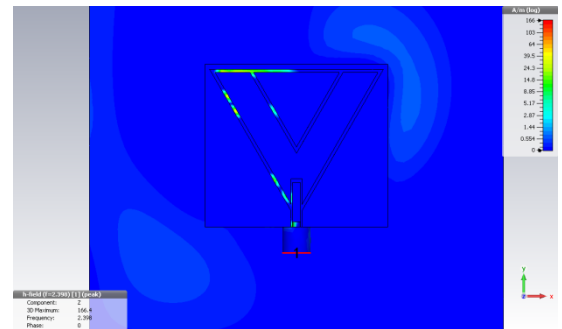


Fig. 3.35. Antenna at 2.4 GHz H-Field, Z component

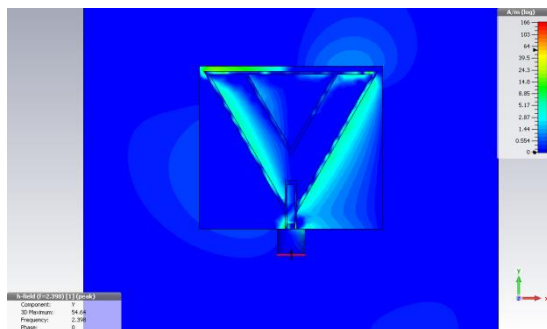


Fig. 3.34. Antenna at 2.4 GHz H-Field, Y component

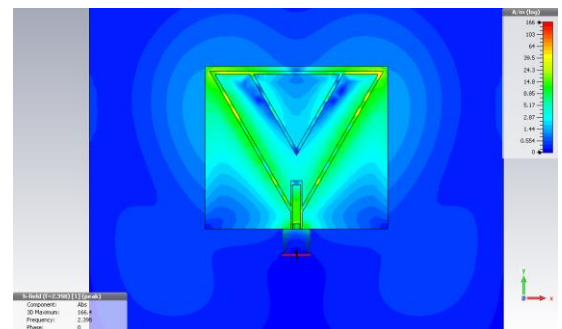


Fig. 3.36. Antenna at 2.4 GHz H-Field, Abs component

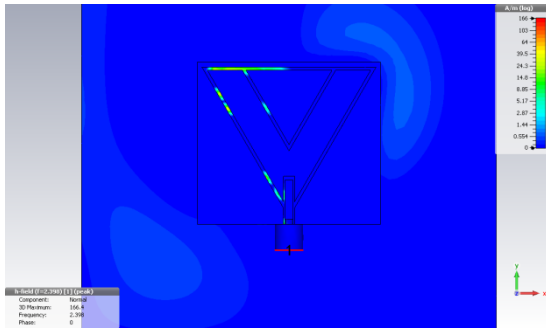


Fig. 3.37. Antenna at 2.4 GHz H-Field, Normal component

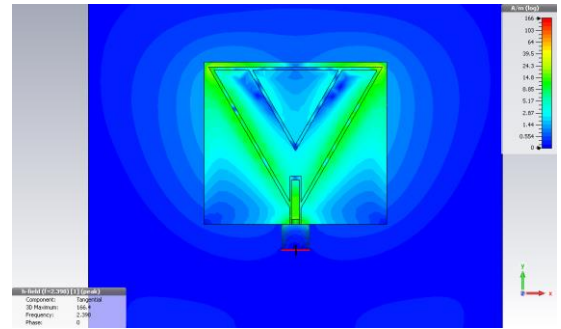


Fig. 3.38. Antenna at 2.4 GHz H-Field, Tangential component

### 3.3.3 E-Field

The electric field (E-field) simulation is shown in this point. The results were also obtained by simulating with CST Microwave Studio. In Fig. 3.39 to 3.45 are shown the results of the mentioned simulation such as vector form (Fig. 3.39) and scalar form with its different components.

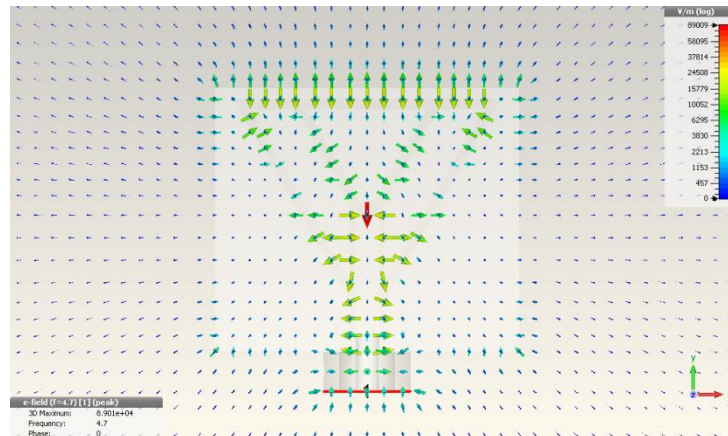


Fig. 3.39. Antenna at 2.4 GHz E-Field vector distribution

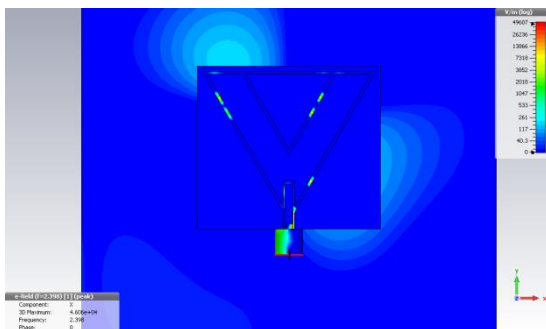


Fig. 3.40. Antenna at 2.4 GHz E-Field, X component

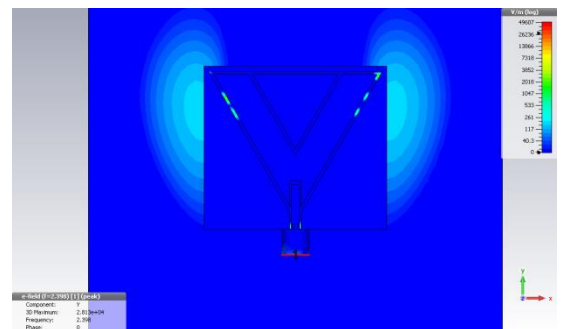


Fig. 3.41. Antenna at 2.4 GHz E-Field, Y component



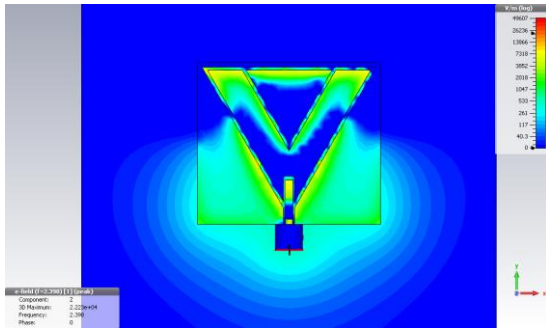


Fig. 3.42. Antenna at 2.4 GHz E-Field, Z component

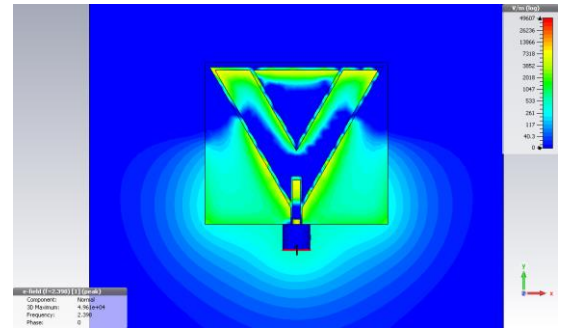


Fig. 3.44. Antenna at 2.4 GHz E-Field, Normal component

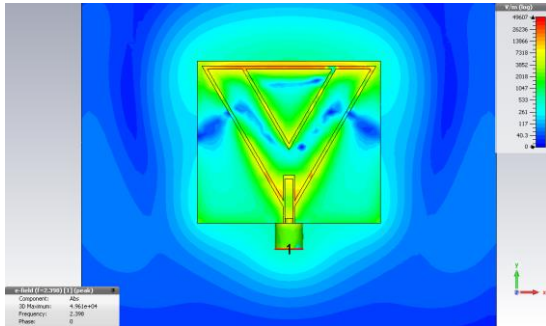


Fig. 3.43. Antenna at 2.4 GHz E-Field, Abs component

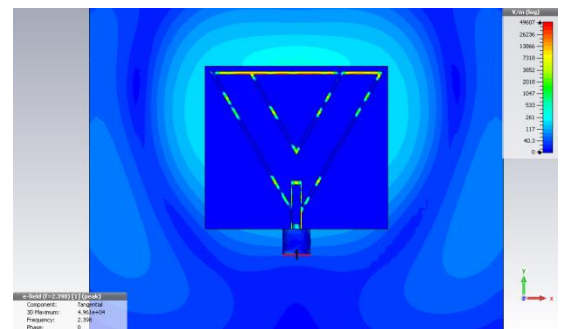


Fig. 3.45. Antenna at 2.4 GHz E-Field, Tangential component

### 3.3.4 Current Distribution

We show in this point the surface current distribution. The results of that simulation are shown in Fig. 3.46 to 3.52 in both ways: vector form (Fig. 3.46) and scalar form with its different components. All these results were also obtained by simulating with CST Microwave Studio.

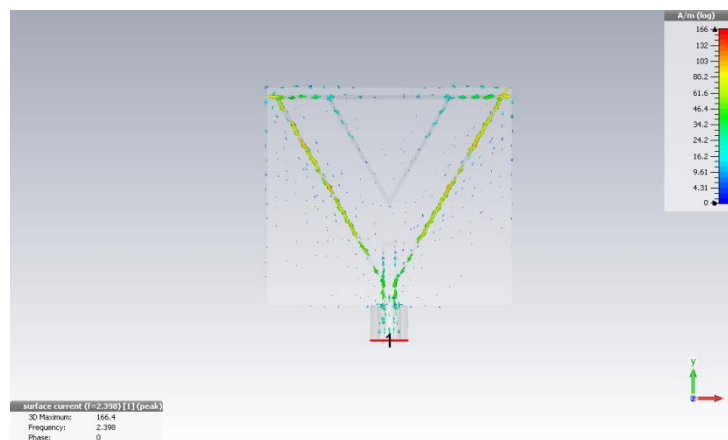


Fig. 3.46. Antenna at 2.4 GHz Current Distribution, vector distribution

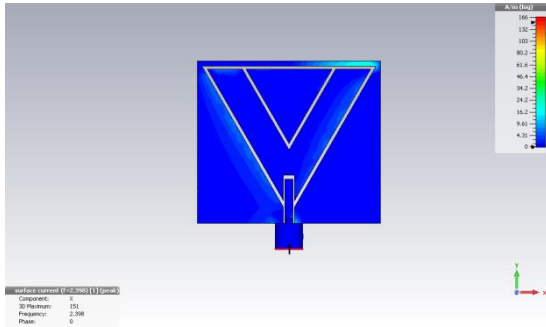


Fig. 3.47. Antenna at 2.4 GHz Current Distribution, X component

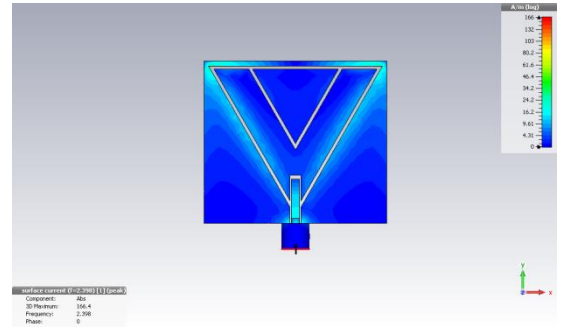


Fig. 3.50. Antenna at 2.4 GHz Current Distribution, Abs component

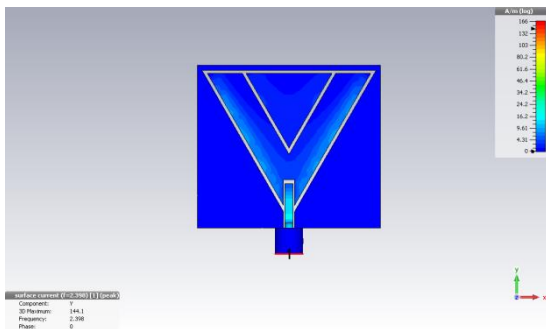


Fig. 3.48. Antenna at 2.4 GHz Current Distribution, Y component

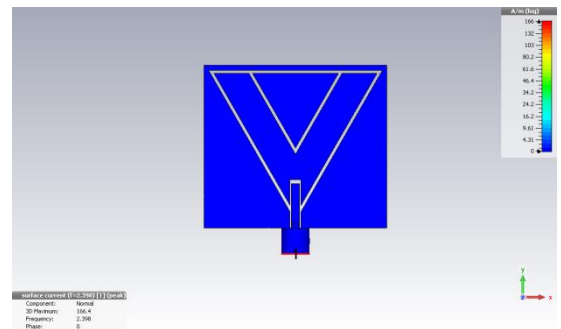


Fig. 3.51. Antenna at 2.4 GHz Current Distribution, Normal component

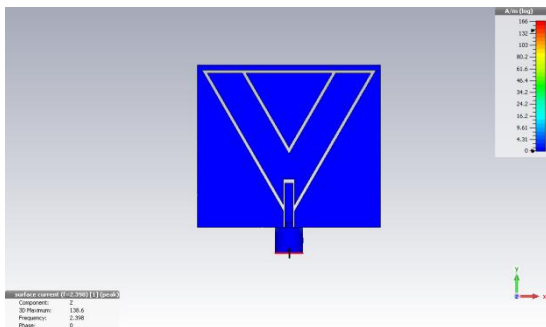


Fig. 3.49. Antenna at 2.4 GHz Current Distribution, Z component

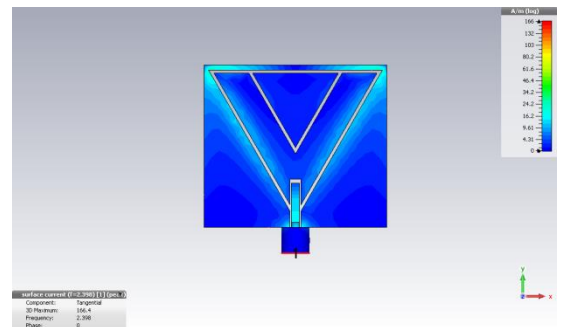


Fig. 3.52. Antenna at 2.4 GHz Current Distribution, Tangential component

### 3.3.5 Farfield

At this point, we will study the radiation patterns of the antenna. First of all, we show the 3D radiation patterns of the Phi component (Fig. 3.54) and the Theta component (Fig. 3.55). In Fig. 3.53 we can see the absolute radiation pattern.

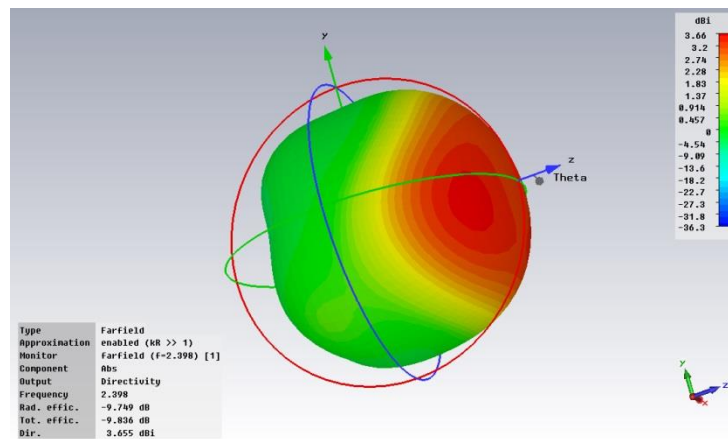


Fig. 3.53. Antenna at 2.4 GHz Abs radiation pattern

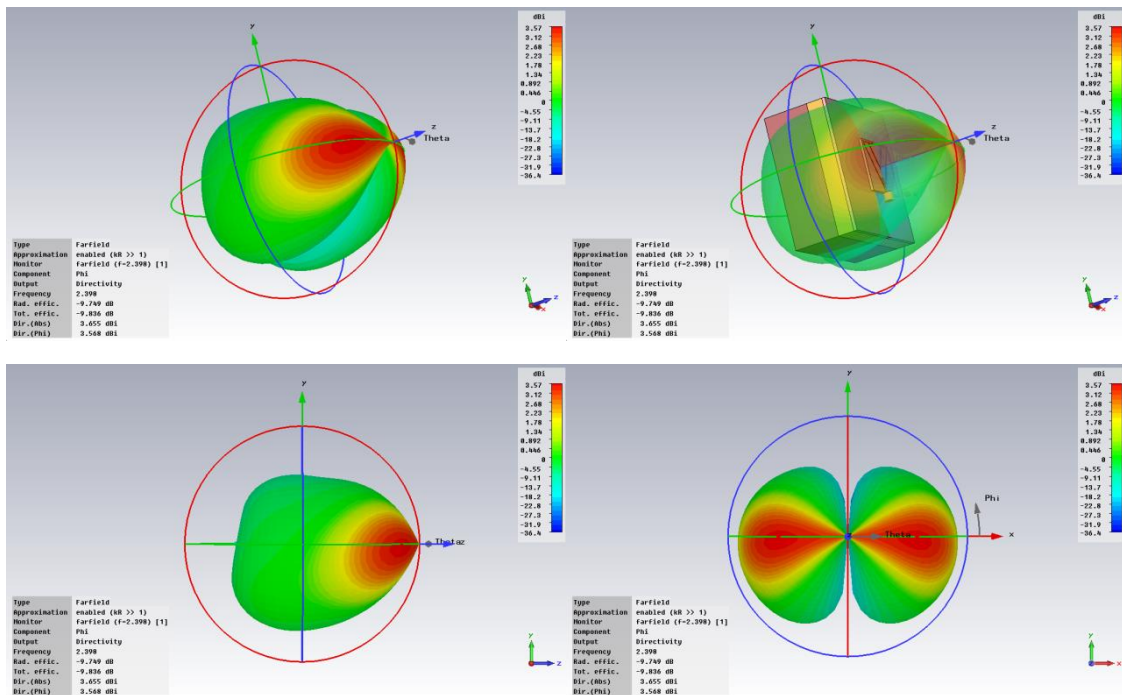
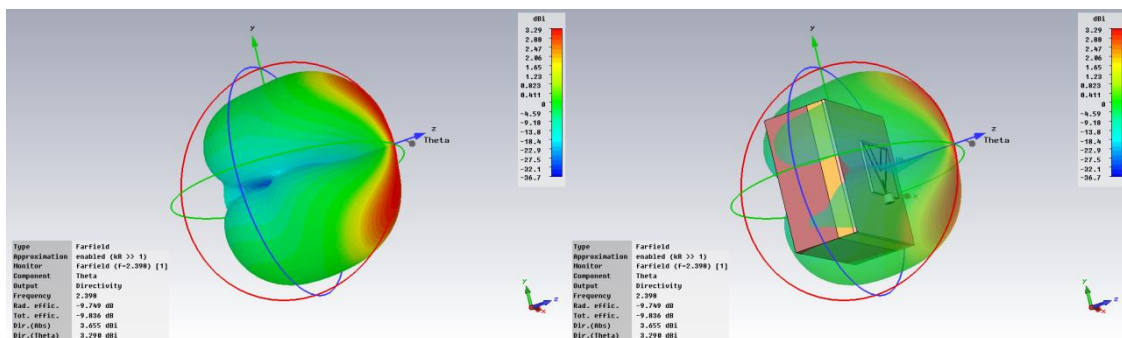


Fig. 3.54. Antenna at 2.4 GHz Phi component 3D radiation pattern



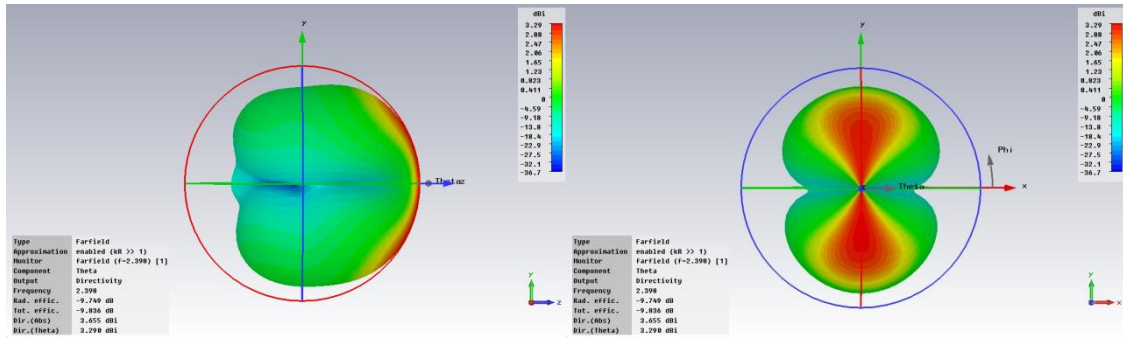


Fig. 3.55. Antenna at 2.4 GHz Theta component 3D radiation pattern

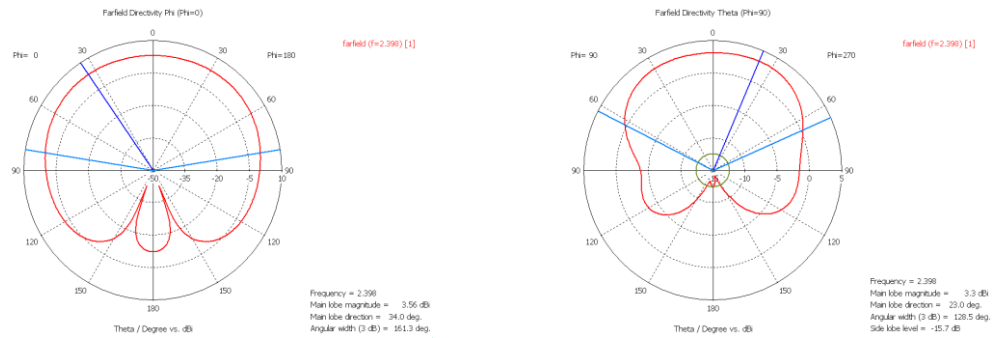


Fig. 3.56. Antenna at 2.4 GHz Directivity pattern: Phi component (Phi=0) (Left) and Theta component (Phi=90) (Right)

At the end of this point, we show the directivity pattern (Fig. 3.56). As we can see, the antenna radiates most of its output power to the front.

### 3.3.6 Conclusions

Looking at the results we can see that because of the changes made to the design we have set the resonant frequency at 2.4 GHz, which was the main objective. Also we obtained an improvement on the reflection coefficient. On the other hand, we have suffered a loss of bandwidth because of these changes. Also the gain has been affected by these changes because in this new design the antenna has a lower gain than the original one.

## 3.4 NEW SUBSTRATE

To finish our design, we were asked to change the antenna substrate to CuClad 217LX, since this substrate is more flexible than its predecessor and thus could better adapt to the curves of the human body. The change of substrate should not affect the resonant frequency of the antenna, that is, the resonance frequency should be maintained at 2.4 GHz. So if we change the substrate and we want to keep the resonance frequency, we must also make slight changes at design dimensions.

### 3.4.1 Substrate CuClad 217LX

CuClad laminates are woven fiberglass/PTFE composite materials for use as printed circuit board substrates. Using precision control of the fiberglass/PTFE ratio, CuClad laminates offer a range of choices from the lowest dielectric constant and loss tangent to a more highly reinforced laminate with better dimensional stability. [28]

CuClad217 uses a low fiberglass/PTFE ratio to provide the lowest dielectric constant and dissipation factor available in fiberglass reinforced PTFE based laminates. Together, these properties offer faster signal propagation and higher signal/noise ratios. [28]

### 3.4.2 Simulations

We made the new design based on CuClad 217LX, whose  $\epsilon_r$  is equal to 2.17, using CST Microwave Studio program, and later we simulated it using the same program. At this point, we show the final design and all the simulations done.

Therefore, since the parameters of the antenna are as shown in Fig 3.57, the dimensions of this new design are shown in Table 3.5. It is important to notice the changes made in several parameters from the previous design. All length parameters are given in millimeters.

Parameter	Value
Substrate	CuClad 217LX
$\epsilon_r$	2.17
Metallic Thickness	0.1
Substrate Thickness	1.54
X	59.85
Y	50.995
a1	53.472
a2	45.594
l1	3.10
l2	4.19
l3	8.5
Width of the signal strip	1.5
Gap between signal strip and the ground plane	0.3

Table 3.5. Final design value of the antenna parameters

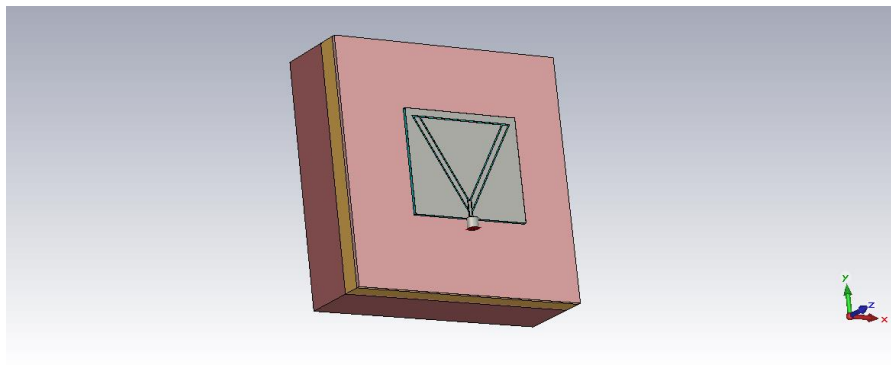
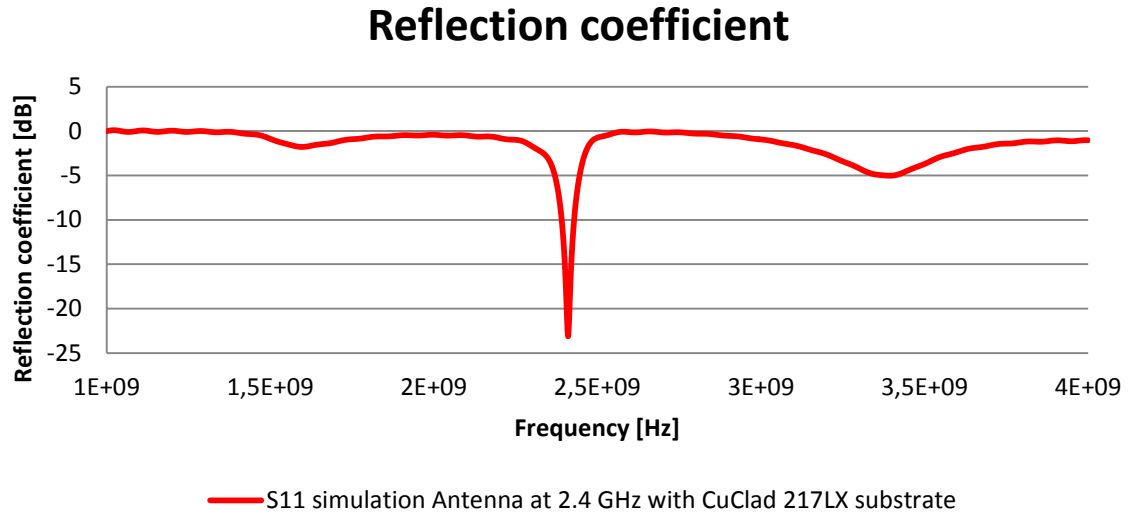


Fig. 3.57. Final antenna design, with CuClad 217LX substrate

### 3.4.2.1 Frequency Response S11

The Reflection Coefficient of our antenna was simulated by CST Microwave Studio and it is shown in Fig. 3.58:



*Fig. 3.58. Final design Frequency response of the reflection coefficient of the antenna*

The Table 3.6 shows the resonant frequency, which is the minimum value of the reflection coefficient:

Frequency	Reflection Coefficient	Bandwidth	Frequency Range
2.41 GHz	-23.121411 dB	1.61%	2.39 GHz-2.4288 GHz

*Table 3.6. Final design Resonant Frequency results obtained by CST*

### 3.4.2.2 H-Field

In this point we show the distribution of the magnetic field (H-field) at the surface of our antenna. The results were obtained by simulating with CST Microwave Studio. In Fig. 3.59 to 3.65 are shown the results in two different ways: vector form (Fig. 3.59) and scalar form with its different components.



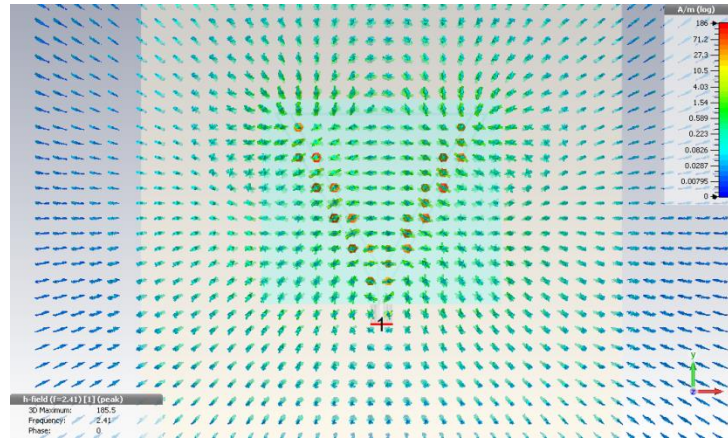


Fig. 3.59. Final design H-Field vector distribution

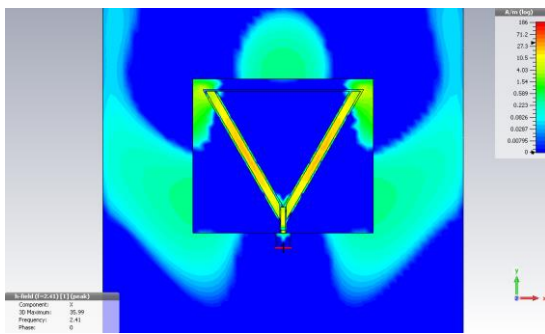


Fig. 3.60. Final design H-Field, X component

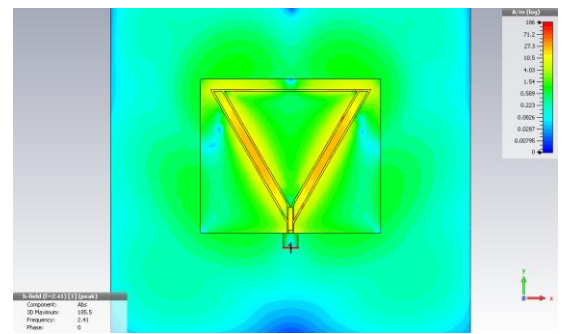


Fig. 3.63. Final design H-Field, Abs component

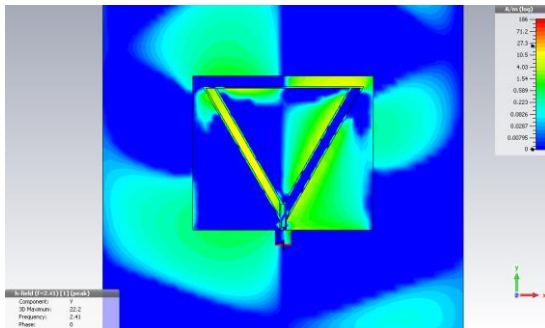


Fig. 3.61. Final design H-Field, Y component

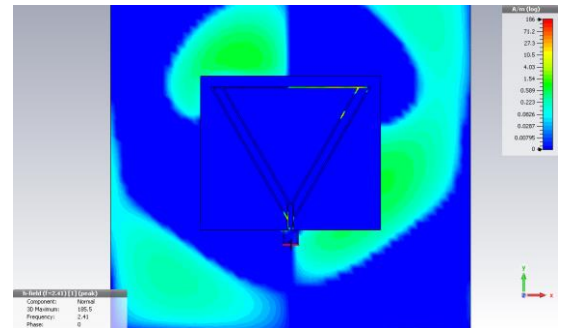


Fig. 3.64. Final design H-Field, Normal component

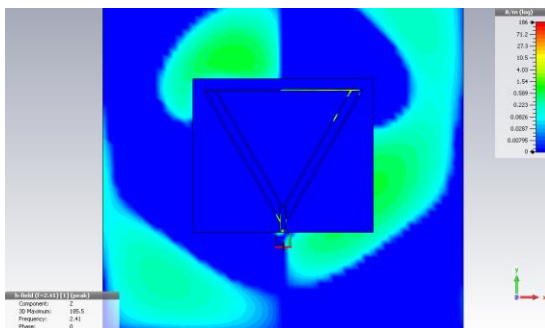


Fig. 3.62. Final design H-Field, Z component

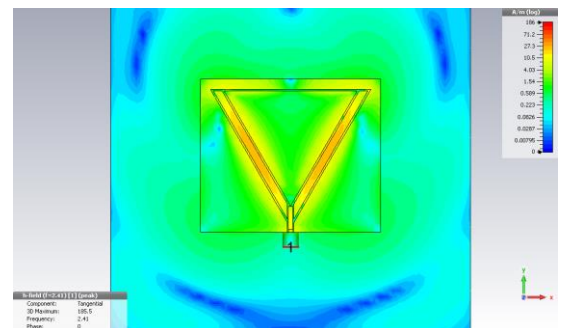


Fig. 3.65. Final design H-Field, Tangential component

### 3.4.2.3 E-Field

The electric field (E-field) simulation is shown in this point. The results were also obtained by simulating with CST Microwave Studio. In Fig. 3.66 to 3.72 are shown the results of the mentioned simulation such as vector form (Fig. 3.66) and scalar form with its different components.

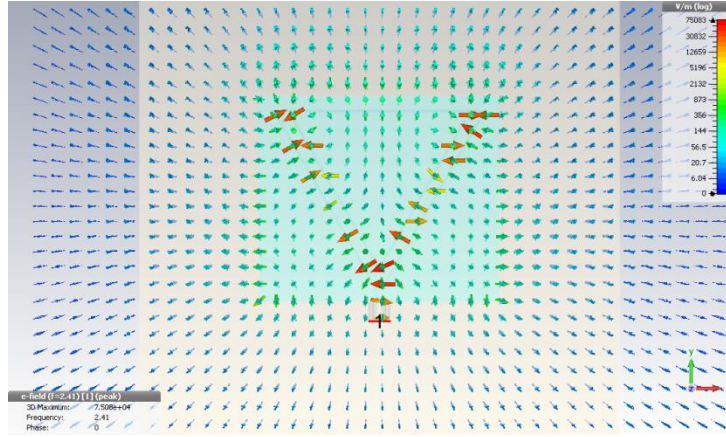


Fig. 3.66. Final design E-Field vector distribution

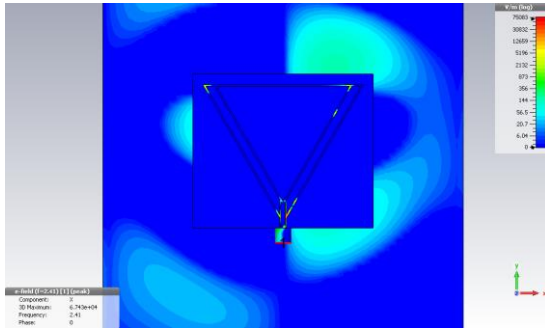


Fig. 3.67. Final design E-Field, X component

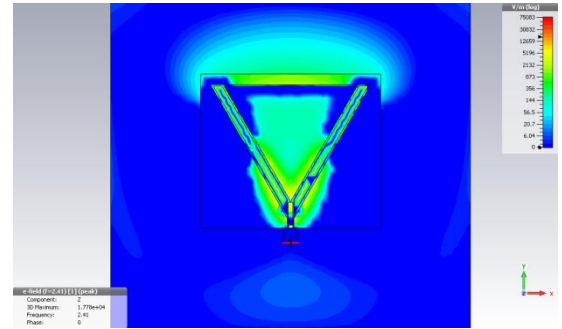


Fig. 3.69. Final design E-Field, Z component

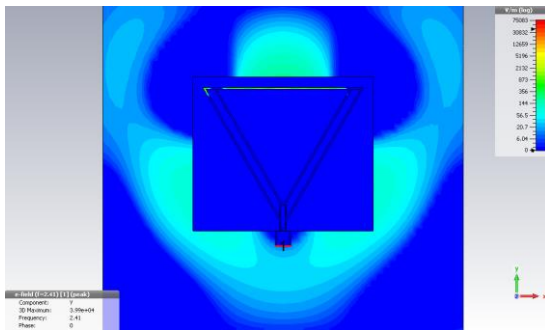


Fig. 3.68. Final design E-Field, Y component

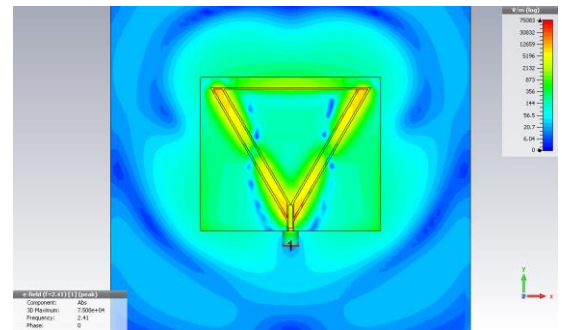


Fig. 3.70. Final design E-Field, Abs component



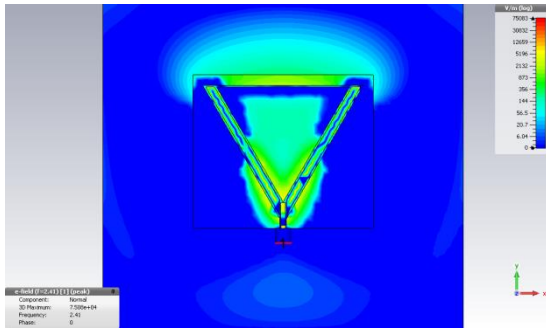


Fig. 3.71. Final design E-Field, Normal component

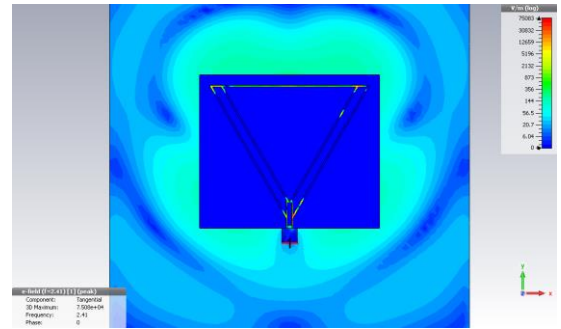


Fig. 3.72. Final design E-Field, tangential component

### 3.4.2.4 Current Distribution

We show in this point the surface current distribution. The results of that simulation are shown in Fig. 3.73 to 3.79 in both ways: vector form (Fig. 3.73) and scalar form with its different components. All these results were also obtained by simulating with CST Microwave Studio.

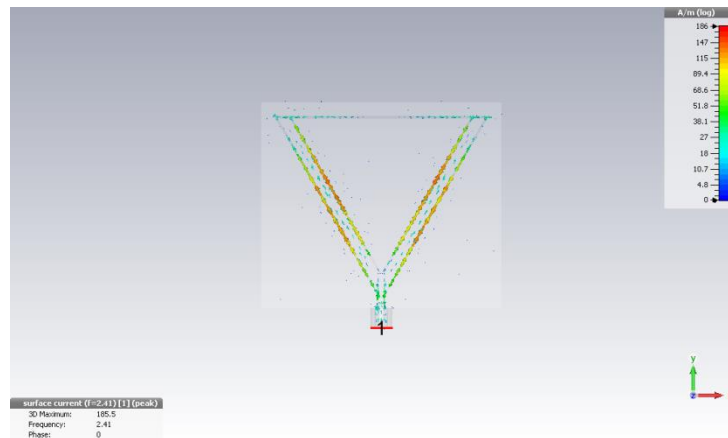


Fig. 3.73. Final design Current Distribution, vector distribution

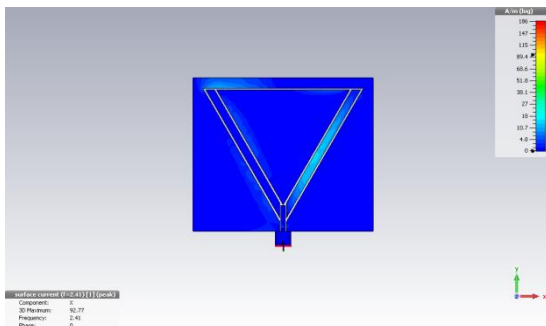


Fig. 3.74. Final design Current Distribution, X component

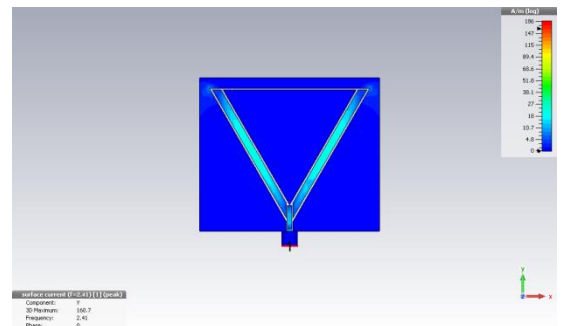


Fig. 3.75. Final design Current Distribution, Y component

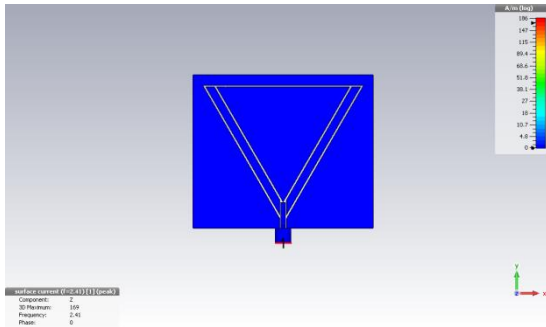


Fig. 3.76. Final design Current Distribution, Z component

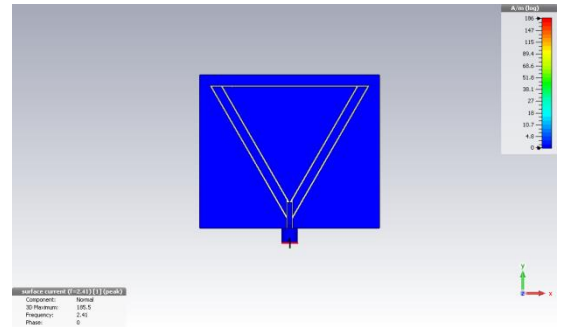


Fig. 3.78. Final design Current Distribution, Normal component

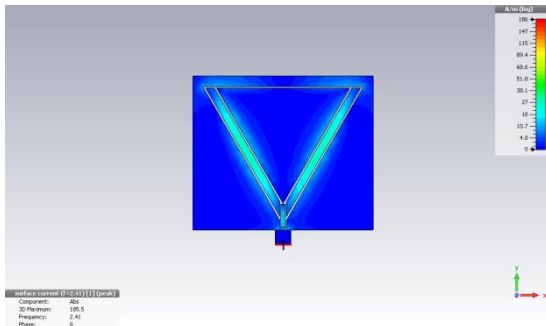


Fig. 3.77. Final design Current Distribution, Abs component

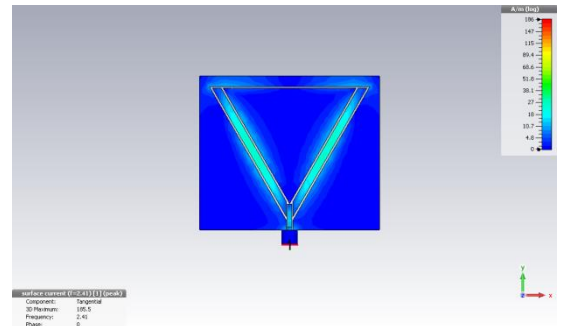


Fig. 3.79. Final design Current Distribution, Tangential component

### 3.4.2.5 Farfield

At this point, we will study the radiation patterns of the antenna. First of all, we show the 3D radiation patterns of the Phi component (Fig. 3.81) and the Theta component (Fig. 3.82). In Fig. 3.80 we can see the absolute radiation pattern.

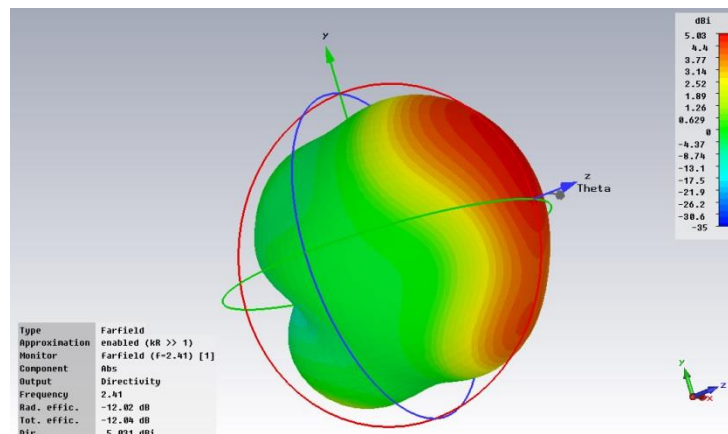


Fig. 3.80. Final design Abs radiation pattern

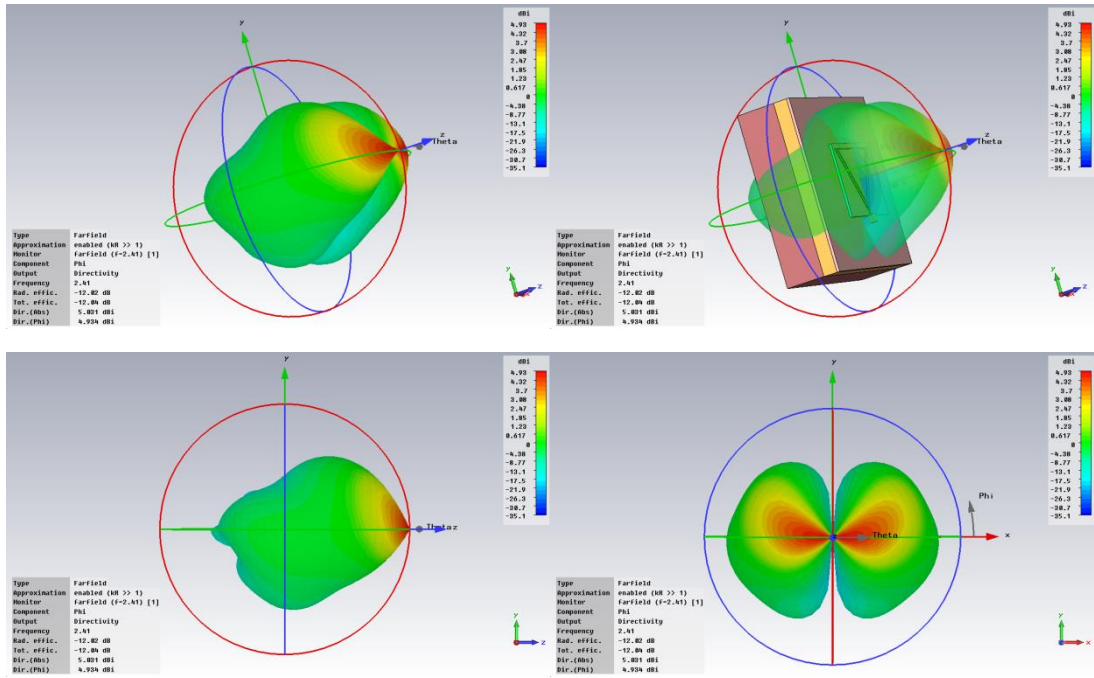


Fig. 3.81. Final design Phi component 3D radiation pattern

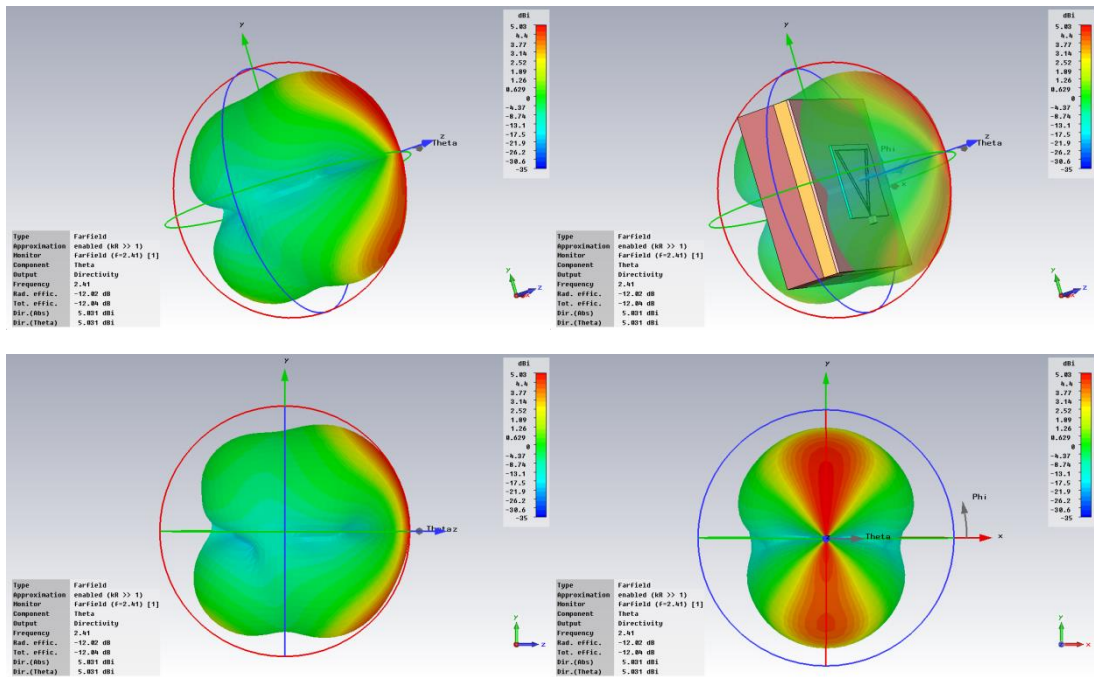


Fig. 3.82. Final design Theta component 3D radiation pattern

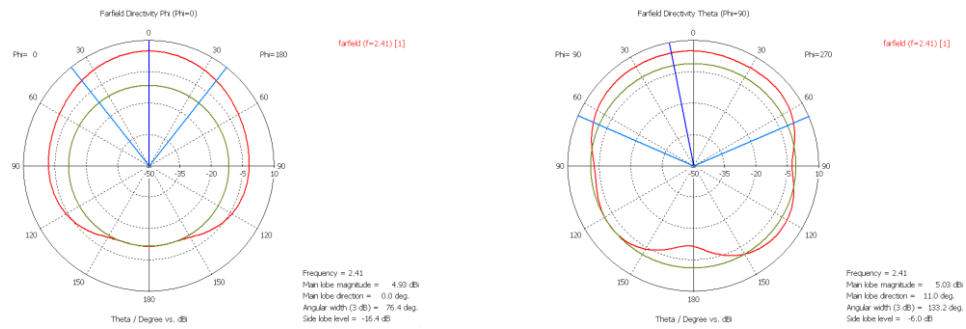


Fig. 3.83. Final design Directivity pattern: Phi component (Phi=0) (Left) and Theta component (Phi=90) (Right)

At the end of this point, we show the directivity pattern (Fig. 3.83). As we can see, the antenna radiates most of its output power to the front, although in this case the antenna radiates somewhat backward power due to the properties of the new substrate.

### 3.4.3 Conclusions

After the changes made, looking at the results we notice that we have managed to maintain the resonance frequency of 2.4 GHz in addition to obtain an improvement in the reflection coefficient. But on the other hand, we slightly reduced the bandwidth again making it even narrower.

In Figure 3.84 we can see a comparison between the S11 parameter of the antenna designed at 2.4 GHz with Arlon substrate and the antenna at the same frequency with the substrate CuClad 217LX. The differences that we observe between the two antennas are not only due to the change of substrate, as also various changes were made to the dimensions of the antenna to reattach the resonant frequency at 2.4 GHz. In comparison we see that the new design get a better coefficient of reflection but instead lose bandwidth.

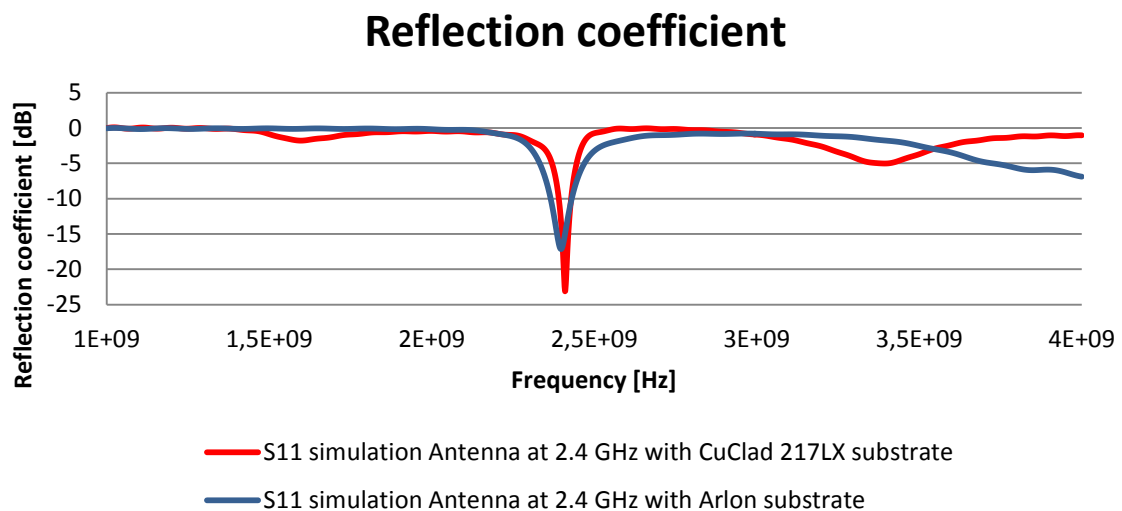


Fig. 3. 84. Comparison S11 parameter between antenna with arlon substrate and antenna with CuClad 217LX substrate

If you look at the directivity pattern, we notice that the final design with the substrate CuClad 217LX has improved gain of around 2 dB over the previous design.

## 4. MEASUREMENTS

---

In this chapter we talk about the antenna's fabrication and measurement processes to verify the antenna correct working. In the first part, we describe the fabrication of the antenna and the measurement methods and measurement tools used. Then, in the second part, we show the results of measurements made in the laboratory of the reflection coefficient and transmission coefficient. Finally, we make some comparisons between measured data and design simulations to verify that the antenna works as expected.

### 4.1 FABRICATION AND MEASUREMENT METHODS

The antenna which was finally built is the one shown in section 3.4, using the substrate CuClad 217LX. The antenna is shown in Fig. 4.1.

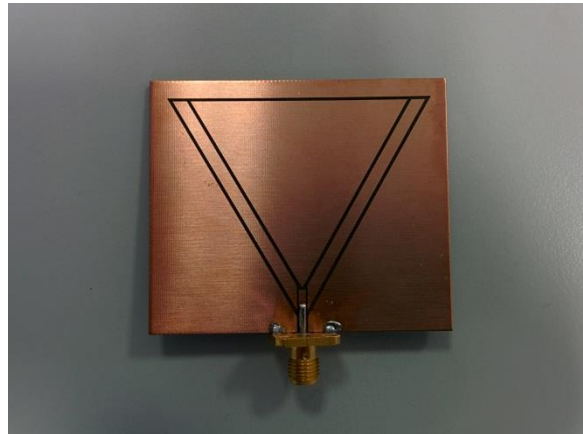


*Fig. 4.1. Triangular-Slot antenna finally built*

The antenna was built in the workshop of the Faculty of Electrical Engineering and Communication belonging to Brno University of Technology.

In the laboratory, the reflection coefficient of the antenna and the transmission coefficient were measured. For both measures, the network analyzer Rohde & Schwarz ZVL was used.



*Fig. 4.2. Network Analyzer used in the measurements*



To measure the reflection coefficient, three measurements were made: with the antenna in free space, on a phantom head and on our own body. The phantom used to measure the reflection coefficient is shown in Fig. 4.3.



*Fig. 4.3. Phantom used for S11 measurement*

The way to measure on phantom and on our own body is as shown in Figs 4.4.

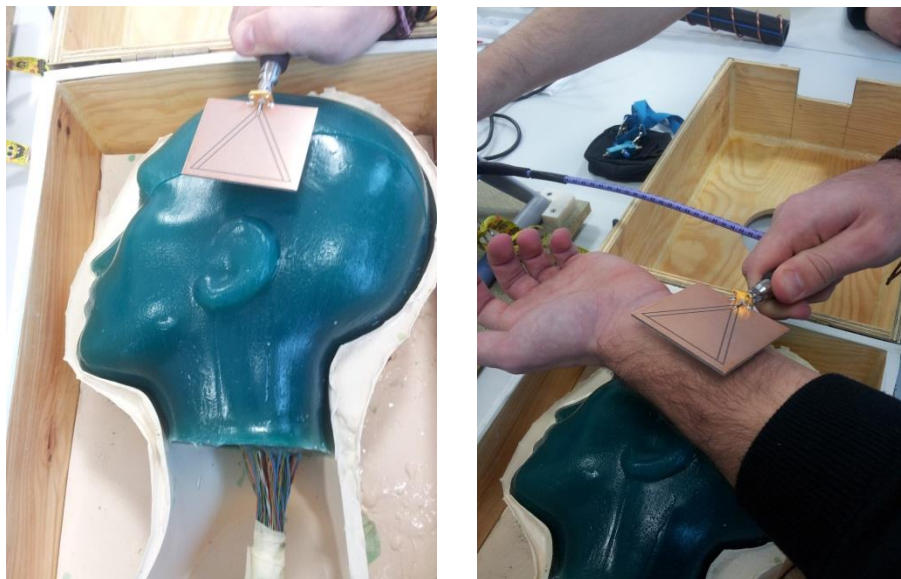


*Fig. 4.4. Phantom measure (Right) and real body measure (Left)*

To measure the transmission coefficient of the antenna an anechoic chamber and a reference antenna, whose resonance frequency is 2.4 GHz as our antenna, were used. Two measures of the transmission coefficient were made: with our antenna in free space and with our antenna on a phantom. The phantom used is an Agar gelatin of 20x20 cm and has a relative permittivity of 50, which seems to be a human muscle. This phantom is shown in Fig. 4.5.

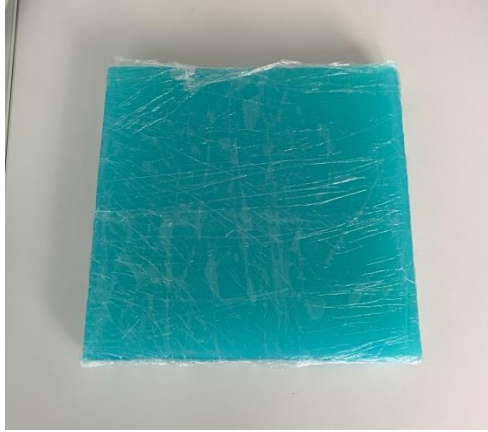


*Fig. 4.5. Phantom used in the transmission coefficient measurement*

The antennas were placed at a distance of 1.6 m and the configurations of both measurements were as shown in Fig 4.6 and Fig. 4.7. The antenna was placed vertical because of its vertical polarization, as we demonstrate on Appendix A.

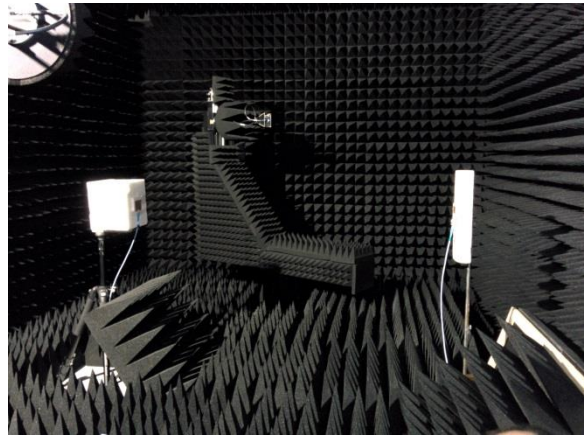


*Fig. 4.6. Transmission coefficient measurement in free space*

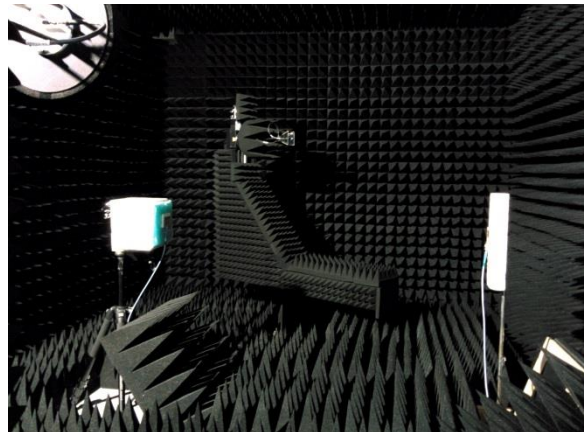


*Fig. 4.7. Transmission coefficient measurement with the phantom*

The results of these measurements are shown in the next section.



## 4.2 MEASUREMENTS RESULTS

In this section we show the results of all measurements made. First of all, the reflection coefficient measurement was made. The graphic result of these measures is shown in Figure 4.8.

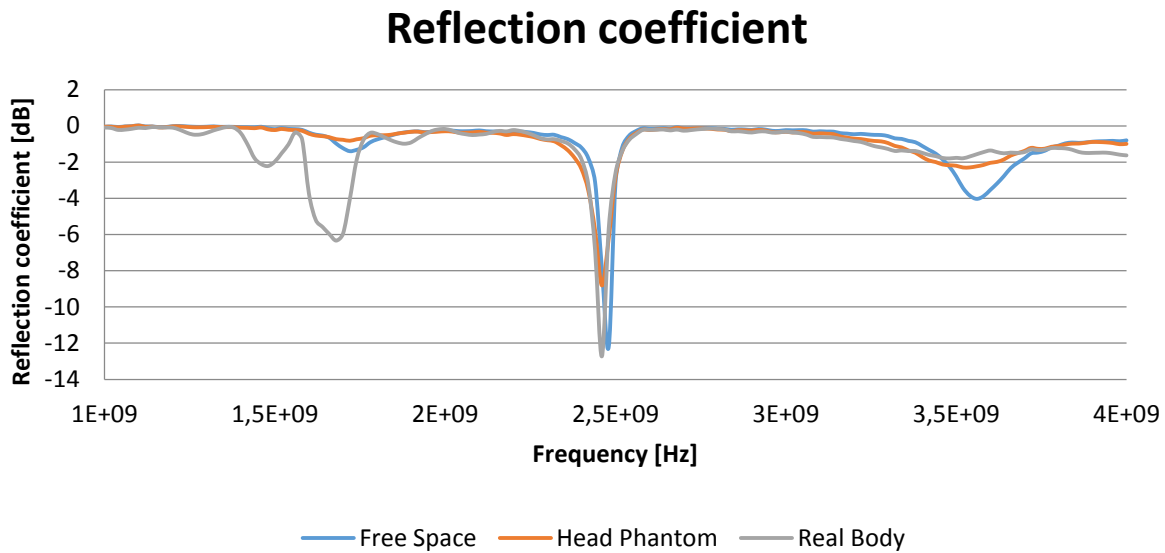


*Fig. 4.8. Reflection coefficient measurements*

The values of the measurements obtained are shown in Table 4.1. These values are an approximation since only samples each 20 MHz were used.

Measuring type	Frequency [GHz]	Reflection coefficient	Bandwidth
Free Space	2.48	-12.22 dB	1.61%
Head Phantom	2.46	-8.81 dB	#
Real Body	2.46	-12.72	1.62%

*Table 4.1. Values of reflection coefficient measurements*

As we can see from the results in Table 4.1, there are no differences between measurements made on tissue and those in free space, which is one of the objectives of on-body communications systems. The measurements on the head phantom are unreliable due to bad parameters of this phantom. The "Like- fractal dipole antenna" project, by Francisco Ruiz González, was done in parallel with this one and the results obtained by measuring on the head phantom were as bad as those obtained in this project.

In a second part, we made measurements of the transmission coefficient. As explained in section 4.1, a reference antenna whose resonance frequency was 2.4 GHz was used. The results of these measurements are shown in Fig 4.9.

## Transmission coefficient

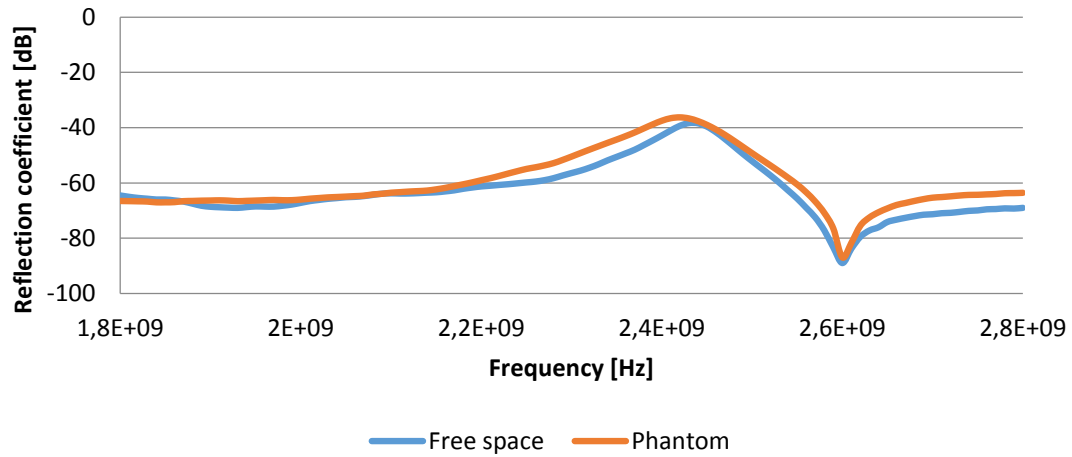


Fig. 4.9. Transmission coefficient measurements

The very low transmission coefficient results are due to the fact that measurements were made at 1.6 meters. In Appendix A, we show several simulations with 5 cm distance between both antennas where it is found that the transmission coefficient is better with lower distances.

### 4.3 COMPARISON BETWEEN MEASUREMENTS AND SIMULATIONS

In this section we make a comparison between the measurements obtained in the laboratory and the simulations done with CST Microwave Studio. First of all, we show the comparison of measurements and simulation of the reflection coefficient, first in free space (Fig. 4.10) and then on human tissue (Fig. 4.11).

## Reflection coefficient

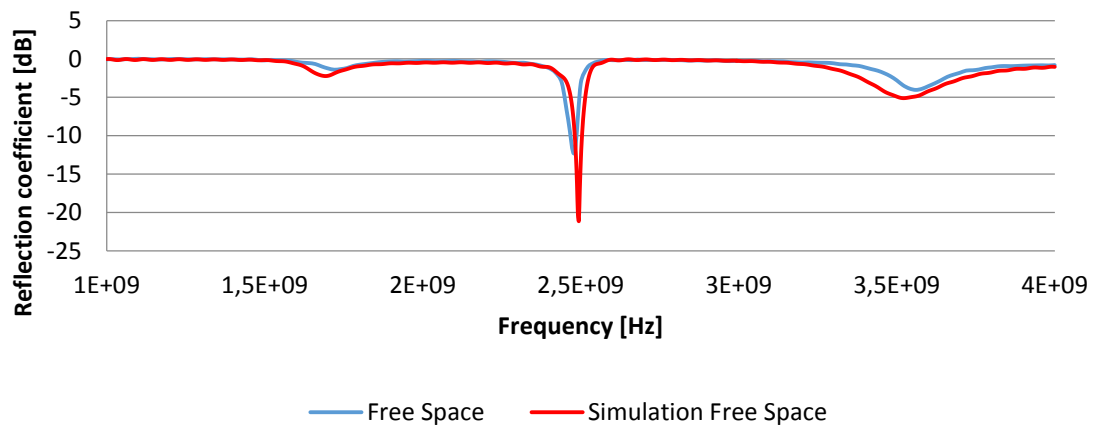
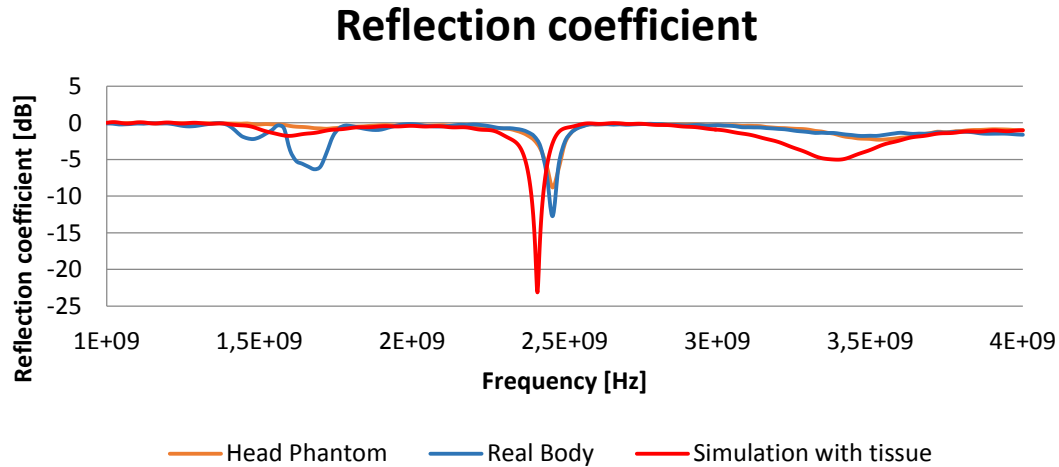


Fig. 4.10. Comparison between measurements and simulation in Free Space



*Fig. 4.11. Comparison between measurements and simulation on human tissue*

As we can see in the comparisons of the reflection coefficient, the measured results are very similar to the simulated ones, as expected. In the measurements on human tissue we found small differences. They are due to differences in the parameters of the phantom used in simulation and measurement.

Then, we show the comparison between the measurements and simulation of the transmission coefficient. The measurements were made in free space and on the phantom, while the simulation was done in free space only.

The configuration of the experiment is shown in Fig. 4.12. The triangular monopole is placed in free space to receive signals transmitted by an antenna placed on a body.

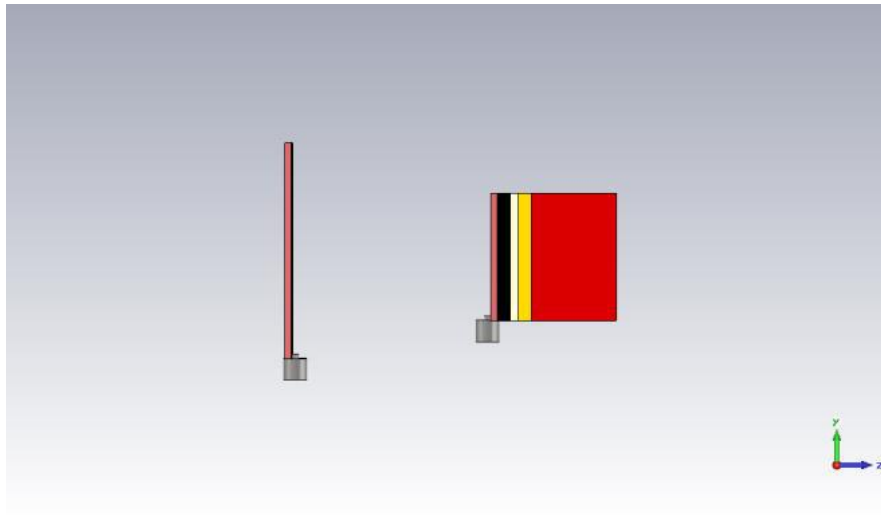


*Fig. 4.12. Configuration of an experiment for measuring transmission between two antennas*

For the transmission, we used a fractal-line slot dipole antenna. This antenna is depicted in Fig. 4.13, and its parameters are given in Table 4.2.

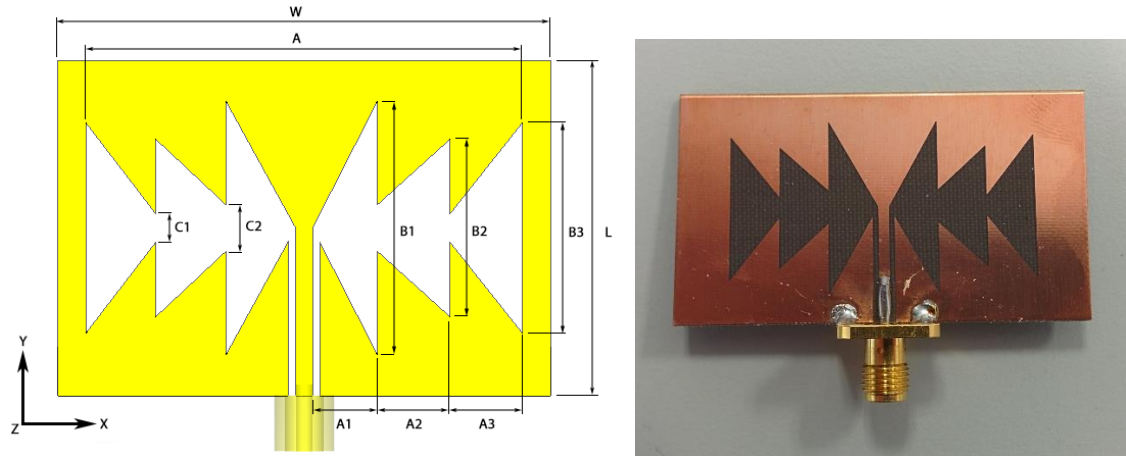


Fig. 4.13. Transmit antenna: fractal-line slot dipole

Parameter name	Value
$\epsilon_r$	2.17 (CuClad217LX)
L	30
W	54
A	40.34
A1	6.474361
A2	6.474361
A3	6.474361
B1	22.75
B2	15.88
B3	18.84
C1	2.55
C2	4.19
h (height of substrate)	1.52

Table 4.2. Parameters of fractal-line slot dipole antenna on CuClad217LX substrate.

Results of the experiments are shown in Fig. 4.14.

At the operating frequency  $f = 2.45$  GHz, both the antennas are well matched: magnitude of the reflection coefficient at the input of antennas (red line and orange line) is lower than  $S_{11} < -10$  dB,  $S_{22} < -10$  dB.

The transmission between antennas reaches its maximum at the operation frequency (green line). Magnitude of the transmission coefficient at the operation frequency is higher than  $S_{21} > -30$  dB.

The difference between the simulation and measurements are because the simulation needs a small grid to simulate small antennas like our antenna, so, in this case, the antennas are separated by 1.6 m and we must increase the grid because if not, calculation matrices are so large and the simulation time is unreasonable. Thus, although we get a reasonable simulation time, the results will be less accurate.

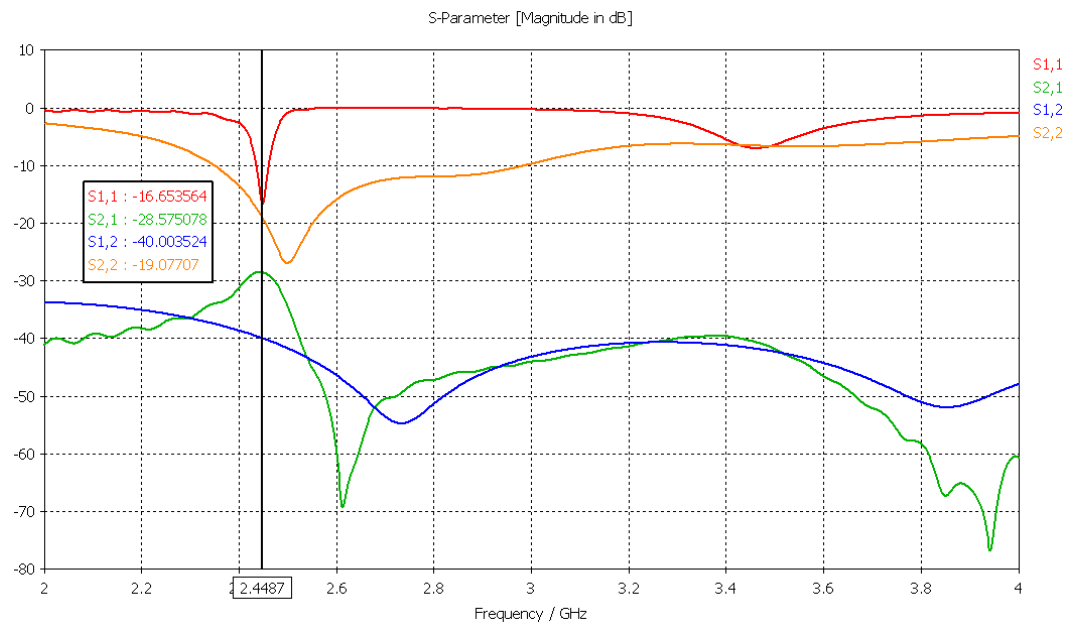


Fig. 4.14. Comparison of frequency response of reflection coefficient at the input of antennas (red, orange) and transmission coefficient (green).

## 5. CONCLUSIONS AND FUTURE WORK

---

The aim of our project was based on an antenna previously designed to work in the human body in the ISM frequency band 5.725 GHz to 5.875 GHz, modify its design to work on another ISM frequency band at 2.4 GHz and change the substrate to CuClad 217LX, since it is more flexible than the previous substrate used and thus it will be better adapted to the curves of the human body.

In a first step we had to recreate the original antenna design with CST Microwave Studio. In this first step we had to face the challenge of learning to use this program. Some dimensions and parameters that we were provided on the antenna were not those actually used in the original design, so we had to adapt them to achieve similar results in simulations that were shown in the paper of the original antenna. Still, the results were not exactly the same but quite similar, we obtained the frequency response we hoped that was what we wanted.

In a second step we change the whole design of the antenna to adapt its working frequency 2.4 GHz. This is achieved by increasing the size of the antenna. The results were good although the frequency response of the new design gave us a bandwidth too narrow. By placing the new substrate in this new design, we had to redo changes in the parameters of the antenna since the frequency was shifted from 2.4 GHz. After all, in the final design with CuClad substrate we achieved the expected frequency response although the bandwidth was narrower. The gain of this final design is also quite small, so that the transmission coefficient measurements we made in the laboratory leave us some pretty low results, since we performed measurements at a distance of 1.6 meters between the antennas.

Initially, we intended to design planar antennas to be used for on-body communication. Such antennas should produce vertically polarized wave (intensity of electric field is perpendicular to human body), and the maximum of the radiation should appear in the plane of a skin. The presented results show that we have succeeded in the radiation of the vertically polarized wave, but the maximum of the radiation appears in the direction which is perpendicular to the human skin. In order to solve the described problem, a detailed numerical analysis of modes of magnetic currents in the slot has to be performed. Unfortunately, CST Microwave Studio is not a proper tool for such an analysis. For the described analysis, ANSYS HFSS is recommended.

In the future work, the numerical model of the designed antenna has to be converted to ANSYS HFSS, a detailed analysis of modes of magnetic currents has to be performed and the design has to be modified to reach the required radiation. Also, we can try to improve all parameters of the antenna in order to achieve an improvement in the bandwidth of it and a better gain. It would also be interesting getting down the antenna size to make it more comfortable to use on the human body. We can achieve this by PIFA design techniques or working in higher frequency bands like 60 GHz. Finally, to take advantage of the flexibility of the CuClad substrate, we can employ a more flexible conductor than copper like graphene, which is a better conductor and much more flexible but on the other hand, is much more expensive than copper conductor.

## REFERENCES

---

- [1] S. I. Woolley, J. W. Cross, S. Ro, R. Foster, G. Reynolds, C. Baber, H. Bristow, and A. Schwartz, "Forms of Wearable Computer," IEE Eurowearable'03, Birmingham, UK, 2003.
- [2] P.S. Hall1, Y. Hao, Y. I. Nechayev, A. Alomainy, C. C. Constantinou, C. Parini, M. R. Kamarudin, T. Z. Salim, David T. M. Hee, R. Dubrovka, A. S. Owadally, W. Song, A. Serra, P. Nepa, M. Gallo and M. Bozzetti, "Antennas and Propagation for On-Body Communication Systems", IEEE Antennas and Propagation Magazine, Vol. 49, No. 3, June 2007.
- [3] M. S. Wegmüller, "Intra-Body Communication for Biomedical Sensor Networks", Dissertation, ETH Zurich, Zurich, 2007.
- [4] GPS World staff (2012, September 10). Optimizing Small Antennas for Body-Loading Applications. [Online]. Available: <http://www.gpsworld.com>
- [5] Hebelka, V.; Lacik, J.; Pitra, K.; Raida, Z., "Slot antennas for on-body communication," Applied Electromagnetics and Communications (ICECom), 2013 21st International Conference on, vol., no., pp.1,6, 14-16 Oct. 2013
- [6] P. J. Bevelacqua, "Antenna Theory". [Online]. Available: <http://www.antenna-theory.com>
- [7] Em:talk, "Electronics and Microwave Engineering". [Online]. Available: <http://www.emtalk.com/>
- [8] P-N Designs, Inc (2012, October 31). [Online]. Available: <http://www.microwaves101.com>
- [9] D. Orban and G.J.K. Moernaut, "The Basics of Patch Antennas". [Online]. Available: <http://www.orbanmicrowave.com>
- [10] W. F. Richards, Y. T. Lo, and D. D. Harrison, "An improved theory for microstrip antennas and applications", IEEE Trans. Antennas Propag., vol. AP-29, pp. 38–46, 1981.
- [11] D. M. Pozar and D. H. Schaubert, Microstrip Antennas: The Analysis and Design of Microstrip Antennas and Arrays. Editors, Wiley/IEEE Press, 1995.
- [12] K. F. Lee, Advances in Microstrip and Printed Antennas. Editor, John Wiley, 1997
- [13] R. Bancroft, Microstrip and Printed Antenna Design. Noble Publishing, 2004, chapter 2-3
- [14] R. Waterhouse, Handbook of Antennas in Wireless Communications. Edited by Lal Chand Godara, 2002, Chapter 6.
- [15] Blumlein, Alan (1938-03-07), "Improvements in or relating to high frequency electrical conductors or radiators", British patent no. 515684
- [16] Y-W. Jang, "Characteristics of a Wide-band, High Gain, Eight-element Slot Antenna for PCS, IMT-2000 and WLL-band". [Online]. Available: <http://www.microwavejournal.com>
- [17] Integrated Publishing, Basic Slot Antenna and Its Complementary Dipole. [Online]. Available: <http://www.electriciantraining.tpub.com>
- [18] A. K. Beesetti, K. Lalitha and R. Valluri, "Performance analysis of rectangular patch antenna using coaxial feeding and microstrip line feeding methods", International Journal of Electrical, Electronics & Communication Engineering, Vol. III Issue VIII August 2013.

- [19] D. Jefferies, "Microstrip". [Online]. Available: <http://personal.ee.surrey.ac.uk>
- [20] Wen, C.P., "Coplanar Waveguide: A Surface Strip Transmission Line Suitable for Nonreciprocal Gyromagnetic Device Applications," Microwave Theory and Techniques, IEEE Transactions on, vol.17, no.12, pp.1087-1090, Dec 1969
- [21] Forman, M. A. (December 2006). "Low-loss LIGA-fabricated coplanar waveguide and filter". APMC 2006 12: 905–1907.
- [22] "Design and Characterisation of Coplanar Waveguide". [Online]. [http://websupplements.net/projects/virtual\\_labs](http://websupplements.net/projects/virtual_labs)
- [23] I. Rosu. Microstrip, Stripline, and CPW Design. [Online]. Available: [http://www.qsl.net/va3iul/Microstrip\\_Stripline\\_CPW\\_Design/Microstrip\\_Stripline\\_and\\_CPW\\_Design.pdf](http://www.qsl.net/va3iul/Microstrip_Stripline_CPW_Design/Microstrip_Stripline_and_CPW_Design.pdf)
- [24] Coplanar Waveguide versus Microstrip [Online]. Available: <http://www.imst.de/coplan/introduction/introduction.html>
- [25] Computer Simulation Technology, CST Microwave Studio reference manual. 2013.
- [26] Hebelka, V.; Raida, Z., "CPW-fed double triangular slot antenna for biomedical applications," Microwave Techniques (COMITE), 2013 Conference on , vol., no., pp.43,45, 17-18 April 2013
- [27] Jin-Sen Chen, "Studies of CPW-fed equilateral triangular-ring slot antennas and triangular-ring slot coupled patch antennas," Antennas and Propagation, IEEE Transactions on, vol.53, no.7, pp.2208,2211, July 2005
- [28] PTFE/Woven Fiberglass Laminates: Microwave Printed Circuit Board Substrates. ARLON Company



1. POLARIZATION CST EXPLANATION

The vertical and horizontal polarization is often requested to be visualized in a farfield plot. Because the vertical or horizontal orientation of the polarization is related to the position of the antenna structure, it is just a matter of adequately choosing the coordinate system. The default coordinate orientation in CST can be changed in the “Farfield Plot > Properties > Axes” to define a new local reference system. Afterwards, the available Phi and Theta components enable the visualization of vertical or horizontal polarization parts, yet only at some especial locations in space. The relevant facts to be considered in this context are demonstrated in our antennas:

(Note: The initial orientation of the antennas is shown in Figure 14)

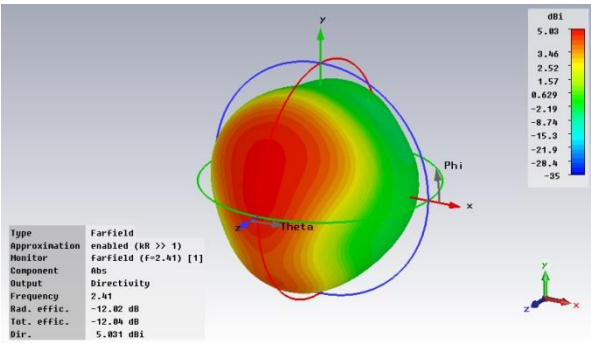


Figure 1. Abs-component

On the image above, the farfield result of an antenna structure is shown having its main lobe in the Z direction that represents the north pole of the system’s orientation. However, as you can see in the pictures below, due to the default coordinates system the plots of the Phi and Theta components barely give an impression of the polarization orientation at the main radiation direction.

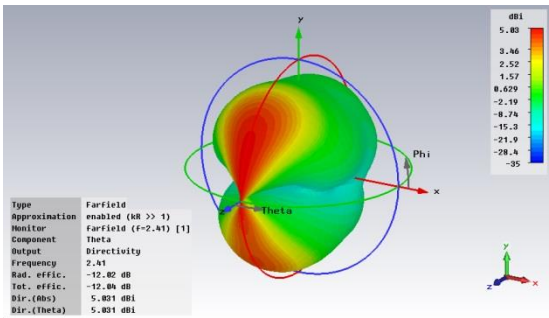


Figure 2. Theta component

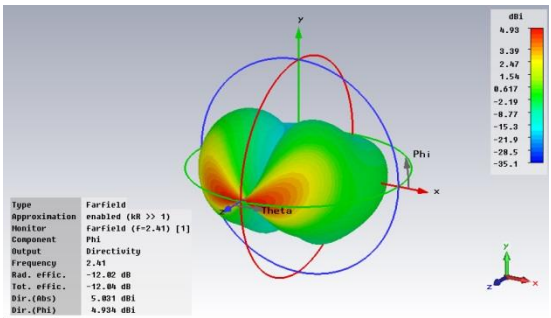


Figure 3. Phi component

To enable a somehow more plausible visualization, the local coordinates system in the “Farfield Plot > Properties > Axes” is changed in an appropriate way. Regarding the farfield orientation, the new Z axis is now represented by the Y axis defining the start for the angle Theta and analogous the new X axis is given by the Z axis defining the start for the angle Phi:

Start for theta (z'-axis) X: <input type="text" value="0"/> Y: <input type="text" value="0"/> Z: <input type="text" value="1"/>	→	Start for theta (z'-axis) X: <input type="text" value="0"/> Y: <input type="text" value="1"/> Z: <input type="text" value="0"/>
Start for phi (x'-axis) X: <input type="text" value="1"/> Y: <input type="text" value="0"/> Z: <input type="text" value="0"/>		Start for phi (x'-axis) X: <input type="text" value="0"/> Y: <input type="text" value="0"/> Z: <input type="text" value="1"/>

Figure 4. Axes change

In the 3D plots, the new coordinate axes  $x'$ ,  $y'$  and  $z'$  are marked by a stroke and are displayed in the farfield plot for a better understanding. As a result of the system's rotation, the farfield plots of the Phi and Theta components have changed in a relevant manner, while the lobe of the absolute value has remained the same as before.

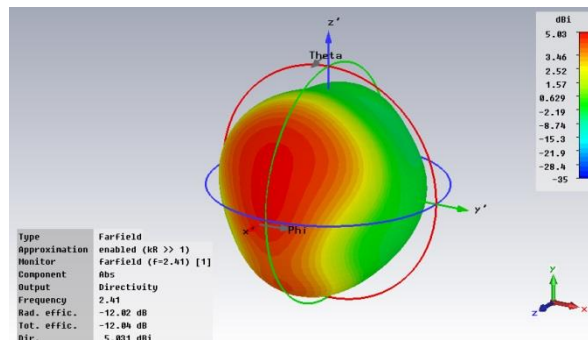


Figure 5. Abs-component with axes changed

The main lobe of the antenna structure is now positioned in the x-direction. As you can see in the pictures below, the Theta component is quite similar to the absolute value and consequently the Phi component is extremely small.

Now regarding the main lobe ( $\text{Theta}=90^\circ$ ,  $\text{Phi}=0^\circ$ ), the Theta and Phi components represent exactly the vertical and horizontal polarization. Therefore, assuming that in practice the antenna radiates in x-direction, we see that the main part of the field is vertically polarized.

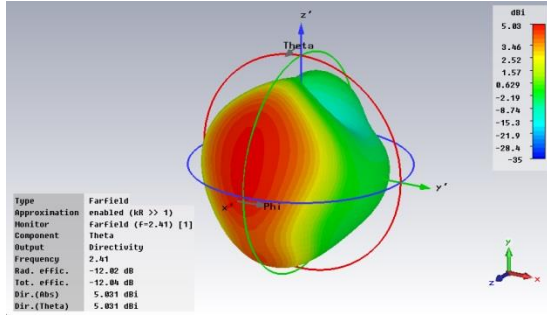


Figure 6. Theta component with axes changed

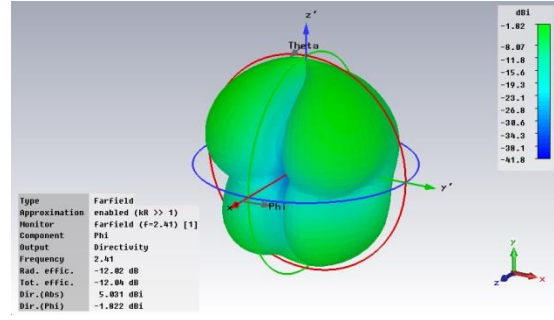


Figure 7. Phi component with axes changed

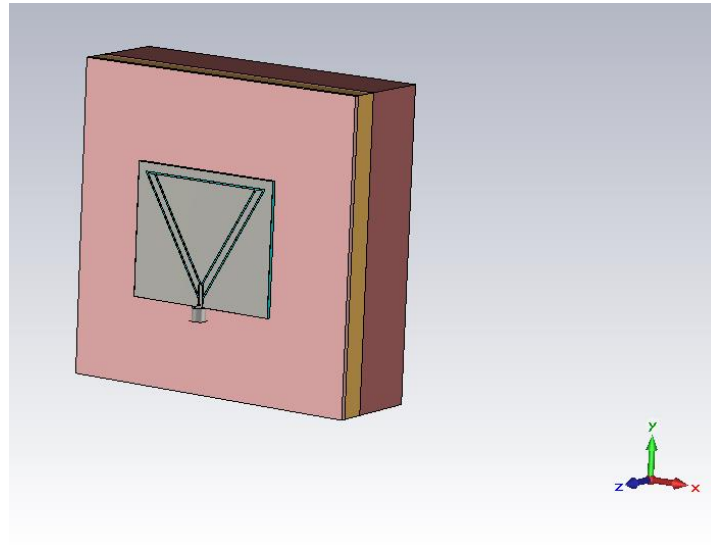


Figure 8. Orientation of antennas

During the next section we are going to simulate the transmission between our antenna and the antenna from “Like-Fractal dipole antenna” project by Francisco Ruiz González in order to compare the previous theoretical explanation with the necessary simulations.

## 2. TRANSMISSION COEFFICIENT SIMULATION

The following simulations are between our antennas (Fractal dipole and Triangular monopole). The separation between the antennas is 5 cm.

We are going to show several simulations varying the position of the antennas. The configuration will be:

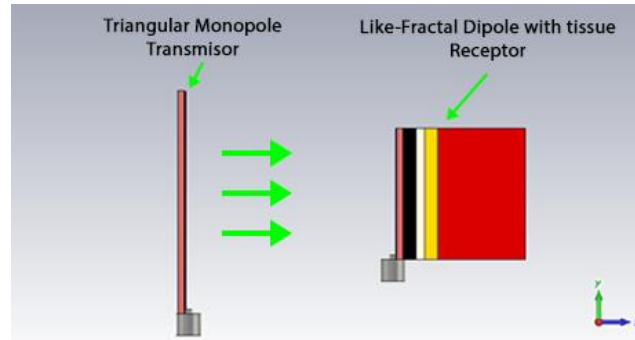


Figure9. Transmission configuration

The results for the configuration in Figure 9 are:

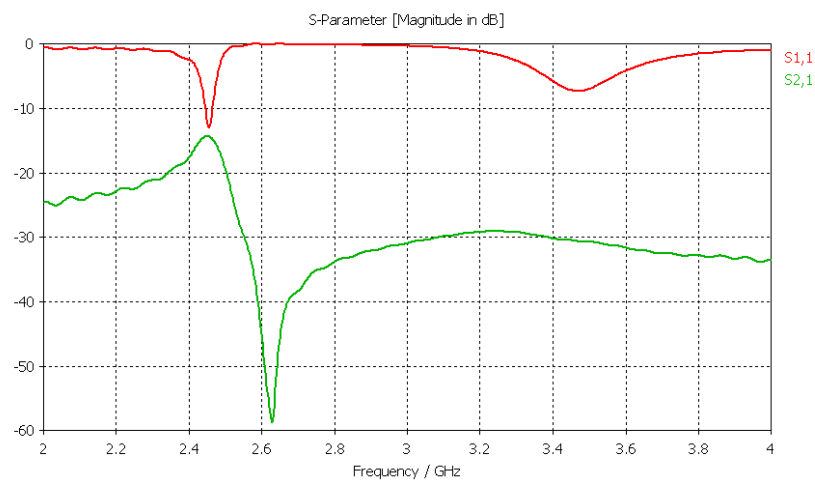


Figure10. S11 and S21 parameters

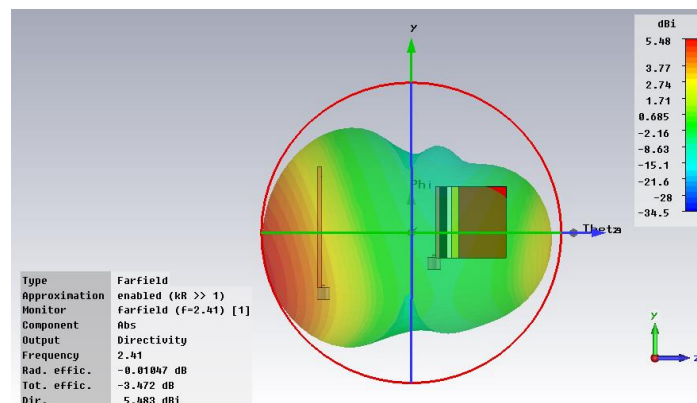


Figure 81. Farfield with antennas structure

- Configuration N°2 (Dipole rotated 90° in Z axis):

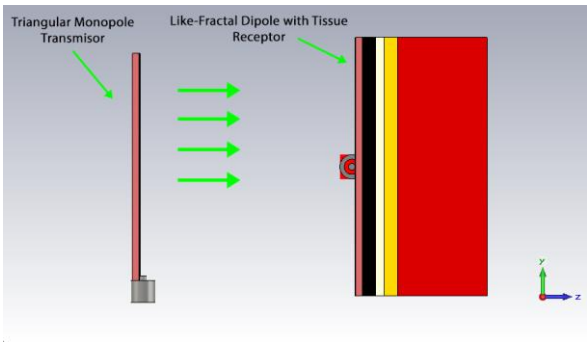


Figure 92. Transmission configuration

The results for the configuration in Figure 12 are:

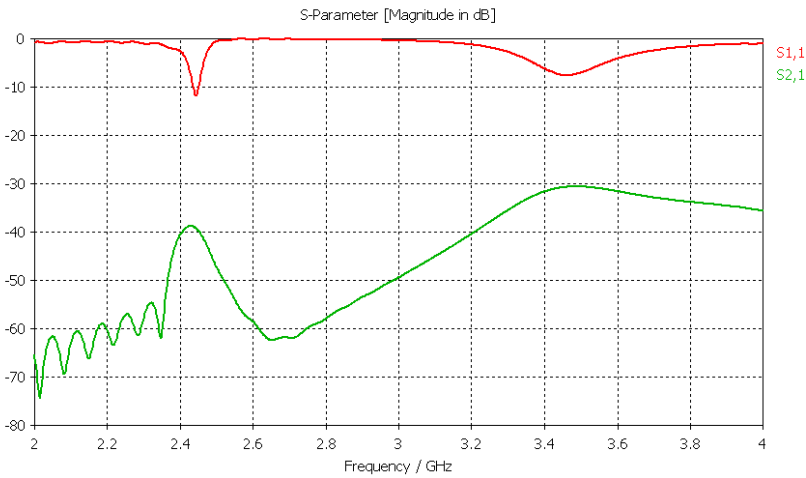


Figure 103. S11 and S21 parameters

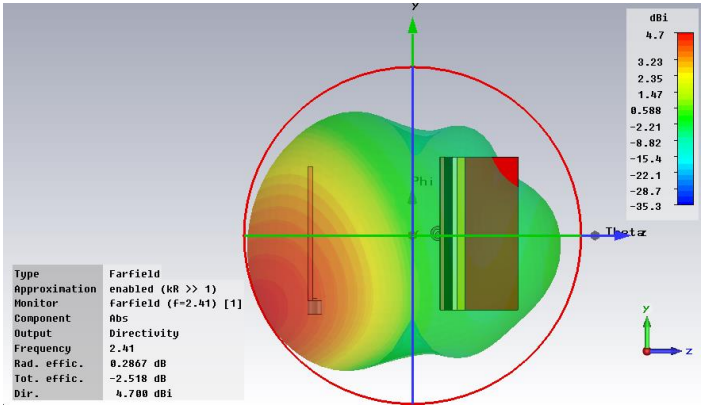


Figure 14. Farfield with antennas structure

- Configuration N°3 (Monopole rotated 180° in Y axis and 90 in X axis):

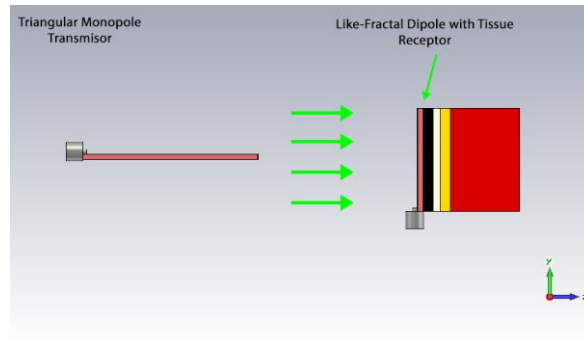


Figure 15. Transmission configuration

The results for the configuration in Figure 15 are:

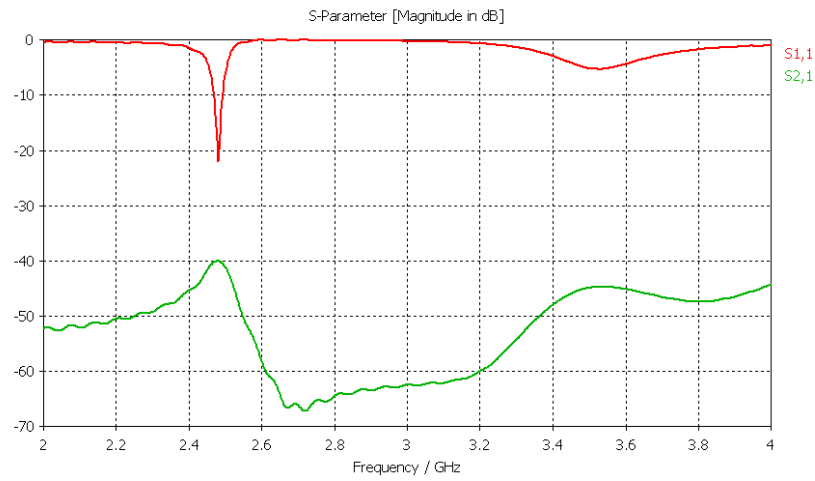


Figure 16. S11 and S21 parameters

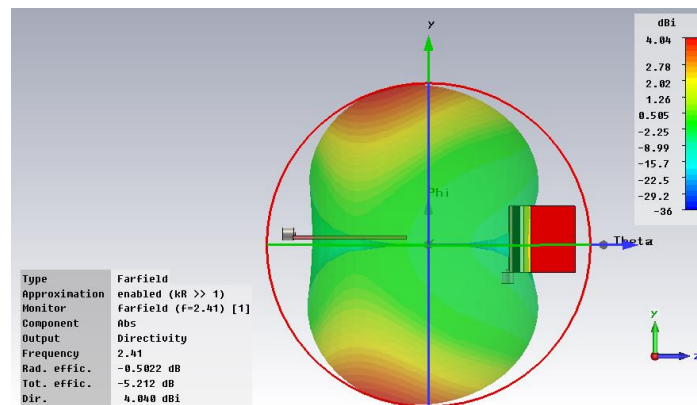


Figure17. Farfield with antennas structure

As we can see in Figure 10, 13 and 16, the results are better with the first configuration.

### 3. PARAMETER S22 OF FIGURE 15 CONFIGURATION

---

The following antennas configuration is the same as shown in Figure 9, but now we added a new source port in the Like-Fractal dipole antenna (Port 2). The aim of this simulation is to view the S22 and S21 parameters of this configuration. The results are shown bellow.

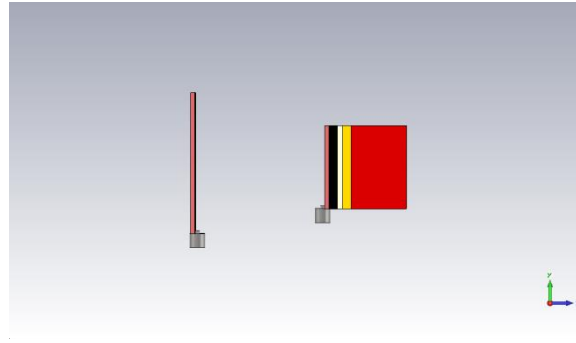


Figure 18 Transmission configuration

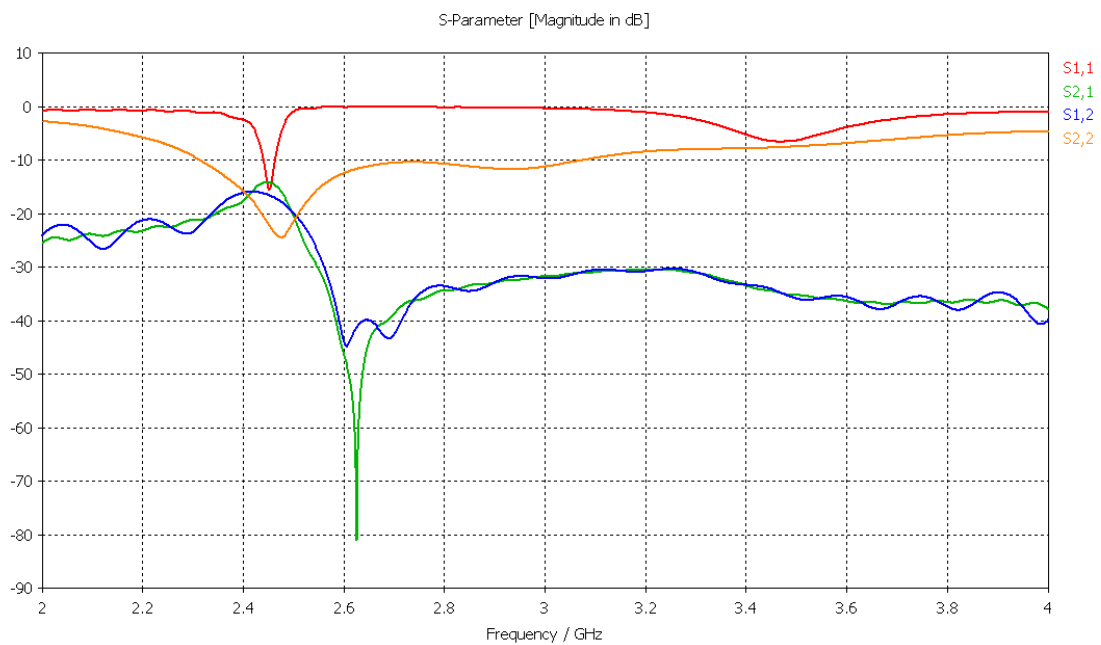


Figure 19 S parameter of Figure 24 configuration

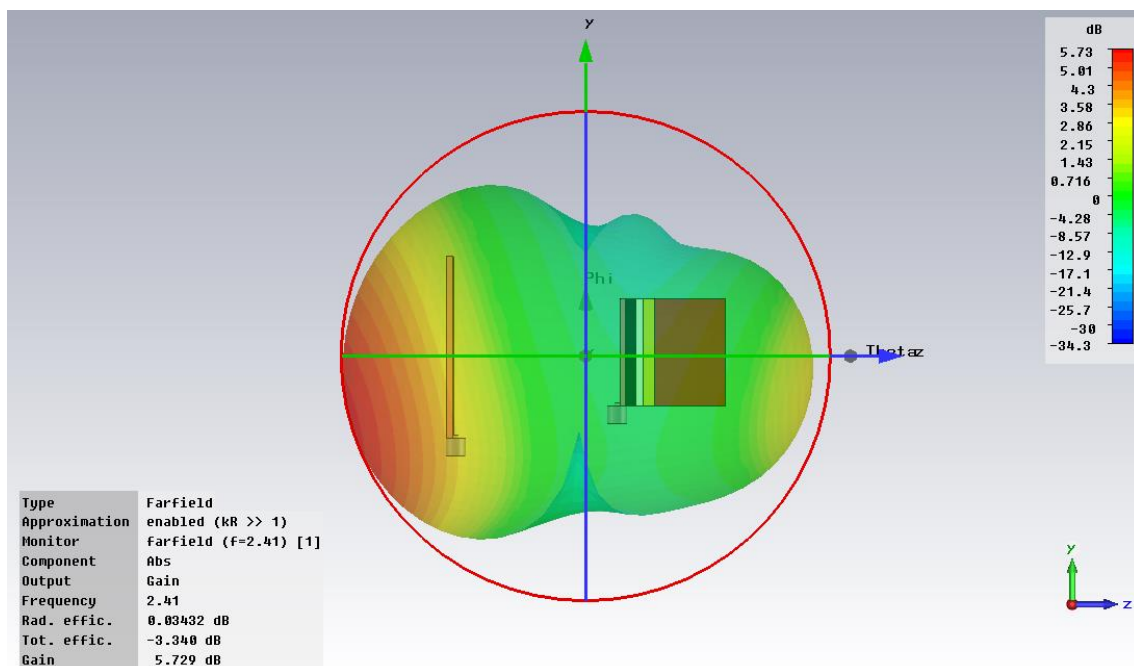


Figure 20 Farfield from Port 1 (Triangular monopole antenna)

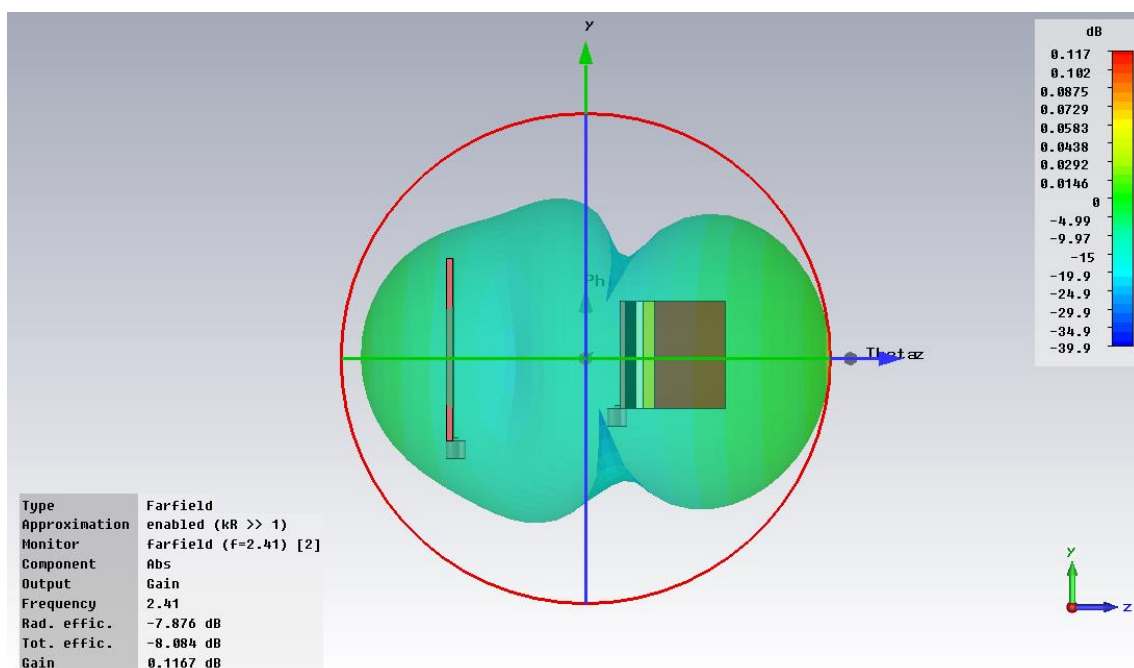


Figure 111 Farfield from Port 2 (Like-Fractal dipole antenna)



#### 4. MEASUREMENTS AT 4 LAMBDA DISTANCE (40 CM)

The following antennas configuration is the same as in the point 3, but now the separation between the antennas is 40 cm so we are in the far-field region. The results are shown bellow.



Figure 122 Transmission configuration

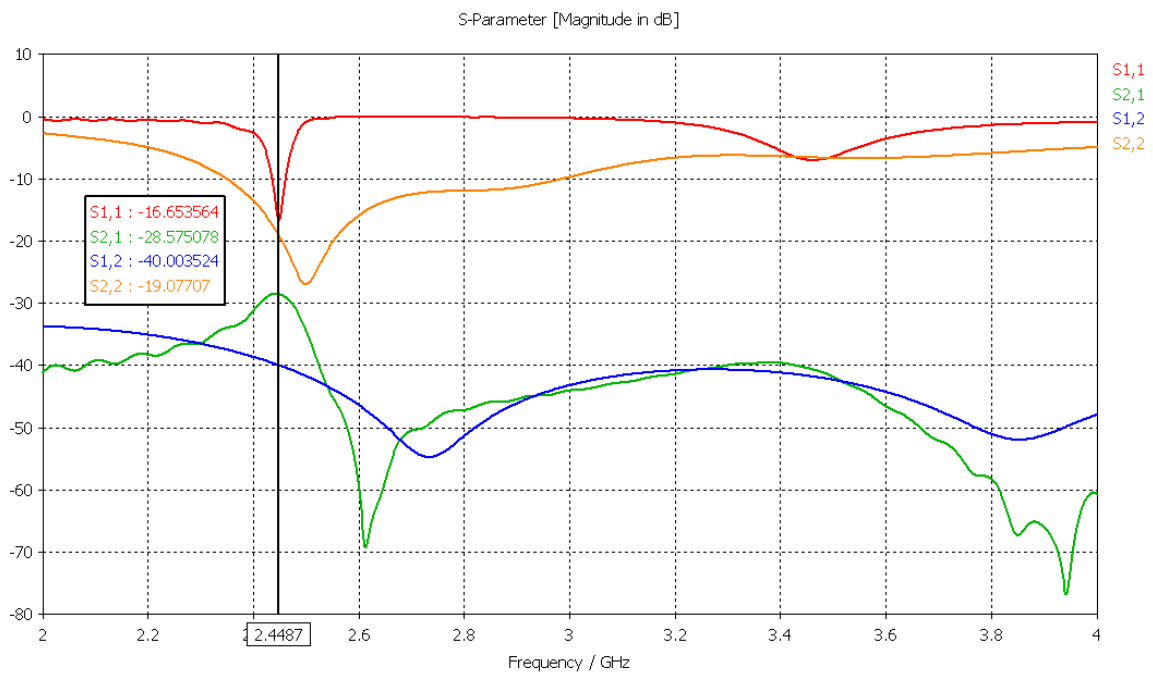


Figure 133 S parameter of Figure 28 configuration

- Gain and directivity, source port 1 (Triangular monopole antenna)

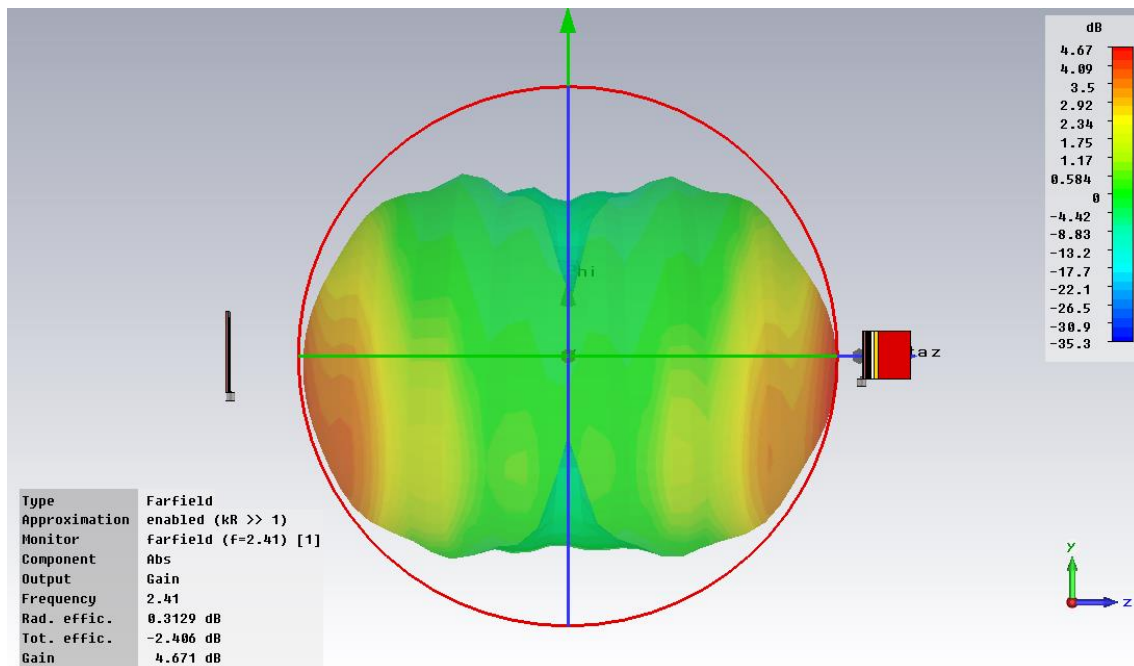


Figure 24 Gain from Port 1 (Triangular monopole antenna)

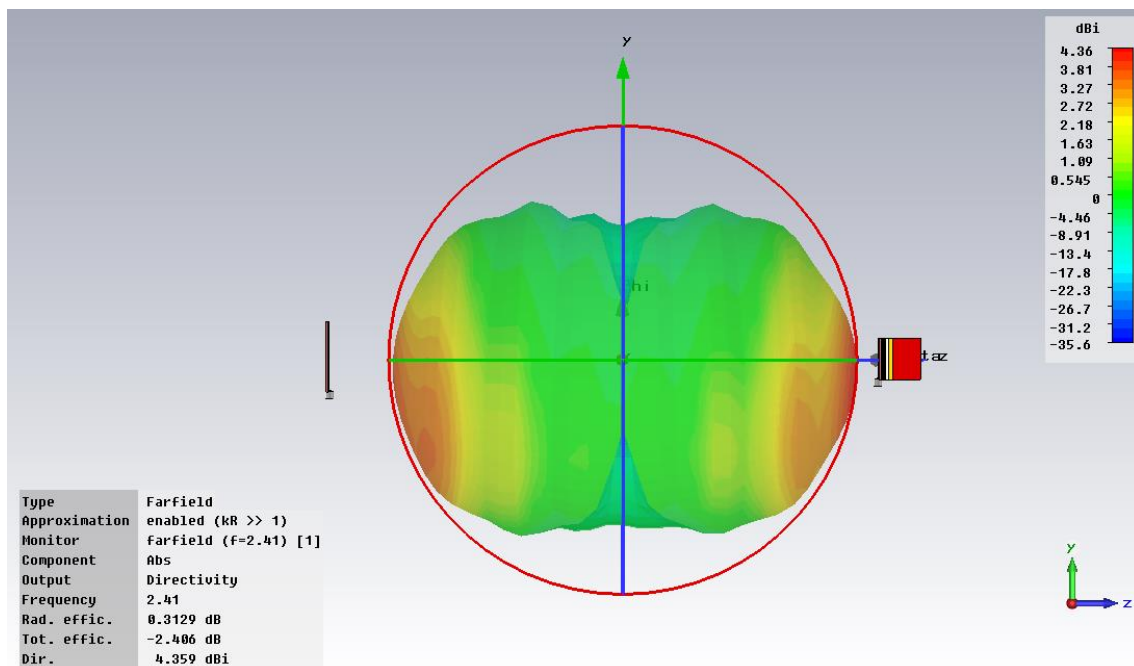


Figure 25 Directivity from Port 1 (Triangular monopole antenna)

On the one hand, when we use the Triangular monopole antenna as the source, we can notice in Figures 24 and 25 that the value of the directivity (4.359dBi) and the gain (4.671dB) is almost the same.

- Gain and directivity, source port 1 (Like-fractal dipole antenna)

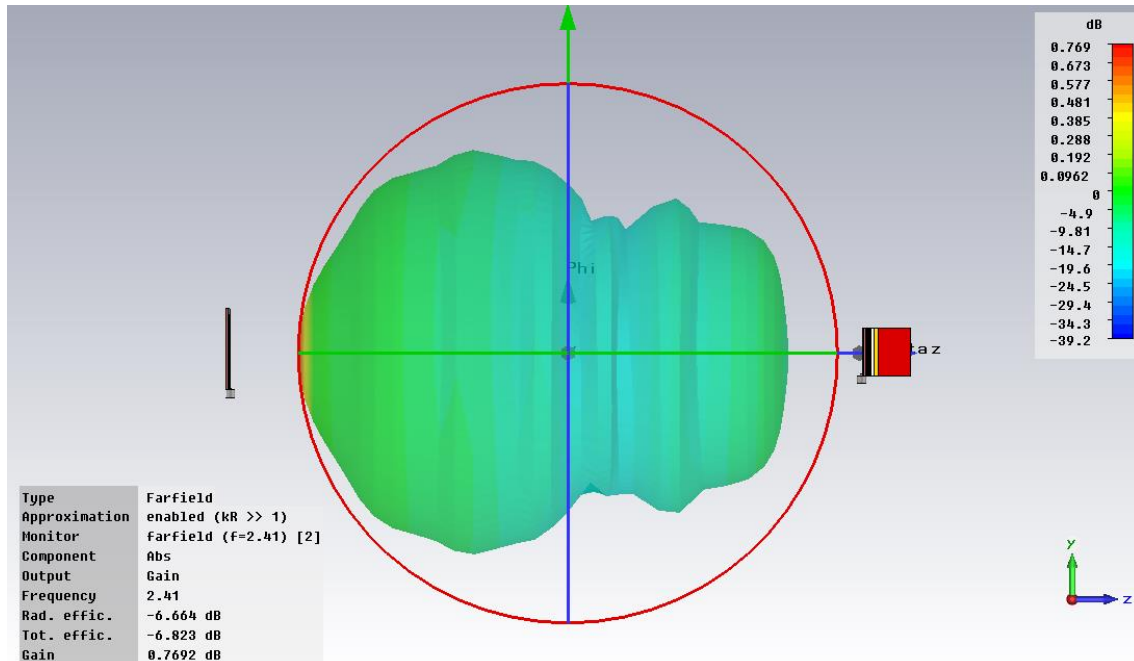


Figure 26 Gain from Port 2 (Like-Fractal dipole antenna)

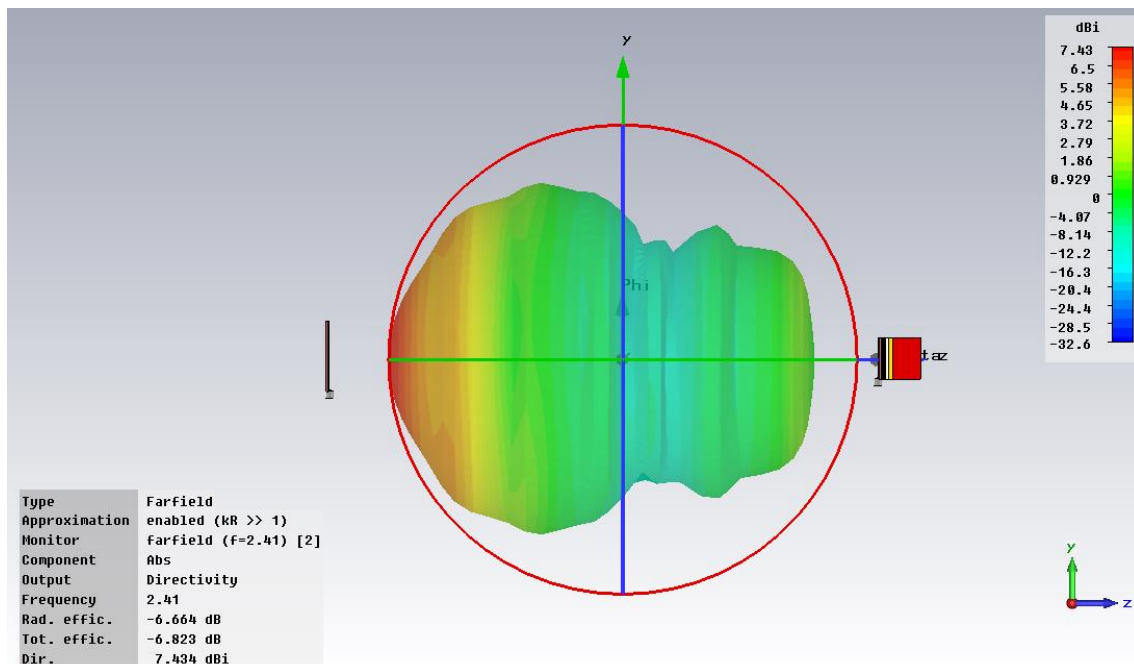


Figure 27 Directivity from Port 2 (Like-Fractal dipole antenna)

On the other hand, as it is depicted in Figures 26 and 27, the directivity (7.434dBi) of the Like-Fractal dipole antenna is right but the gain (0.7692dB) is too low.